The superconducting phases of UPt_3

Robert Joynt

Department of Physics and Applied Superconductivity Center, University of Wisconsin–Madison, Madison, Wisconsin 53706

Louis Taillefer

Canadian Institute for Advanced Research and Department of Physics, University of Toronto, Toronto, Ontario, Canada M5S 1A7

(Published 11 March 2002)

The heavy-fermion compound UPt_3 is the first compelling example of a superconductor with an order parameter of unconventional symmetry. To this day, it is the only unambiguous case of multiple superconducting phases. Twenty years of experiment and theory on the superconductivity of UPt_3 are reviewed, with the aim of accounting for the multicomponent phase diagram and identifying the superconducting phases. First, the state above the superconducting critical temperature at $T_c = 0.5$ K is briefly described: de Haas–van Alphen and other measurements demonstrate that this state is a Fermi liquid, with degeneracy fully achieved at T_c. This implies that the usual BCS theory of superconductivity should hold, although the strong magnetic interactions suggest the possibility of an unconventional superconducting order parameter. The role of the weak antiferromagnetic order below $T_N = 5$ K in causing phase multiplicity is examined. A comprehensive analysis of which superconducting states are possible is given, and the theoretical basis for each of the main candidates is considered. The behavior of various properties at low temperature ($T \ll T_c$) is reviewed. The experiments clearly indicate the presence of nodes in the superconducting gap function of all three phases. In particular, the low-temperature low-field phase has a gap with a line node in the basal plane and point nodes along the hexagonal c axis. The phase diagram in the magnetic-field–temperature plane has been determined in detail by ultrasound and thermodynamic measurements. Experiments under pressure indicate a coupling between antiferromagnetism and superconductivity and provide additional clues about the order parameter. Theoretically, Ginzburg-Landau theory is the tool that elucidates the phase diagram, while calculations of the temperature and field dependence of physical quantities have been used to compare different order parameters to experiment. On balance, the data point to a two-component order parameter belonging to either the E_{1g} or the E_{2u} representation, with degeneracy lifted by a coupling to the symmetry-breaking magnetic order. However, no single theoretical scenario is completely consistent with all the data. The coupling of superconductivity and magnetism may be the weakest link in the current picture of UPt_3, and full understanding depends on the resolution of this issue.

CONTENTS

I. INTRODUCTION

A. History and basic facts

The superconductivity of the heavy-fermion compound UPt_3 presents a fascinating challenge for both theoretical and experimental physicists. The normal state of the material appears to be a Fermi liquid above the critical temperature $T_c=0.5$ K and there is an antiferromagnetic transition at $T_N=5$ K. Since the discovery of superconductivity in 1984 by Stewart *et al.* (1984), it has been anticipated that the usual theory of Bardeen, Cooper, and Schrieffer (1957) (BCS) holds, with one very big exception: because of the momentum-dependent inter-*f*-electron potential, we may need to consider nontrivial forms for the Cooper-pair wave function. In contrast to the situation in elemental superconductors, the wave function may deviate in an essential way from complete crystal symmetry. This leads to a gap function that varies on the Fermi surface. The example of superfluid ^{3}He tells us to expect complex patterns of symmetry breaking and a rich phase diagram. Discovering the origin and consequences of this unconventional superconductivity is the challenge for the theorist. Devising and carrying out critical experiments on a material that is complex but that can be made in very pure form is the challenge for the experimentalist.

Uranium-platinum compounds were studied in the early 1980s to understand the effect of hybridization on the nature of the U $5f$ wave functions (Schneider and Laubschat, 1981). Valence-band photoemission, which measures (roughly speaking) the occupied density of states, was performed on UPt_n, with $n=0,1,2,3,5$, as well as on pure platinum. This systematic study showed a peak below the Fermi energy (E_F) associated with U $5f$ electrons. The peak is quite pronounced in pure uranium and gradually disappears as n is increased. The peak is only a shoulder in UPt_3, suggesting that this compound might be in an interesting intermediate hybridization range.

The specific heat C_V of UPt_3 was measured by several groups in the 1980s. The measurements showed no sign of magnetic or other ordering above T_c. They did show an upturn in the curve of C_V/T vs T^2 as temperature was reduced (see de Visser, Menovsky, and Franse, 1987). This is an anomalous behavior often associated with spin fluctuations. Indeed, the data were later shown to fit the law $C_V=\gamma T+\beta T^3+\delta T^3\ln(T/T_{SF})$ (Pethick *et al.*, 1986). The strong logarithmic term ($\delta \approx 2$ mJ/mol K^4) was considered to be a measure of the fluctuations, with a characteristic energy T_{SF}. (Interestingly, it is not present in other heavy-fermion systems.) In addition, γ was found to be very large: $\gamma \approx 440$ mJ/K^2 mol U, compared to 1.2 mJ/K^2 mol for aluminum. The elementary formula

$$\gamma=\frac{V_m k_F k_B^2}{3\hbar^2}m^*, \tag{1}$$

where k_F is the Fermi wave vector, V_m is the molar volume, and m^* is an effective mass, explains why UPt_3 is called a "heavy-fermion" system. The heavy-fermion family of materials is a rather loosely defined collection of intermetallic compounds with *f* electrons at the Fermi surface, typically made of Ce or U ($4f$ or $5f$ electrons, respectively) and other elements, with a strong degree of electron correlations and narrow quasiparticle bands, as reflected in a large γ, typically in excess of 100 mJ/K^2 mol.

Measurements of the resistivity, specific heat, and ac susceptibility to lower temperatures established that UPt_3 is a bulk superconductor (Stewart *et al.*, 1984). In 1984, UPt_3 and UBe_{13} (Ott *et al.*, 1984) joined $CeCu_2Si_2$ (Steglich *et al.*, 1979) to make up the early trio of heavy-fermion superconductors. Since then, other heavy-fermion superconductors have been discovered: UPd_2Al_3 (Geibel *et al.*, 1991a) and UNi_2Al_3 (Geibel *et al.*, 1991b), both of which have coexisting antiferromagnetic and superconducting orders like UPt_3, and compounds such as $CeCu_2Ge_2$ (Jaccard and Vargoz, 1998) and $CePd_2Si_2$ (Mathur *et al.*, 1998). All of them have $T_c\leqslant 2$ K. Since the heavy mass was believed to be due to magnetic fluctuations, reminiscent of ^{3}He, UPt_3 was speculated from the beginning to be an unconventional superconductor. ("Unconventional" will receive its precise definition in the next section.) These suspicions received confirmation from the absence of the characteristic activated [$\sim\exp(-\Delta_0/k_BT)$] temperature dependence of thermodynamic and transport quantities seen in standard superconductors at low temperature.

Great impetus was given to the field when it became clear that there were not one but several superconducting phases in UPt_3. Reports of finite field anomalies in ultrasound attenuation (Müller *et al.*, 1987; Qian *et al.*, 1987; Schenstrom *et al.*, 1989) and upper critical field (Rauchschwalbe *et al.*, 1985; Taillefer, Piquemal, and

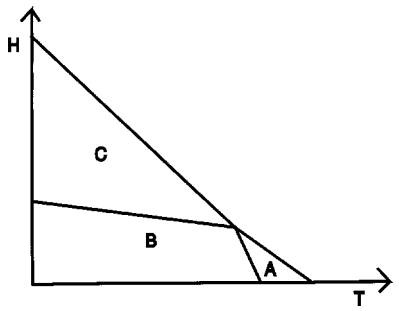

FIG. 1. Schematic superconducting phase diagram of UPt_3 in the magnetic field-temperature plane. Note the three distinct superconducting phases, labeled A, B, and C, which exist below an upper critical field line $H_{c2}(T)$ that separates them from the normal state. Note also that these phases all meet at a tetracritical point ($T^\star$, $H^\star$).

Flouquet, 1988) pointed to the possible presence of additional transitions, and it was the resolution of a second jump in the specific heat, first by Fisher *et al.* (1989) on two polycrystals and soon after by Hasselbach, Taillefer, and Flouquet (1989) on a single crystal, that brought clear thermodynamic evidence for a multiphase superconducting regime. The phase diagram is shown in Fig. 1. The names of the three phases shown—A, B, and C—have now become standard.

There is now little doubt that UPt_3 is an unconventional superconductor with a multicomponent superconducting order parameter. One should know that this is a rare occurrence. With the possible exception of UBe_{13} when doped with Th impurities in the narrow concentration window of 2–6 % Th (see Heffner and Norman, 1996), UPt_3 is the only compelling instance in nature of a superconductor with multiple phases. Because it exhibits this exciting new physical phenomenon and because it can be prepared in very pure single-crystalline form, its physical properties are now probably the best studied of any superconducting binary compound.

The primary aim of this extensive research has been to determine the form of the superconducting order parameter, in particular its momentum dependence. In having such a dependence, unconventional superconductivity is to conventional superconductivity as antiferromagnetism is to ferromagnetism. However, the student of magnetism has the luxury of being able to consult neutron diffraction data from which the magnetic structure can be read off. In superconductivity, the order parameter sets up no measurable field and there is no experimental probe which couples directly to it. Precisely for the reason that experiments to determine the order parameter structure are so indirect, a very close connection between experiment and theory is essential. This connection has indeed marked the nearly 20-year history of UPt_3 studies. We hope it marks this review as well.

B. Unconventional superconductors and superfluids

Superconductivity is defined as a state in which the order parameter spontaneously breaks gauge symmetry. Unconventional superconductivity is defined as a superconducting state in which the order parameter also breaks the crystal symmetry. The order parameter of an unconventional superconductor may also have more than one component, but this is not part of the definition.

The superfluidity of ^{3}He is both unconventional (the order parameter breaks rotation symmetry) and multicomponent (for a review, see Leggett, 1975). As a result, it became a paradigm for research in heavy-fermion superconductivity, so we briefly summarize the comparison to UPt_3. ^{3}He is a strongly interacting system. The enhancement of its specific heat over the free-particle value depends on pressure, but is generally in the range of 4–5. This is less than in UPt_3, where the enhancement over the value given by band calculations is about 20. There are strong magnetic fluctuations in ^{3}He but these are concentrated near zero momentum, i.e., ferromagnetic fluctuations. By contrast, in UPt_3, antiferromagnetic fluctuations and ordering are predominant. Magnetic interactions are surely the most important part of the pairing interaction in ^{3}He and almost certainly also in UPt_3. But the difference in the momentum-space weighting of the magnetic fluctuation spectrum in the two means that the symmetry of the ordering in the two systems is also likely to be different.

The electrons in UPt_3 move on a lattice of considerable complexity; this feature is not present in ^{3}He. Spin-orbit coupling, a tiny (but important) force in ^{3}He, is very strong in UPt_3. This complicates the band structure of UPt_3, but in some respects it simplifies the phenomenological theory of the superconducting state. This paradox comes about in the following way. ^{3}He is a spin-triplet superfluid—the Cooper pairs are in an $S=1$ spin state. The orbital wave function in this rotationally invariant system belongs to the $\ell=1$ representation. Due to the weakness of the spin-orbit force, this gives a ninefold degeneracy before nonlinear effects are considered. This multiplicity of low-lying degrees of freedom gives rise to great complexity (or richness, according to your taste) when calculating the collective modes or vortex structures. In UPt_3, on the other hand, the spin-orbit coupling locks the spin and orbital angular momenta, reducing the degeneracy from 9 to 3 in the triplet case. The absence of complete rotational symmetry reduces this further, to two or one, which are the possible dimensions of the representations of the point group. In the spin-singlet case, there is no spin degeneracy to start with: we end up again with a degeneracy of two or one for the pair state.

^{3}He exhibits two superfluid phases as a function of temperature and pressure, the A and B phases. UPt_3 has three phases as a function of temperature and applied magnetic field: the A, B, and C phases. However, it is unlikely that the transitions between different superfluid states in the two systems are caused by similar factors. The interaction strength, as measured by the dimensionless parameters of Fermi-liquid theory, is a very strong function of pressure in ^{3}He. The A-B transition is associated with this dependence. There is no analogous de-

pendence of these numbers on field in UPt_3. Furthermore, the applied field in UPt_3 breaks the point-group symmetry and can lift the degeneracy of the two components in linear order. Pressure can have no such effect. The transitions in UPt_3 are more analogous to the A-A′ transition in ^{3}He, where A′ is a phase which exists only at finite magnetic field.

High-T_c materials are likely to be the most familiar unconventional superconductors to the modern reader (for recent reviews, see Orenstein and Millis, 2000 and Tsuei and Kirtley, 2000). The analogy between UPt_3 and high-T_c superconductors is in some ways close. In both cases, the role of antiferromagnetic correlations (and ordering) is likely to be of central importance. Although the energy scales are two orders of magnitude higher in the cuprates, the ratio of magnetic to superconducting temperatures is similar: 5–10 in the cuprates and 10 in UPt_3. However, the nature of magnetism and its interplay with superconductivity are quite different. The strength of the intersite coupling is greater in the cuprates, which may account for some part of the difference in the superconducting critical temperatures. Scaling of the energies from one class of materials to the other is not likely to work, however, as there are a number of clear qualitative differences: high-T_c materials are quasi-two-dimensional, spin-orbit coupling is quite weak, the Fermi surfaces are rather simple (or at least have few sheets), and these materials are doped Mott insulators. None of these properties describe UPt_3. One of the most fundamental differences may lie in the nature of the normal (nonsuperconducting) state: while it is a Fermi liquid in UPt_3, albeit with strong mass renormalization, it is widely believed not to be a Fermi liquid in the cuprates.

There is a consensus that the order parameter in high T_c is predominantly one-component d wave (singlet; Tsuei and Kirtley, 2000). This is consistent with the fact that there appears to be no phase transition in the order-parameter structure in high-T_c cuprates. Thus the analogy is probably of little use in understanding the phase diagram of UPt_3. Nonetheless, the properties of the superconducting state will be seen to have many similarities and the theories developed to explain them are typically applicable to both cases. It is interesting that experimental breakthroughs in the two fields have come from very different measurements. Photoemission spectroscopy, microwave absorption, and phase-sensitive measurements have proven enormously fruitful in investigating cuprate superconductivity, but not in UPt_3. Pressure studies and sound attenuation have played a key role in our understanding of UPt_3, but they have not been very important in high T_c.

A number of review articles on particular aspects of UPt_3 have already appeared. General reviews of heavy-fermion systems which include discussion of UPt_3 are those by Stewart (1984) and Ott and Fisk (1987), who discuss early work, and later on by Grewe and Steglich (1991), Lawrence and Mills (1991), and Hess, Riseborough, and Smith (1993). Reviews on the general topic of superconductivity in heavy-fermion systems are those of Lee *et al.* (1986), Gor'kov (1987), and Taillefer, Flouquet, and Lonzarich (1991). Two comprehensive and useful reviews of unconventional superconductivity in general are those by Sigrist and Ueda (1991) and Volovik and Gorkov (1985). The theoretical background presented by Sigrist and Ueda is detailed enough that it makes sense to follow the notation established by their paper. We shall do this as far as possible. The most recent, and very useful, review in the area of heavy-fermion superconductivity is that of Heffner and Norman (1996). Reviews more specifically covering UPt_3 are those of Joynt (1992), which is a comparison of experiment with various theories, Taillefer (1994), and Löhneysen (1994), fairly comprehensive summaries of experimental data, and Sauls (1994), which is particularly good on the E_{2u} theory.

C. Outline and summary

In what follows, we cover experiments and theories that shed light directly on the superconducting phases of UPt_3. This is the central problem in this material. We shall attempt to give enough introductory material in each section that the article can be read by newcomers to the area, but go deep enough that that it should also be useful to experienced researchers. We limit the choice of topics to those in which meaningful comparison of theory and experiment can be made. This has led us to largely or partially omit certain topics, most importantly a large number of experiments on the effects of various impurities. Theories of vortices and vortex lattices are discussed only briefly, and theories of surface effects, Andreev scattering, and collective modes not at all. We discuss the pairing mechanism only very briefly. This is an issue of central interest but on which little can be said with any certainty at this stage.

Our strategy for the comparison of theory and experiment is to classify theories and experiments into groups. Within a class of theories, the predictions for experiment are rather similar. Within a class of experiments, the constraints on theories also resemble each other to some extent.

The theories are divided into three groups:

(a) two-dimensional representations, mainly E_{1g} and E_{2u};

(b) three-dimensional representations or spin-triplet theories;

(c) mixed-representation theories.

Other theories are mentioned, but space prevents us from investigating them in detail.

The experiments are also divided into three groups:

(a) phase diagram;

(b) nodal structure of the gap;

(c) Cooper-pair spin structure and spectroscopy.

The theories in one section of course do not all give precisely the same predictions, nor do all the experiments in one section point to the same theory. Nevertheless, there is enough commonality that comparison of classes of theories to classes of experiments often makes sense.

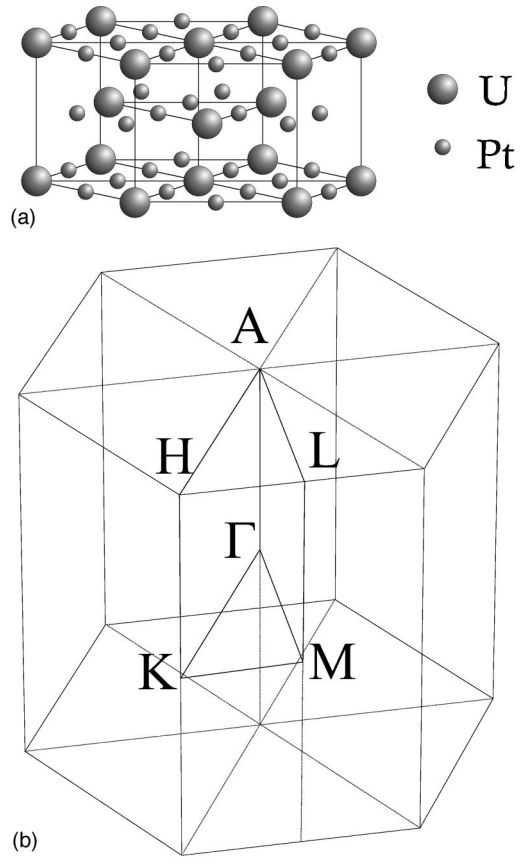

FIG. 2. Crystal structure of UPt_3 (a) and its first Brillouin zone (b).

We begin in Sec. II with a brief description of the normal state. Section III contains the background for understanding the three classes of theories of the superconducting state. The peculiar phase diagram of the superconductor is the topic of Sec. IV. The physical properties of the material in each of the superconducting phases, particularly in phase B, are discussed in detail in Sec. V, which is thus devoted to experiments in classes (b) and (c). In Sec. VI, we summarize the current status of our understanding of UPt_3 and suggest ways to further that understanding.

II. NORMAL STATE

A. Crystal lattice

UPt_3 crystallizes in the $MgCd_3$-type structure shown in Fig. 2. The uranium atoms form a closed-packed hexagonal structure with the platinum atoms bisecting the planar bonds. There are two formula units per unit cell. The compound belongs to the space group $P6_3/mmc$ and the point group D_{6h}. The lattice parameters are $a=5.764$ Å and $\tilde{c}=4.899$ Å, so that $\tilde{c}/a=0.845$, not too far from the hard-sphere value of 0.816. Here $\tilde{c}$ is the distance between neighboring planes, not the length of the unit cell. When discussing transport properties, the b axis is usually defined to be perpendicular to the a axis (i.e., parallel to the a^* axis). In terms of reciprocal space, we have $a\|\Gamma K$ and $b\|\Gamma M$. The nearest U-U distance is between atoms in adjacent layers, equal to 4.132 Å. Correspondingly, as we shall see in Sec. II.C, the conductivity is greatest along the c axis. The volume of the unit cell is 140.96 $Å^3$, the molar volume $V_m=42.43\times10^{-6}$ m^3/mol U, the mass density 1.940×10^4 kg/m^3, and molar weight 823.3 g. The mean atomic volume is 17.62 $Å^3$.

In 1993, a study of the crystal structure of UPt_3 using transmission electron microscopy (TEM) discovered a complex set of incommensurate structural modulations at room temperature, corresponding to several $\vec{q}$ vectors of magnitude around 0.1π/a (Midgley *et al.*, 1993). A similar TEM study performed on a whisker of UPt_3 found a well-developed incommensurate modulation with a single $\vec{q}=(0.1,-0.1,-0.1)$, i.e., of the same magnitude, corresponding to a modulation of wavelength ≈70 Å, coherent over microns (Ellman, Zaluska, and Taillefer, 1995). However, a subsequent x-ray investigation of the structure of a whisker by Ellman *et al.* (1997) found no trace of any incommensurate modulation, at the level of one part in 10^5 (see also Walko *et al.*, 2001). This suggests that the structural distortions seen with TEM may be the result of the rather violent surface preparation techniques used to thin the samples (e.g., ion milling). We conclude that the intrinsic crystal structure of UPt_3 is perfectly hexagonal. (Note, however, a recent x-ray study which reports the observation of a slight trigonal distortion; Walko *et al.*, 2001.) Deviations from this correspond to extrinsic lattice defects (such as stacking faults), which of course are present to a varying degree in different samples, as discussed in Sec. II.E.

The basic elastic properties of UPt_3 are well described by de Visser, Menovsky, and Franse (1987). Longitudinal acoustic waves travel at a speed of 3860 and 3993 m/s parallel and perpendicular to the c axis, respectively. The two transverse acoustic modes propagate at 1385 m/s along the c axis and 1388 m/s (2076 m/s) along the b axis with polarization parallel (perpendicular) to the c axis. The Debye temperature is found to be 217 K, in agreement with an estimate from specific heat (Sec. II.C.1). The compressibilities are calculated by de Visser, Menovsky, and Franse (1987):

$$\kappa_a=-\frac{1}{a}\frac{da}{dP}=0.164,\quad \kappa_c=-\frac{1}{c}\frac{dc}{dP}=0.151,$$
$$\kappa_V=2\kappa_a+\kappa_c=0.479\ \text{Mbar}^{-1}. \tag{2}$$

B. Quasiparticle spectrum

1. Band structure

UPt_3 is the archetype of a heavy-fermion system. It has the qualitative properties of a Fermi liquid, but the magnitude of the effective masses, reflected in the specific heat and magnetic susceptibility, is very much larger than the free-electron value. The heaviness of the electrons is generally attributed to electron correlations which come from the strong repulsions on the U sites.

Models of this phenomenon are usually based on simplified Hamiltonians such as the Anderson lattice model. Approximate solutions of this model show an enhanced specific heat and high magnetic susceptibility combined with (elastic) transport properties which do not show strong renormalizations. This is the pattern observed in UPt_3, so we may be said to have a reasonable qualitative understanding of the ground state and the low-energy excitations. Details of the theories may be found in Fulde, Keller, and Zwicknagl (1988) and Hewson (1993). These theories are usually based on models that greatly oversimplify the uranium atom. There has been some progress in models with more realistic atomic physics, and mass renormalization appears to take place in a fashion similar to that in the simplified models (Rasul and Harrington, 1987; Evans and Gehring, 1989).

In the theories, correlations give a strong frequency dependence to the self-energies of the electrons, but very little wave-vector dependence. Thus one may hope to calculate accurately the position of the Fermi surface using density-functional theory. We would not expect that such calculations would yield the mass enhancement. In fact, UPt_3 has attracted a great deal of interest from band-structure theorists, particularly when it became clear that reliable experimental information on the Fermi surface could be obtained by measurements of the de Haas–van Alphen (dHvA) effect. The calculations are based on the local-density approximation to the exchange-correlation potential taking the U $5f$ electrons to be itinerant, as opposed to localized in the core (Oguchi and Freeman, 1985; Sticht and Kübler, 1985; Strange and Gyorffy, 1985; Albers, Boring, and Christensen, 1986; Oguchi, Freeman, and Crabtree, 1987; Wang *et al.*, 1987; Norman *et al.*, 1988). All calculations lead to similar results, confirmed again in more recent calculations (Kimura *et al.*, 1995; Julian *et al.*, 2000). The band structure of UPt_3 thus calculated consists of five separate bands crossing the Fermi level, all with strong f character, giving rise to five (or six) Fermi surface sheets. For a brief review of the calculations and a comparison with experimentally determined surfaces, see

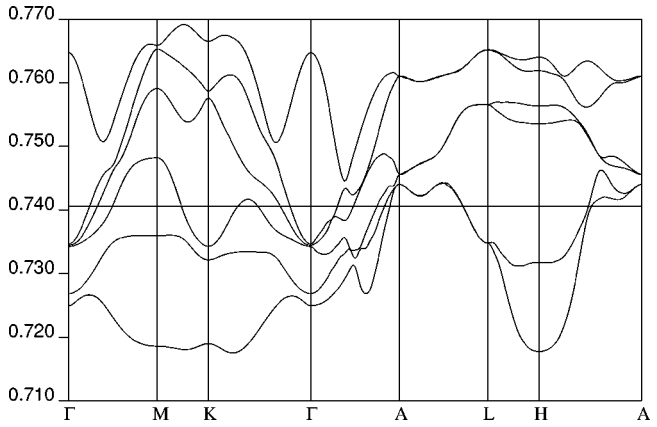

FIG. 3. The band structure of UPt_3 calculated using density-functional theory within a linearized augmented plane-wave basis. The nature of each band is described in the text. From Wang *et al.*, 1987.

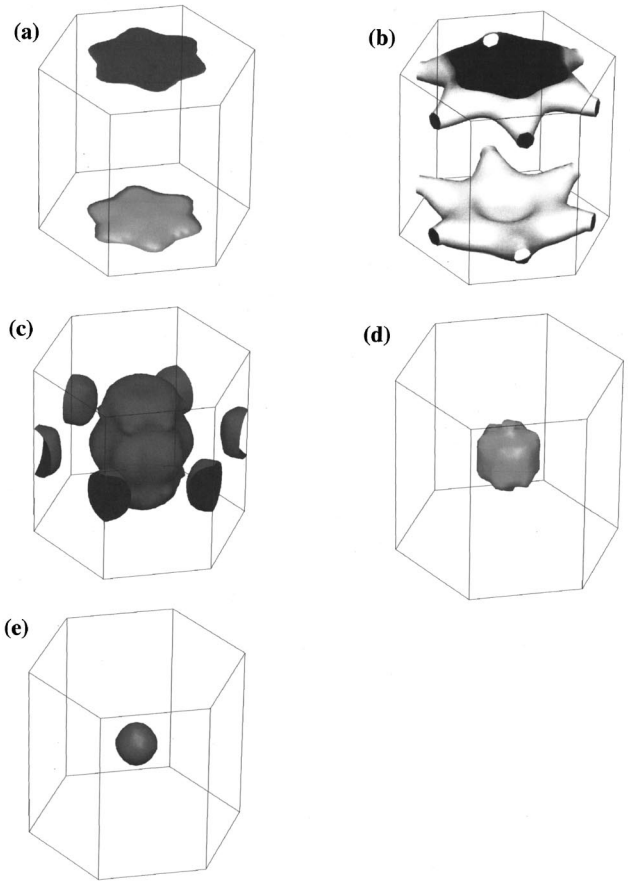

FIG. 4. Three-dimensional Fermi surfaces calculated under the assumption that the $5f$ electrons are included in the Fermi volume (Julian, 2000). For convenience, we label these as follows: (a) the starfish, (b) the octopus (both centered on point A), (c) the Γ-centered oyster surrounded by six K-centered urchins, and (d) the mussel and (e) the pearl (both centered on Γ).

Norman and Koelling (1993). In Fig. 3 we plot dispersion curves taken from Wang *et al.* (1987), who used the method of "linearized augmented plane waves," generally regarded as the most accurate of those applied to UPt_3. These calculations are relativistic so that spin-orbit coupling is properly treated.

The corresponding Fermi surface is shown in Fig. 4 in a 3D representation (Julian *et al.*, 2000). It is seen to consist of five or six separate sheets: two hole sheets centered on A, which we call the "starfish" and the "octopus," and three electron sheets centered on Γ which we call the "oyster," the "mussel," and the "pearl." In addition, there may be a set of six "urchins" surrounding the oyster, each centered on K.

These curves are the eigenvalues of the Kohn-Sham equations and represent the single-particle states. The differences in atomic configuration energies thus appear only in an average way. This being given, however, the bands are not difficult to understand. Since uranium is near the beginning of the actinide row, Hund's rules imply that the single-particle states near the Fermi energy are the $\ell=3$, $s=1/2$, and $j=5/2$ states. At the Γ point, these six states transform according to the repre-

sentations of the full hexagonal point group, and are therefore split into three doublets by the crystal field. These may be labeled by their values of j_z: $j_z=\pm 1/2$, $j_z=\pm 3/2$, and $j_z=\pm 5/2$. The splitting between the $\pm 5/2$ states and the $\pm 3/2$ states is seen to be roughly twice that between the $\pm 3/2$ and $\pm 1/2$ states. The situation in UPt_3 is further complicated by having two uranium atoms in the unit cell. There is a bonding and antibonding combination for each momentum state. The total number of bands is thereby doubled, yielding the six bands that one sees in the vicinity of the Fermi level. The bonding-antibonding (even-odd) splitting in the unit cell may be seen from form-factor arguments to be very small on the zone faces $k_z=\pm\pi/c$, particularly at the A and L points. This is convenient since it allows us to estimate the crystal field and bonding-antibonding energies separately.

At the Γ point, the identification of the states as being derived from a given j_z is reasonable if crystal fields are not too strong. Following the bands to the zone face allows us to distinguish between even and odd as well. This procedure leads to the conclusion that the even-odd splitting potential matrix element ranges from a few mRy to about 10 mRy, or roughly 10–100 meV. The splittings between pairs at the Γ point may be attributed to the crystal field. These splittings are of order 5 mRy, comparable to the even-odd splitting.

The dispersion of the bands comes from hybridization of the U $5f$ shell with the Pt $5d$ shell. Direct overlap of the U atoms is negligible since the minimum U-U distance is 4.13 Å, well beyond the Hill limit of 3.4 Å at which $5f$ orbitals cease to overlap. The bandwidth varies a bit from band to band, but is generally about 20 mRy, roughly $\frac{1}{4}$ eV.

The fact that the bandwidth is greater than the crystal-field splitting means that orbitals of different j_z will mix over most of the Brillouin zone and we may not classify states in this way, except near the Γ point.

The band calculations, combined with experiment, can help to estimate the on-site interaction U and overlap parameter V in model Hamiltonians such as the periodic Anderson model (for details of the model, see Hewson, 1993). Spectroscopic experiments on free neutral uranium atoms give values for U ranging from 2.3 to 2.6 eV, which is probably reduced to something like 1.5 eV in the metallic ion (see Norman, 1995a for references). Putting in a bandwidth B ($\approx 2zV$, z being the coordination number) of about 0.25 eV then leads to a sizable dimensionless interaction strength $U/B\approx 6$, and substantial mass renormalization is to be expected.

By evaluating the Fermi velocity $\vec{v}_F=\hbar^{-1}\nabla_{\vec{k}}E(\vec{k})$ at all points on each surface one can evaluate the average velocity $\langle v_F\rangle_i$ in the i direction, and obtain the cyclotron mass for a particular orbit:

$$m_c=\frac{\hbar}{2\pi}\int_{orbit}\frac{d\vec{k}}{|\vec{v}_F(\vec{k})|}. \tag{3}$$

The thermodynamic mass, or equivalently the density of states at the Fermi energy for each surface, is given by

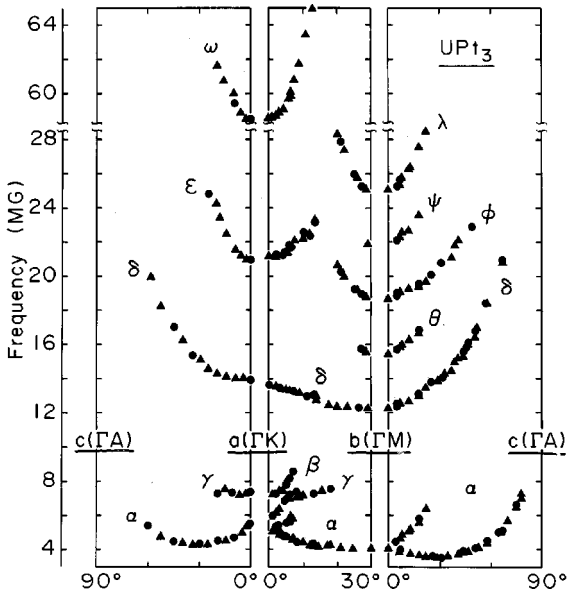

FIG. 5. Variation of the de Haas–van Alphen frequencies with orientation of the magnetic field in the crystallographic planes a-b, a-c, and b-c. From Taillefer and Lonzarich, 1988.

$$N_{FS\ sheet}(E_F)=\frac{1}{8\pi^3}\int_{FS\ sheet}\frac{dS}{|\vec{v}_F(\vec{k})|}. \tag{4}$$

2. de Haas–van Alphen effect

Measurements of quantum oscillatory phenomena such as the de Haas–van Alphen (dHvA) and Shubnikov–de Haas effects allow for a test of the validity of these band-structure calculations. The dHvA study of UPt_3 by Taillefer and co-workers (Taillefer *et al.*, 1987; Taillefer and Lonzarich, 1988) revealed a number of different frequency components, plotted in Fig. 5 as a function of the angle between the applied magnetic field and the crystal axes. Most of the observed dHvA frequency branches, and certainly all of those that correspond to large fractions of the Brillouin zone, can be satisfactorily identified with specific cyclotron orbits on the calculated Fermi surface (Taillefer and Lonzarich, 1988; Norman *et al.*, 1988). In Fig. 4, the identification of the dHvA frequency branches α, δ, γ, λ, ϵ, and ω to certain predicted orbits is given. Five of the six Fermi-surface sheets are sampled in the dHvA measurement, and most of the dHvA frequencies find a natural explanation and are in quantitative agreement with the calculated band structure. This includes the nontrivial structure for $H\|b\|\Gamma M$ (Fig. 5), made of five equally spaced frequencies (δ, θ, ϕ, ψ, and λ), naturally explained in terms of magnetic breakdown between two orbits centered on point A, respectively supported by the starfish (δ orbit) and the belly of the octopus (λ orbit) (see Taillefer and Lonzarich, 1988).

Recently, Julian *et al.* (2000) succeeded in resolving a number of dHvA frequencies for $H\|c$, not detected in the early studies. In particular, they could extend the δ and ω branches (around the mussel and the oyster) all the way from the a to the c axis, for which they find an

effective mass m^* varying from 25 to 43 m_e and from 82 to 110 m_e, respectively. They also identify an orbit around the urchins close to $H\|c$, with $m^* \simeq 60$. Kimura *et al.* (1995) also reported the observation of two dHvA frequencies for $H\|c$, with $F=27$ and 49 MG. They attribute the larger frequency to a new branch, labeled τ, assigned to an orbit around the "belly" of the octopus. Such a closed orbit would only exist for $\vec{H}$ very close to the c axis, as it seems to. (Note that Julian *et al.*, 2000 do not see this orbit.) As for the lower frequency, which one would naturally associate with the rising δ branch (or even the ϵ), these authors interpret it in terms of a new orbit on the inside of a gaping hole within the octopus. This proposed hole is said to result from a slight shift of the Fermi level in their band calculation (see Kimura *et al.*, 1995). They invoke the lack of saturation in their transverse magnetoresistance study as evidence for this central void. Indeed, without this void, the octopus supports open orbits along both a and b directions and the magnetoresistance should saturate for a current along those directions (given that UPt_3 is a compensated metal). However, the authors seem not to have been aware of a previous study by Taillefer, Flouquet, and Joss (1988), performed at lower temperature on a crystal of longer mean free path, such that the maximum $\omega_c\tau$ was 10 times higher, where saturation was very clearly established for a field along both the a and the b directions. Note also that a hole in the center of the octopus would eliminate the possibility of magnetic breakdown mentioned above. We conclude that no such hole exists (our octopus has a full belly!), and the Fermi surface of UPt_3 is very much as shown in Fig. 4. The oyster and the octopus are the only two Fermi-surface sheets that are thermodynamically significant, enclosing a large fraction of the Brillouin-zone volume and accounting for most of the density of states. The cyclotron mass on the oyster is the largest ever measured in any metal so far. Julian, Teunissen, and Wiegers (1992) were able to resolve what appears to be the two spin-split components of that Fermi surface and found a mass of 135 m_e for the upper branch.

In summary, we have good reasons to believe that standard band-structure calculations reproduce well the complex topology of the Fermi surface of UPt_3 and that the surfaces of Fig. 4 provide a fairly complete picture. In great contrast, however, no such agreement is found for the measured cyclotron masses, which range from 15 m_e for the smallest orbits to 90 m_e or more for the ω branch (oyster). Since the calculated band mass, m_c, of the various orbits is never more than 5 m_e (Norman *et al.*, 1988), this gives a mass enhancement that varies by a factor 2 with an average of about 20:

$$\frac{m^*}{m_c} = 12\text{–}29. \tag{5}$$

The same factor is found in the thermodynamic mass, which is just an average of the cyclotron mass over the entire Fermi surface [see Eqs. (3) and (4)]. The ratio of measured to calculated linear coefficient of the specific heat (Norman *et al.*, 1988) works out to be $\gamma_N/\gamma_{calc} = 17$, where $\gamma_{calc} = \pi^2 k_B^2 N(E_F)/3$. In this sense, the large effective mass one extracts from the specific heat is in excellent agreement with the cyclotron masses measured for various orbits around the Fermi surface. A mass enhancement of 17 is enormous, much higher than seen in any other class of materials before. It is of course the defining characteristic of a heavy-fermion compound and is due to the strong electron-electron correlations not included in the band-structure calculations. It is interesting that even in the presence of such strong correlations, there is no evidence of any breakdown of Fermi-liquid theory. The standard Lifshitz-Kosevich formula for the field and temperature dependence of the amplitude of quantum oscillations is perfectly verified down to 10 mK and up to 18 T (Lonzarich and Julian, 1994).

The picture that emerges for UPt_3 is then one of a liquid of Fermionic quasiparticles with uniformly high effective masses and a Fermi surface consisting of six sheets. By uniformly high masses we mean that there are no unrenormalized quasiparticles; one way of seeing this is via the Fermi velocities, all of which are within 15% of the same (extremely low) value:

$$\langle v_F \rangle_{bc} \simeq \hbar \langle k_F \rangle_{bc}/m^* = 5000 \text{ m/s} \tag{6}$$

for orbits in the b-c plane (Taillefer *et al.*, 1987). This is extremely slow; these fermions are not much faster than a typical phonon.

Even though this detailed picture has been known for over ten years, the Fermi surface of UPt_3 is still frequently approximated by a single sphere, with a radius $k_F = (3\pi^2 Z^2/V_m)^{1/2} = 1.08$ Å^{-1}, where Z is the valence number (usually taken to be 6, assuming only the three $5f$ electrons of each U atom contribute to the Fermi-surface volume) and V_m is the molar volume, with an effective mass $m^* = 3\hbar^2 \gamma_N/k_B^2 k_F V_m = 180\, m_e$, which gives a Fermi velocity of 6800 m/s. The experiments demonstrate that this is a highly oversimplified approximation.

The dHvA studies provided another useful piece of information: the impurity scattering rate. Indeed, by measuring the field dependence of the amplitude of a particular frequency component (i.e., the usual Dingle-plot analysis), the scattering rate along the associated quasiparticle orbit was obtained. For a sample with residual resistivity $\rho_0 \simeq 0.1\ \mu\Omega$ cm $(J\|c)$, Taillefer *et al.* (1987) deduced mean free paths $\ell_{dHvA} = 1000$, 1500, and 2200 Å for the α, ϵ, and ω orbits in the b-c plane, respectively, or scattering rates $1/\tau_{dHvA} = 5.6$, 3.3, and 2.5 $\times 10^{10}$ s^{-1}.

C. Thermodynamic and transport properties

1. Specific heat

The specific heat of UPt_3 is linear in temperature in the range $0.5 < T < 1.5$ K and given by $C(T) = \gamma_N T$, with $\gamma_N = 0.44 \pm 0.02$ J/(K^2 mol U). The coefficient of the linear term is enormous, two to three orders of magnitude larger than in simple metals, reflecting the huge effective

masses seen in dHvA. A large γ_N is usually taken to be the defining characteristic of the heavy-fermion state. In other heavy-fermion compounds, γ_N ranges from ~ 100 (as in UPd_2Al_3 and URu_2Si_2) to ~ 1000 mJ/(K^2 mol U) (in UBe_{13}). At temperatures above 1.5 K, contributions to $C(T)$ from excitations other than quasiparticles become important, certainly phonons and probably also spin fluctuations. A phonon T^3 term of ~ 0.8 J/(K^4 mol U) was extracted by Frings (1984), corresponding to a Debye temperature of ~ 210 K, comparable to that of pure platinum, 230 K, and in agreement with the value of 217 K derived from sound velocity measurements (see Sec. II.A). In the presence of an applied magnetic field greater than 3 T [i.e., above $H_{c2}(T=0)$], two features are worth mentioning: a large upturn in C/T at very low T, visible below about 100 mK (Brison *et al.*, 1994a), and a peak at 20 T, at the so-called metamagnetic transition (Müller, Joss, and Taillefer, 1989). Although less pronounced, the upturn is also present in zero field, i.e., in the superconducting state. Its origin is not understood (see also Schubert, Strickler, and Andres, 1992).

2. Thermal expansion

In a system with nearly localized quasiparticles, a shortening of the interatomic separation is expected to rapidly decrease the degree of correlation. This is indeed the case in UPt_3, as seen by a number of experiments. The usual measure of the sensitivity of the electronic system to a change in volume is the dimensionless Grüneisen parameter:

$$\Gamma = \frac{V_m}{\gamma_N}\left(\frac{\partial \gamma_N}{\partial V}\right)_T . \tag{7}$$

It has been estimated in two ways. From the pressure dependence of the specific heat below 4 K, Brodale *et al.* (1986) obtain $\partial \ln \gamma_N/\partial P \simeq -24$ Mbar^{-1}, so that $\Gamma = -(1/\kappa_V \gamma_N)(\partial \gamma_N/\partial P)_T \simeq 50$, where κ_V is the bulk compressibility (see Sec. II.A). Alternatively, one can use the linear coefficient of thermal expansion, $\alpha_V = \partial \ln V/\partial T$, and the appropriate Maxwell thermodynamic relation to obtain $\Gamma = (V_m/\kappa_V \gamma_N)(\partial \alpha_V/\partial T)_V$. At low enough temperature that both $C(T)$ and $\alpha_V(T)$ are linear in T, one finds $\Gamma(T \to 0) \simeq 60$ (de Visser, Franse, and Menovsky, 1985), compared to a value of 1–2 in simple metals. This extremely high sensitivity of the average effective mass in UPt_3 to a change in volume has been interpreted as arising from a sensitivity in the magnetic correlations, e.g., spin fluctuations (Brodale *et al.*, 1986; van Dijk, 1994). Given this sensitivity, we expect dramatic effects of pressure on the electronic properties and on superconductivity. These effects will be very anisotropic, since a crystal of UPt_3 expands along the a and b axes upon heating from $T=0$, but contracts along the c axis, at least initially (de Visser, Franse, and Menovsky, 1985).

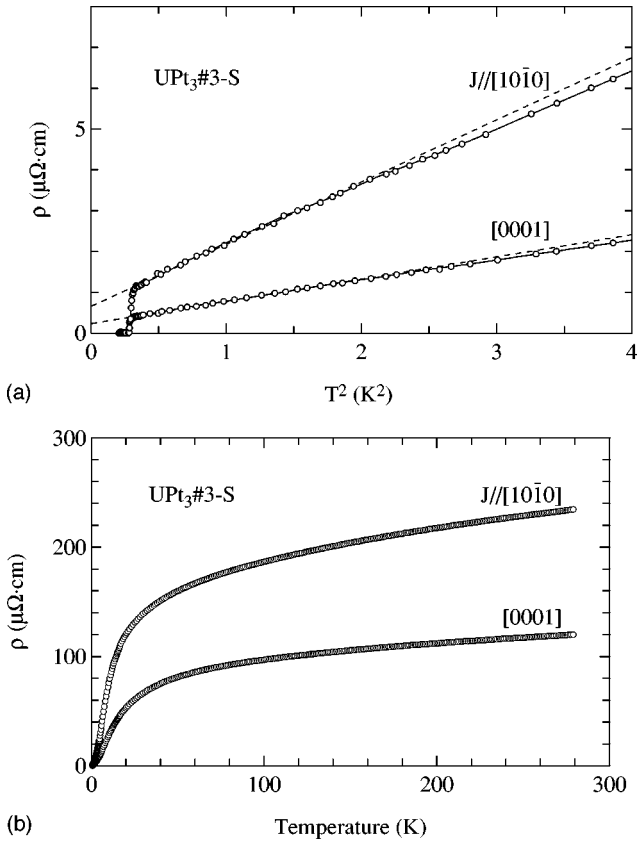

FIG. 6. Temperature dependence of the electrical resistivity of a high-quality single crystal of UPt_3 for current directions parallel ([0001]) and perpendicular to the hexagonal c axis. From Kimura *et al.*, 1995.

3. Charge conduction

The heavy itinerant quasiparticles in UPt_3 can carry charge and heat. This transport is anisotropic, with conduction along the c axis always better than perpendicular to it. Both elastic and inelastic scattering processes are important at temperatures of order 1 K, being roughly of the same magnitude at T_c in high quality crystals.

The electrical resistivity of UPt_3 is shown as a function of temperature up to 300 K in Fig. 6(b), for a current along each of the two high-symmetry directions, $J \| c$ and $J \perp c$. (No difference is seen between $J \| b$ and $J \| a$.) The first noteworthy result is the absence of a peak: $\rho(T)$ never increases with decreasing temperature, as it usually does in heavy-fermion compounds, a feature attributed to the single-impurity Kondo effect. Second, at all temperatures an anisotropy of about 2 is observed, with $\rho_{a,b} \simeq 2\rho_c$. The absolute value of the resistivity at room temperature, if residual impurity scattering can be neglected (as in the best samples), is $\rho_{a,b}(300\ \mathrm{K}) = 230\ \mu\Omega$ cm and $\rho_c(300\ \mathrm{K}) = 130\ \mu\Omega$ cm to within 10% or so (de Visser, Menovsky, and Franse, 1987; Kimura *et al.*, 1995). The low-temperature behavior is shown in Fig. 6(a). It is characterized by a well-defined T^2 law, valid for both directions up to a temperature of about 1.5 K: $\rho(T) = \rho_0 + AT^2$. Most studies on single crystals (e.g., Lussier, Ellman, and Taillefer, 1994;

Kimura *et al.*, 1995; Suderow *et al.*, 1997b; Kycia *et al.*, 1998) obtain a value for the inelastic scattering coefficient in agreement with $A=1.55\pm0.1$ $\mu\Omega$ cm K^{-2} for $J\|a,b$ and $A=0.55\pm0.05$ $\mu\Omega$ cm K^{-2} for $J\|c$, independent of ρ_0. The magnitude of ρ_0 in nominally pure crystals varies by a factor of 10 or so, with the following range of values representative of single crystals used in most investigations so far: $\rho_0=0.6$–6 $\mu\Omega$ cm for $J\|a,b$ and $\rho_0=0.2$–2 $\mu\Omega$ cm for $J\|c$. Since the impurity scattering rate appropriate for transport will be somewhat lower than the scattering rates obtained from dHvA (the latter is more sensitive to small-angle scattering), we estimate roughly that $1/\tau_0\simeq1\times10^{10}$ s^{-1} for $\rho_0=0.1$ $\mu\Omega$ cm along the c axis, corresponding to $l_0\simeq5000$ Å.

In the low-temperature regime (below ~1 K), the anisotropy in the conduction is roughly independent of temperature (Lussier, Ellman, and Taillefer, 1994), and $\sigma_c/\sigma_b=\rho_b/\rho_c\simeq2.6$. The fact that the anisotropy is the same for the elastic and inelastic terms (ρ_0 and A) suggests that it arises mainly from the Fermi velocities rather than from the scattering rates. An evaluation of the square of the Fermi velocity (or mass tensor) over the various sheets of the calculated Fermi surface gives an anisotropy $\langle v_c^2\rangle/\langle v_b^2\rangle=2.1$ (Norman, 1996). Note that the mass enhancement, neglected in this ratio, could account for the additional anisotropy.

The inelastic electron-electron scattering is enormously stronger (by three or four orders of magnitude) in heavy-fermion materials than it is in normal metals. Like the specific heat, it is governed by the density of states at the Fermi energy and a simple relation $\gamma_N\sim\sqrt{A}$ is fairly well obeyed across the family of compounds (Kadowaki and Woods, 1986). One way to investigate the effect is to apply pressure, thereby reducing the quasiparticle bandwidth. Hydrostatic pressure has little effect on ρ_0 but it decreases A at the rate $d\ln A/dP\simeq-40$ $Mbar^{-1}$ (Willis *et al.*, 1985; Ponchet *et al.*, 1986), roughly twice the corresponding rate for γ_N. Note, however, that the response is highly anisotropic: uniaxial stress applied along the c axis causes A to increase (Taillefer *et al.*, 1992).

A magnetic field lower than 10 T has no effect on A, but it causes an increase in ρ_0. This positive magnetoresistance is linear in field and depends on whether the field is parallel or perpendicular to the c axis (de Visser, Menovsky, and Franse, 1987). For $J\|c$ and $H<10$ T, one has $\rho(T,H)=\rho_0+aH+AT^2$ with $a=6.8$ $(0.25)\times10^{-2}$ $\mu\Omega$ cm T^{-1} for $H\perp c$ $(H\|c)$ (Taillefer, Flouquet, and Joss, 1988).

4. Heat conduction

Thermal conductivity is a tensor that relates the heat current $\vec{J}_Q$ to the associated temperature gradient ∇T: $J_{Q\alpha}=-\Sigma_\beta\kappa_{\alpha\beta}\nabla_\beta T$. In a hexagonal crystal the tensor is diagonal and only two independent quantities are involved. In simple kinetic theory assuming an isotropic medium, the thermal conductivity is given by $\kappa=cv\ell/3$, where $c=c(T)$ is the volume specific heat, v is the speed, and ℓ the mean free path of the carriers. This expression applies equally to electrons and phonons. For normal metals at low temperatures, the electronic conduction is limited by impurity scattering, and κ is linear in temperature since $c(T)=\gamma_N T$, so $\kappa_N=\frac{1}{3}\gamma_N v_F\ell_0 T$.

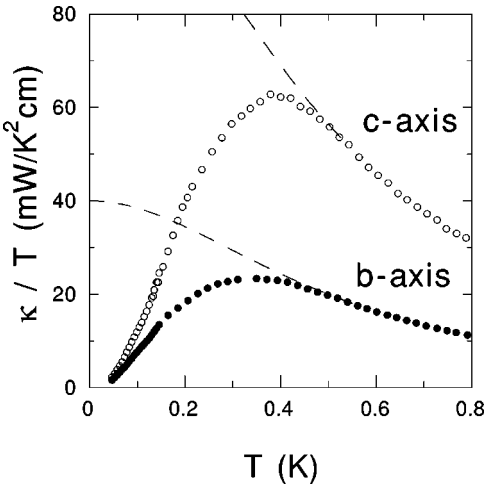

FIG. 7. Thermal conductivity κ_i as a function of temperature, plotted as κ/T vs T for heat currents along the b and c axes. The normal-state thermal conductivity below T_c (dashed lines) is obtained by extrapolating the good fit $\kappa_{N,i}/T=(a_i+b_iT^2)^{-1}$ found for $0.5<T<0.8$ K. From Lussier, Ellman, and Taillefer, 1996.

The thermal conductivity of UPt_3 below 1 K is shown in Fig. 7 for both high-symmetry directions. The normal state is characterized by strong inelastic scattering and an anisotropy of $\kappa_c/\kappa_b\simeq2.7$: $\kappa_N(T)/T=1/(a+bT^2)$, with $a=0.25$ (0.09) m K^2 W^{-1} and $b=1.0$ (0.37) m W^{-1} for $J_Q\|b$ $(J_Q\|c)$ (Lussier, Ellman, and Taillefer, 1994, 1996). Quasiparticle scattering gives rise to the T^2 term, which (in these crystals) grows to be as large as the elastic impurity component at T_c (i.e., $bT_c^2\simeq a$). It is also seen that the anisotropy is independent of temperature in the normal state.

Therefore the picture that emerges for the normal state is remarkably simple: UPt_3 is a slightly anisotropic but three-dimensional Fermi liquid with strong electron-electron interactions. The anisotropy is the same for both particle and energy transport, and for both impurity and electron scattering:

$$\frac{\kappa_c}{\kappa_b}\simeq\frac{\sigma_c}{\sigma_b}\simeq2.7 \tag{8}$$

for $T<0.8$ K (Lussier, Ellman, and Taillefer, 1994). It is tempting to conclude from this that most of the anisotropy comes from the anisotropy in the Fermi velocities and that all scattering is s wave, i.e., that the transport relaxation times $\tau_{elastic}$ and $\tau_{inelastic}$ are almost isotropic. (For a recent discussion of anisotropies, see Kycia *et al.*, 1998.)

The Wiedemann-Franz law is obeyed at very low temperature, i.e., the Lorenz number $L=\kappa/\sigma T$ reaches its expected limiting value: $\rho_0/a=L_0=2.44\times10^{-8}$ W Ω K^{-2} (Lussier, Ellman, and Taillefer, 1994; Suderow *et al.*, 1997b). Of course, $L(T)$ is strongly tem-

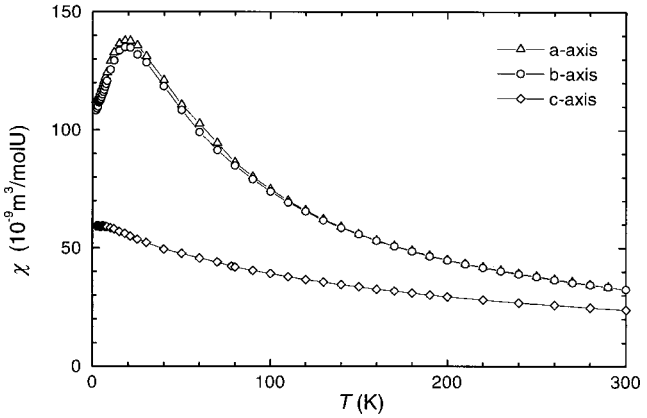

FIG. 8. Uniform magnetic susceptibility as a function of temperature for fields along the three high-symmetry directions. Equality of the linear susceptibility along the a and b axes is a general consequence of hexagonal symmetry. From Frings *et al.*, 1983.

perature dependent, as a result of the inelastic scattering, and $L(0.8\,\mathrm{K})=0.75\,L_0$.

The electrons responsible for the large γ_N are also the carriers of heat. This can be confirmed using the known Fermi velocity (averaged over the various orbits in the b-c plane), $v_{bc}\simeq 5000$ m/s, combined with $\gamma_N=0.44\,\mathrm{J\,K^{-2}\,mol^{-1}}$ and $l_{bc}\simeq 2000$ Å (for $\rho_0=0.23\ \mu\Omega$ cm), giving an estimate of the thermal conductivity due to the quasiparticles: $\kappa_N/T=\frac{1}{3}\gamma v_{bc} l_{bc}=3.5\,\mathrm{W\,K^{-2}\,m^{-1}}$ at $T<0.1$ K. The measured values (in the normal state) are $\kappa_N/T=L_0/\rho_0=4.0$ (10.6) $\mathrm{W\,K^{-2}\,m^{-1}}$, for $J_Q \| b$ ($J_Q \| c$), reasonably close to our rough estimate. This is further confirmation that the Fermi-liquid picture of heavy and itinerant quasiparticles is quantitatively consistent in UPt_3.

D. Magnetic properties

The spin degrees of freedom in strongly correlated electron systems are at the heart of their subtle and exotic low-temperature phenomena. It is interesting that both high-T_c superconductors and heavy-fermion superconductors have low-lying magnetic fluctuations with antiferromagnetic correlations and a proximity to antiferromagnetic order.

1. Uniform magnetic susceptibility

The ac susceptibility of UPt_3 was measured by Frings *et al.* (1983) for fields parallel and perpendicular to the c axis, as shown in Fig. 8. The Knight shift of nuclear magnetic resonance (NMR) frequencies also gives a measure of the susceptibility $\chi(T)$; Tou *et al.* (1996) have reproduced the temperature dependence and anisotropy of χ with ^{195}Pt NMR. The main features of χ are (1) a large value at $T=0$, (2) a weak temperature dependence at low temperature ($T<2$ K), (3) a substantial anisotropy (with the larger response for field in the basal plane), and (4) a peak in χ_{xx} at ~ 20 K.

We can understand this complex phenomenology from the band calculations. As we have seen in Sec. II.B.1, the single-particle states near the Fermi surface are uranium $5f$ electrons in a $j=5/2$ state which are split by the crystal field into three doublets: $j_z=\pm 5/2$, $j_z=\pm 3/2$, and $j_z=\pm 1/2$. The bands constructed from these states all cross the Fermi energy. If we now apply a magnetic field, there will be both a Pauli (intraband) χ_P and a Van Vleck (interband) χ_{VV} contribution to the susceptibility. The former is of order $(g_{eff}\mu_B)^2 N(\varepsilon_F)$ for any band, while the latter is of order $(g_{eff}\mu_B)^2/E_{cf}$ for a pair of bands. Here g_{eff} is an effective g factor for the coupling of the field to the total angular momentum of the band or bands involved, and E_{cf} is a characteristic crystal-field splitting. χ_{VV} comes from a sum over *pairs* of bands [see Eq. (9) below], while χ_P is a sum over single bands. In this highly degenerate multi-f-band metal with $1/N(\varepsilon_F)\sim E_{cf}$ we expect the Van Vleck part of the susceptibility to be comparable to or larger than the Pauli part.

The anisotropy of the two parts is also important. The Van Vleck susceptibility is given by

$$\chi_{ii}=2n\mu_B^2\sum_{\alpha,\beta}\frac{|\langle\alpha|\vec{L}_i+2\vec{S}_i|\beta\rangle|^2}{E_\beta-E_\alpha}f_\alpha(1-f_\beta), \tag{9}$$

where f_α, f_β, E_α, E_β are occupation factors and energies of the states α and β. n is the density of U atoms. If $\vec{H}$ is along the c axis, then $|\langle\alpha|\vec{L}_i+2\vec{S}_i|\beta\rangle|^2=(36/49)j_z^2\delta_{\alpha,\beta}$. In the approximation that states of different j_z do not mix (negligible intersite interactions), the perturbation introduced by $\vec{H}$ is diagonal, and the occupation factors then imply that the Van Vleck susceptibility is zero for this direction. In actual fact, because of the itinerant nature of the f electrons, the mixing of states of different j_z will give some Van Vleck contribution for this direction of the field. If $\vec{H}$ is in the x direction, the corresponding expression for the square of the matrix element is $(36/49)(5/2-j_z)(5/2+j_z+1)$ if the states α and β differ by one unit of j_z and is zero otherwise. The Van Vleck susceptibility comes from four distinct pairs of states: $(j_z=-5/2,-3/2)$, $(-3/2,-1/2)$, (1/2,3/2), and (3/2,5/2), whenever one of the pair is occupied and the other unoccupied. The Pauli contribution to χ_{xx}, on the other hand, comes only from the pair $(-1/2,1/2)$ when this state is occupied. Again, these statements are made in the approximation that intersite mixing of the states is small.

Summing up these considerations, we expect that χ_{zz} will be dominated by the Pauli contribution. We expect that χ_{xx} will be dominated by the Van Vleck contribution and that it will be considerably larger than χ_{zz}. Note that the interactions enhance the susceptibility and that this is expected to affect Pauli and Van Vleck terms alike.

This simple picture is consistent with the data in Fig. 8. A Pauli term is expected to behave as a constant for $k_BT<\varepsilon_F$ and then to cross over to the $1/T$ Curie form. Here ε_F is the effective Fermi temperature. Since it is a measure of the density of states, it should be roughly

proportional to C/T. The Van Vleck term could have a more complex behavior because it depends on various pairwise joint densities of states. Figure 8 shows that χ_{xx} is considerably larger than χ_{zz} at all temperatures, in accord with the expectation that Van Vleck terms tend to dominate the total. Furthermore, the expected Pauli-like dependence on temperature is seen for χ_{zz}, while the temperature dependence of χ_{xx} is anomalous. This is consistent with the hypothesis that χ_{xx} and χ_{zz} come from different sets of transitions.

2. Magnetic correlations

The magnetic fluctuation spectrum of UPt_3 was investigated by Aeppli and his collaborators (Aeppli, Bucher, Broholm, *et al.*, 1988; Aeppli, Bucher, Goldman, *et al.*, 1988) using inelastic neutron scattering. The basic features are as follows: at a gross level, the spectrum at low temperature ($\sim$1 K) is that of a local magnetic moment of $\sim 2\mu_B$ on each U site fluctuating at a characteristic energy of the order of 10 meV. On a finer scale, moments on nearest-neighbor sites (in adjacent planes separated by c) become correlated antiferromagnetically below about 20 K. The appearance of these correlations coincides roughly with the peak in χ_{xx}. These antiferromagnetic correlations are at $\vec{Q}=(0,0,1)$ and they peak in energy at 5 meV (Aeppli, Bucher, Goldman, *et al.*, 1988). At even lower energies, the magnetic behavior of UPt_3 is dominated by a second type of antiferromagnetic correlation, with characteristic energy 0.3 meV and wave vector $\vec{Q}=(\pm\frac{1}{2},0,1)$, and associated effective moment of $\sim 0.1\mu_B$ (Broholm, 1989). This corresponds to antiferromagnetic alignment of neighboring sites within the same a-b plane, along the a^* (or b) axis. The temperature dependence of the inelastic scattering at this wave vector is shown in Fig. 9. Although the role of these fluctuations in either the formation of the heavy-fermion state (mechanism for mass renormalization) or the formation of the superconducting state (pairing mechanism) is not established, it is likely to be of fundamental importance, as is certainly the case for ^{3}He and probably also for the high-T_c cuprates.

One might ask how this picture of fairly localized moments ties in with the fact that at low temperature UPt_3 seems to behave very much as a Fermi liquid. In other words, where are the magnetic fluctuations that must inevitably result from the itinerant quasiparticles carrying spin? They were shown by Bernhoeft and Lonzarich (1995) to exist as long-wavelength magnetic fluctuations ($0.1<q<0.3$ Å) at low temperature ($\sim$1 K) with a dispersive relaxation rate characteristic of a Fermi liquid. This "slow" component of the fluctuation spectrum coexists with the "fast" contribution described above, and it accounts for approximately 20% of the total static susceptibility. It is similar to the well-understood response of nearly or weakly ferromagnetic d transition-metal systems, but further complicated by the strong spin-orbit interaction.

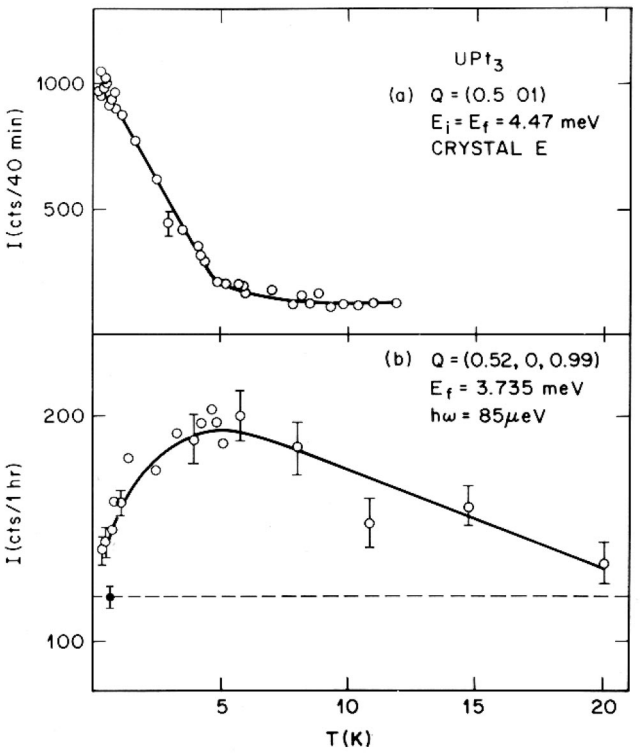

FIG. 9. Temperature dependence of neutron-scattering intensity below 20 K for (a) the elastic peak at $\vec{Q}=(\frac{1}{2},0,1)$ and (b) the inelastic scattering at $\vec{Q}=(0.52,0,0.99)$ for $\hbar\omega=85$ μeV. From Aeppli *et al.*, 1988.

3. Antiferromagnetic order

When the temperature is lowered below about $T_N \simeq 5$ K, an elastic component of the magnetic correlations at $\vec{Q}=(\pm\frac{1}{2},0,1)$ appears, i.e., static antiferromagnetic order sets in, with a very small staggered moment of order $0.01\mu_B$/U atom. This ordering was first noticed in muon spin relaxation measurements by Heffner *et al.* (1989) and was soon confirmed by neutron scattering (Aeppli, Bucher, Broholm, *et al.*, 1988), which established the magnetic structure, shown in Fig. 10. The magnetic order is collinear and commensurate with the crystal lattice, with a moment aligned in the basal plane ($\vec{M}_S \| a^*$) and a propagation vector $\vec{Q}=(\pm\frac{1}{2},0,1)$ parallel to the moment. It doubles the unit cell along a^* and it corresponds to antiferromagnetic coupling within planes and ferromagnetic coupling between planes. The temperature dependence of the scattering intensity (proportional to $\vec{M}_S^2$) is shown in the upper part of Fig. 9. It is linear all the way between T_c and T_N, i.e., $|\vec{M}_S| \sim (T_N - T)^{1/2}$.

All aspects of this ordering were reproduced by later neutron studies on a different crystal (Hayden *et al.*, 1992; Lussier, Taillefer, *et al.*, 1996) and by magnetic x-ray scattering (Isaacs *et al.*, 1995). The moment grows to a maximum magnitude of $0.02-0.03\mu_B$/U atom and the Néel temperature is between 5 and 6 K. On the other hand, in a subsequent muon spin relaxation (μSR) study, Dalmas de Réotier *et al.* (1995) detected no signa-

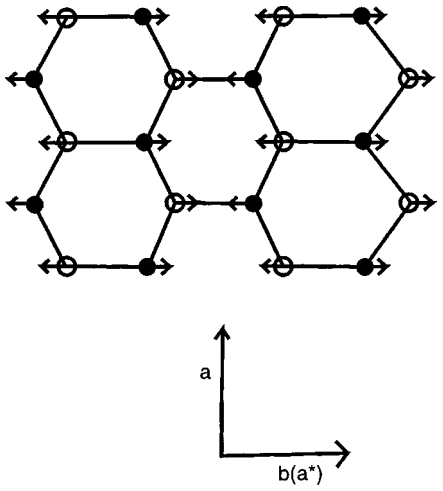

FIG. 10. Configuration of ordered magnetic moments (drawn on the U site) in the antiferromagnetic state below 5 K, as determined by neutron scattering. The magnetic moment lies in the basal plane, parallel to the a^* direction.

ture of the ordering in a high quality annealed single crystal of UPt_3. They attribute the absence of a μSR anomaly to the fact that the implanted muon may well sit in a high-symmetry site in the lattice where the total field resulting from the antiferromagnetically arranged moments would be canceled. In the presence of structural deformations (in crystals of lower quality), however, this cancellation would not be perfect and a small μSR signal could appear (as seen by Luke *et al.*, 1993; see also Yaouanc *et al.*, 2000).

Several observations might suggest an extrinsic origin. For example, addition of a few percent Pd (see de Visser *et al.*, 1997, and references therein) or Th (see Aeppli *et al.*, 1988a, and references therein) causes a large ordered moment ($\sim 0.5\mu_B$/U atom) to appear. The order in pure UPt_3 never seems to develop over a long spatial range: the correlation lengths are invariably of order 300 Å (Broholm, 1989; Isaacs *et al.*, 1995). On the other hand, an identical order has been seen in three distinct crystals (and experiments). Furthermore, Isaacs *et al.* (1995) showed that a heat treatment which strongly modifies the shape of the superconducting transition anomaly in the specific heat has no effect on T_N or $\vec{M}_S$.

One possibility is that the order is not truly static, but only appears so as seen by neutrons. This would explain the absence of an anomaly in all physical properties investigated so far (although the small size of the moment may by itself preclude detection). In particular, no sign of magnetic ordering was seen in the NMR Knight shift (Tou *et al.*, 1996), the specific heat (Fisher *et al.*, 1991), or the magnetization. On the other hand, the experimental resolution of the μSR measurements provides a lower limit of approximately 10 μs for the time scale on which the order persists.

Even if it is intrinsic (and nearly static), as we believe it is, the origin of the small-moment order in UPt_3 is a puzzle, as are most of its properties: Why no true long-range order? Why no domain selection by a magnetic field (Lussier, Taillefer, *et al.*, 1996)? Why a mean-field behavior in temperature but not in pressure (Hayden *et al.*, 1992), etc.? Somewhat similar phenomena are encountered in other heavy-fermion compounds, and a number of authors have attempted to explain the origin of small moments in these systems. We shall not enter into these attempts here (see, for example, Buyers, 1996), but simply take the antiferromagnetic order as given and ask later what its role might be in shaping the superconducting phase diagram.

E. Sample quality

UPt_3 is an intermetallic binary compound which solidifies congruently from the liquid phase at 1700 °C. Depending on the cooling procedure, the material will solidify into a polycrystal or a single crystal. Most recent research has been done on single crystals. These come in two varieties: whiskers and bulk. Whiskers are small needlelike crystals with their length along the hexagonal c axis. They grow in two distinct ways: spontaneously from the melt upon cooling, at the surface of a boule (Menovsky, Franse, and Moleman, 1984), and from a bismuth flux (Fisk and Remeika, 1989). Whiskers are used only rarely because of their small size (typical length <1 mm, typical section $<5000\ \mu m^2$) and their imposed geometry. In addition, there is the complicating factor of flux inclusion in the flux-grown whiskers and the uncontrolled nature of growth in the other type of whisker, leading to widely varying quality. Nevertheless, the longest electronic mean free paths have been found in whiskers, which can have RRR values of up to 3000. (RRR is the residual resistivity ratio, defined as the ratio of the electrical resistance at 300 K to the electrical resistance extrapolated to 0 K.) Thus they have proven to be useful in certain cases, such as in Fermi-surface studies, which depend strongly on $\omega_c\tau$ (Taillefer, Flouquet, and Joss, 1988; Julian, Teunissen, and Wiegers, 1992). They can also have a crystalline structure of extremely high integrity, making them ideal for detailed structure studies, for example, those of Ellman *et al.* (1997). They may also prove to be appropriate for experiments depending on good surface quality, such as tunnel junctions.

The bulk single crystals have been grown by the usual techniques of unidirectional solidification (for a review see, for example, Abell, 1989): the Czochralski pulling method (with either rf induction heating or arc melting), the technique of vertical float zoning (typically with electron-beam heating), or horizontal zoning on a water-cooled crucible (which produces large-grained polycrystalline ingots out of which single crystals can be cut). These techniques have been used by a number of groups around the world.

One advantage of the U-Pt system is the low vapor pressure of both constituents at (or below) 1700 °C. This has meant negligible loss of either component during growth, even when performed in vacuum, allowing the use of electron-beam heating, and long heat treatments in ultrahigh vacuum at fairly high temperatures.

As long as care is taken to work with the purest starting materials (99.97 at. % U, with RRR$\simeq$30, and 99.995 at. % Pt, RRR$\simeq$2000 after annealing), and in a clean environment (typically provided by ultrahigh vacuum technology), all of the above-mentioned techniques can produce high-purity crystals.

Two kinds of defects will exist to some extent in any crystal of UPt_3: chemical (substitutional or interstitial trace impurities, from starting materials and through reaction during growth or annealing), and structural (stacking faults, dislocations, point disorder, low-angle grain boundaries and mosaic, inhomogeneous stoichiometry, built-in strain). Both of these affect the electronic properties and in particular the superconducting properties.

The RRR$\equiv R(300\,\mathrm{K})/R_0$ is probably the simplest and most reliable measure of overall sample quality. R_0 is obtained from fitting the low-temperature resistance to R_0+AT^2 between T_c and 1.5 K. Because this ratio is anisotropic, one needs to specify the current direction in order to make meaningful comparisons. As an indication of current standards, the best single crystals produced by a number of groups have RRR$>$500 or ρ_0 $<0.25\ \mu\Omega$ cm (for $J\|c$). We use this as our definition of a "high quality sample." The highest RRR in a bulk crystal known to us is 1280 (Kycia *et al.*, 1998).

Other common measures of sample quality are the value of T_c (the upper transition) and the width δT_c of that transition, as measured by resistivity, susceptibility, or specific heat. High-quality samples will have a resistive transition with $T_c>530$ mK and $\delta T_c<20$ mK. [The ideal maximum value of T_c is estimated to be 563 mK (Kycia *et al.*, 1998).] The deliberate addition of impurities that go on the U site, such as rare-earth elements, Th, Y, and Zr, or on the Pt site, such as Pd, rapidly suppresses T_c: in most cases, superconductivity is destroyed by an addition of less than 1% (Vorenkamp *et al.*, 1993; Dalichaouch *et al.*, 1995). As a rough indication of the impact of impurity/defect scattering on superconductivity, T_c is decreased to half its maximum value when the mean free path is made to drop to a value roughly equal to the coherence length $\xi\simeq150$ Å (Dalichaouch *et al.*, 1995; Kycia *et al.*, 1998).

The improving effect of annealing on the RRR has been known for a long time (de Visser, Menovsky, and Franse, 1987). Recently, Kycia *et al.* (1998) have carried out a careful study in very pure crystals and show that the RRR can be tripled by lowering the annealing temperature from 1250 to 900 °C. Similarly, annealing is typically needed for producing two distinct well-split superconducting transitions in the specific heat (see Sec. V.A.1; Midgley *et al.*, 1993; Isaacs *et al.*, 1995), and the lower the annealing temperature the better (Brison *et al.*, 1994b). It now appears that the factor that limits the RRR in most high-quality samples is structural imperfection (sensitive to some extent to heat treatment) rather than chemical impurities.

The tremendous sensitivity of the specific heat near T_c to annealing is perhaps not all that surprising: given the huge Grüneisen parameter, any deformation of the lattice structure would be expected to have a large impact on the electronic properties, at least locally. Globally, T_c is rapidly suppressed by stress (Willis *et al.*, 1985; Trappmann, Löhneysen, and Taillefer, 1991; Greiter, Lonzarich, and Taillefer, 1992). Thus stacking faults and other defects that produce strain fields could easily broaden the transition seen in specific heat.

An x-ray and TEM study by Aronson *et al.* (1993) suggests that stacking faults may be the predominant form of structural disorder in some crystals of UPt_3. The stacking sequence becomes ABACABACABAC, which corresponds to a double hexagonal structure. This would have a strong effect on the magnetic susceptibility. In particular, the atoms in the A layer of the double hexagonal sequence are in an environment that has local cubic symmetry, and therefore should have an isotropic susceptibility. A study correlating structural disorder and susceptibility would be illuminating.

These considerations on sample quality point to the need for careful characterization of UPt_3 crystals. This is now being done more and more systematically, and single crystals of UPt_3 can be (and have been) produced with a high degree of crystalline perfection, as can be seen from recent x-ray studies on a whisker (Ellman *et al.*, 1997) and on a bulk crystal (Kycia *et al.*, 1995), and with transport mean free paths approaching 1 μm. Of all the heavy-fermion superconductors, this is by far the one for which sample quality is the highest. Nevertheless, it is pertinent to ask: are any of the interesting properties of this material extrinsic, i.e., the result of defects and ultimately absent in a perfect crystal? In particular, some authors have wondered in the past about the intrinsic nature of the double superconducting transition, the small antiferromagnetic order, and the incommensurate lattice distortion. The situation today allows us to say with some confidence that the first is intrinsic (see Sec. V.A.1), the second probably so (see Sec. II.D.3), and the third probably not (see Sec. II.A). In well-annealed high-purity crystals, several groups have now observed a well-resolved double superconducting transition in specific heat and antiferromagnetic order with neutrons on one and the same crystal, with the very same characteristics (Hayden *et al.*, 1992; Brison *et al.*, 1994a; Dalmas de Réotier *et al.*, 1995; Isaacs *et al.*, 1995). For those samples (or any other), no lattice modulation has ever been seen by x-ray or neutron scattering.

III. SUPERCONDUCTING STATE—THE FRAMEWORK

A. Classification of superconducting states

The great interest in UPt_3 arises from the possibility of unconventional superconductivity, i.e., that the ground state breaks lattice symmetry as well as gauge symmetry. The phase diagram alone shows unambiguously that the superconductivity of UPt_3 has unconventional symmetry. The s-wave state is unique, so at least two of the three phases of UPt_3 must have novel symmetry. The discovery of this phenomenon is analogous to, and is as fundamental as, the discovery of antiferro-

magnetism, which, unlike the ferromagnetism known from ancient times, breaks translation symmetry. The comparison can be carried further. Antiferromagnetism vastly increases the types of magnetism that can occur in nature. Unconventional superconductivity vastly increases the types of superconductivity beyond isotropic s wave. Furthermore, it is almost certainly caused by a new mechanism, not the electron-phonon interaction that causes conventional s-wave superconductivity, so the study of the phenomenon carries us to the deepest waters of correlated electron physics.

The analysis of symmetry limits and defines the possible superconducting states, allowing us to construct a framework for the interpretation of experimental data. Before plunging into the technical details, we can give the overall scheme. The classification is done by looking at the form of the Cooper-pair wave function, just as one would classify states in atomic physics by orbital angular momentum and spin. This part of the classification is dictated by symmetry, namely, the way the wave function changes when rotated or reflected by the operations that leave the crystal unchanged, i.e., the point group. The analog of the point group in atomic physics is the rotation group. There is also an analog to the principal quantum number of atomic wave functions, as we shall see. The principal quantum number is not related to symmetry. In the atom, if we neglect spin-orbit coupling (the $\vec{L}\cdot\vec{S}$ term), the states may be classified by $\vec{L}$ and $\vec{S}$ separately, each being conserved. Spin-orbit coupling breaks down this classification, and only the total angular momentum $\vec{J}=\vec{L}+\vec{S}$ and parity are still conserved. This carries over to the Cooper-pair case. The Cooper-pair case is actually simpler than the atomic physics case: the point group is finite, and therefore the number of representations is finite.

The formal analysis begins by writing down the Hamiltonian for superconductivity. This is

$$\begin{aligned}\mathcal{H}-\mu\mathcal{N}=&\sum_{n\vec{k}s}\varepsilon_{n\vec{k}s}a^{\dagger}_{n\vec{k}s}a_{n\vec{k}s}\\&+\sum_{n\vec{k}n'\vec{k}'}\sum_{s_1s_2s_3s_4}V_{s_1s_2s_3s_4}(n\vec{k},n'\vec{k}')\\&\times a^{\dagger}_{n,-\vec{k}s_1}a^{\dagger}_{n\vec{k}s_2}a_{n'\vec{k}'s_3}a_{n',-\vec{k}'s_4},\end{aligned}\tag{10}$$

where n and n' are band indices which keep track of the crystal field and even-odd splittings, $\varepsilon_{n\vec{k}s}$ are the band energies relative to the chemical potential μ, $\vec{k}$ and $\vec{k}'$ are crystal momenta, and s and s' are two-valued variables which represent the "pseudospin." They are defined by adiabatic continuation. The spin-orbit coupling is turned on gradually and the spin-up energy eigenstate evolves into the $s=+$ energy eigenstate and the spin-down energy eigenstate evolves into the $s=-$ energy eigenstate. In UPt_3, we can identify these indices in a less abstract fashion. At the Γ point, j_z is a good quantum number and the states j_z and $-j_z$ are degenerate. These states may be split by an infinitesimal magnetic field in the z direction into the $j_z>0$ state and the $j_z<0$ state. We then identify the $s=+$ band as the one containing the $j_z>0$ state at the Γ point and $s=-$ as the band containing the $j_z<0$ state. In the absence of a field, the energy is independent of s throughout the band. The energies $\varepsilon_{n\vec{k}+}=\varepsilon_{n,-\vec{k}+}=\varepsilon_{n\vec{k}-}=\varepsilon_{n,-\vec{k}-}$ are in fact fourfold degenerate because of time reversal and parity symmetry (Anderson, 1984).

The mean-field treatment of the Hamiltonian of Eq. (10) proceeds by defining the gap function

$$\begin{aligned}\Delta_{ss'}(n\vec{k})=&-\sum_{n'\vec{k}'s_3s_4}V_{s'ss_3s_4}(n\vec{k},n'\vec{k}')\\&\times\langle a_{n'\vec{k}'s_3}a_{n',-\vec{k}'s_4}\rangle\end{aligned}\tag{11}$$

and neglecting its fluctuations. This leads to the equation for the critical temperature:

$$\begin{aligned}v\Delta_{s_1s_2}(n\vec{k})=&-\sum_{n'\vec{k}'s_3s_4}V_{s_2s_1s_3s_4}(n\vec{k},n'\vec{k}')\\&\times\Delta_{s_3s_4}(n'\vec{k}')\,\delta(\varepsilon_{n'\vec{k}'}),\end{aligned}\tag{12}$$

where v is related to T_c by $k_BT_c=1.14\omega_ce^{-1/v}$. ω_c is the cutoff for the interaction potential $\hat{V}$. It is Eq. (12), a linear integral eigenvalue equation, which is taken as the basis for discussion of the symmetry of the gap function. From it we draw the following conclusions:

(1) the eigenfunctions of the the equation transform according to a definite representation of the symmetry group of V;
(2) if the representation is multidimensional, then the order parameter has more than one component;
(3) the critical temperature is a monotonically increasing function of the eigenvalue, hence the eigenfunction belonging to the highest eigenvalue is realized in the system;
(4) generically, there are no symmetries in the set of band indices n, so the eigenvectors will generally have nonzero components in all "directions" in this space, and superconductivity occurs simultaneously in all bands, even in bands where the interaction is repulsive. The relative magnitude of coefficients of V belonging to different bands may be very different. The gap may be much smaller in some bands than others, and can even change sign.

Since UPt_3 has many disconnected pieces in its Fermi surface, these possibilities are difficult to analyze even from a phenomenological point of view.

It is convenient to express the gap function in a different form:

$$\Delta_{ss'}(n\vec{k})=i[\psi(n\vec{k})+\vec{d}(n\vec{k})\cdot\vec{\sigma}]\sigma_y.\tag{13}$$

Here $\vec{\sigma}_i$ are the Pauli matrices. The definition in Eq. (11) and the fermion anticommutation relations give $\psi(n\vec{k})=\psi(n,-\vec{k})$ and $\vec{d}(n\vec{k})=-\vec{d}(n,-\vec{k})$.

A state in which $\vec{d}(n\vec{k})=0$ is said to be a "singlet" state, and a state in which $\psi(n\vec{k})=0$ is said to be a "triplet" state. This misleading, but standard, terminology is

borrowed from the theory of ^{3}He. It does not reflect anything about actual degeneracies for our case. In a singlet state, each electron is paired with its time-reversed partner with a pairing amplitude $\psi(n\vec{k})$ which may depend on the particular position on the Fermi surface. The Cooper-pair wave function has even parity in real space. For the triplet states, the parity is odd. However, the physical interpretation of $\vec{d}(n\vec{k})$ is in general somewhat complicated. If $\vec{d}(n\vec{k})=[0,0,d_z(n\vec{k})]$, then only time-reversed states are paired, but with the other relative sign as compared with the singlet state. Take a case in which the states at the Fermi surface of band n are pure $\pm j_z$ states. Then if $\vec{d}(n\vec{k})$ is in the z direction, $|j_z,\vec{k}\rangle$ is paired only with $|-j_z,-\vec{k}\rangle$. When $\vec{d}(n\vec{k})$ has components in the x or y directions, then there is also a pairing amplitude between $|j_z,\vec{k}\rangle$ and $|j_z,-\vec{k}\rangle$. The azimuthal angle of $\vec{d}(n\vec{k})$ in the x-y plane determines the phase of this amplitude relative to the $|j_z,\vec{k}\rangle, |-j_z,-\vec{k}\rangle$ amplitude. We see that the $\vec{d}(n\vec{k})$ vector is a rather abstract quantity, useful more for its formal properties than as a physical indicator. It is important to note that $\vec{d}(n\vec{k})$ does *not* represent the direction of zero spin projection, as in ^{3}He, or of zero total angular momentum projection of the atomic wave functions. The band energies are much greater than the gap energies, so the eigenstates at a given $\vec{k}$ are determined by the starting crystal Hamiltonian while the direction of $\vec{d}(n\vec{k})$ represents the values of the pairing coefficients in the three-dimensional triplet part of the four-dimensional residual degeneracy space of the crystal Hamiltonian.

The symmetry group of the Hamiltonian is the space group of UPt_3 ($P6_3/mmc$). Usually it is assumed that the Cooper pair has zero center-of-mass momentum. When this is the case, the translation group may be ignored. We shall discuss theories in which nonzero momentum is postulated in Sec. III D, but here restrict ourselves to the zero-momentum case. Then only the point group D_{6h} is relevant. It contains 24 operations, 12 proper rotations $\mathcal{R}_i$, and the inversion $\mathcal{I}$ which commutes with all the operations of the group. There are six representations of the pure rotation group D_6 obtained by dividing out the (normal) inversion subgroup. A_1, A_2, B_1, and B_2 are one dimensional, while E_1 and E_2 are two dimensional, so that the functions belonging to them come in degenerate pairs. Then we add back in the transformation property under $\mathcal{I}$. This is either even or odd, indicated by the subscript g ("gerade") for even parity or u ("ungerade") for odd parity, giving A_{1g} and A_{1u}, and so on for all the representations.

The number of eigenfunctions of Eq. (12) is infinite. Since the number of representations is very much finite, each representation owns many eigenfunctions. If we were to label these within one representation, the label would be analogous to the principal quantum number, as mentioned above. Only one function, or one pair of functions, has the highest eigenvalue and is the gap function (or functions) chosen by the system.

Two further characteristics of special states are best defined here for future reference. A *unitary state* is a triplet state for which $\vec{d}\times\vec{d}^*=0$. A state that breaks time-reversal symmetry is one for which $\Delta^*\neq e^{i\phi}\Delta$, where $e^{i\phi}$ is a phase (which may be removed by a gauge transformation).

The framework based only on symmetry sets strong constraints on theories of superconducting order in UPt_3: any candidate order parameter should be drawn from a single representation of D_{6h}. Because it has seemed difficult to explain all or some experiments within this framework, a number of proposals for the superconducting state of UPt_3 have been made which are outside it.

If spin-orbit coupling were negligible, then the symmetry group would be $D_{6h}\times SU(2)$. In addition to the operations already mentioned, which would act only on the orbital degrees of freedom ($\vec{k}$), we would have a three-dimensional rotation group acting only on the spin degrees of freedom (s). In particular, the $\vec{d}$ vector would be free to rotate relative to the crystal axes. Since the expectation value of the spin-orbit coupling term in uranium wave functions is of the order of 1 eV [incorporated into $\epsilon_{n\vec{k}s}$ in Eq. (11)], it is obvious that it cannot be neglected in the wave functions. On the other hand, the role that this coupling plays in the pairing interaction $V_{s's s_3 s_4}(n\vec{k},n'\vec{k}')$ in Eq. (10) is less clear. This has not been investigated, but it seems unlikely that the symmetry of V would be higher than that of the crystal. However, if one assumes that it can be neglected, there are representations that are one or two dimensional in the space group, but three dimensional (spin 1) in the spin rotation group (see Sec. III.D.2).

A further interesting possibility is that two different representations are nearly degenerate, in the sense that the eigenvalues v in Eq. (12) corresponding to the two representations are nearly the same. To the extent that weak-coupling theory is valid, so that the exponential relation between T_c and v holds with $v\ll 1$, even a small difference in eigenvalues leads to a large difference in critical temperatures. This picture is not ruled out by symmetry, of course, but raises questions about tuning of parameters or of hidden symmetry in the system (see Sec. III.D.3).

Finally, as seen above, it is perfectly permissible to include appropriate translations, since they are also genuine symmetries of the system. One may then choose the gap function to belong to a nontrivial representation of the translation group. This increases the possible number of superconducting states, since it means pairing between $\vec{k}$ and $-\vec{k}+\vec{Q}$, with $\vec{Q}\neq 0$ (see Sec. III.D.4).

A related issue is whether, on dynamical grounds, we can say anything about the SC state. Take the case of a single band, and assume that the pairing interaction has the form $V_{s_1s_2s_3s_4}(\vec{k},\vec{k}')=g\vec{J}_{s_1s_3}\cdot\vec{J}_{s_2s_4}$ which is the simplest angular-momentum-dependent interaction. This

TABLE I. Illustrative polynomial functions and functions that form a complete periodic basis for the singlet representations of D_{6h}. For work involving the full Fermi surface, the final column should be used. $f_x(\vec{k}) \equiv \sin(k_x a) + \sin(k_x a/2)\cos(\sqrt{3}k_y a/2)$, $f_y(\vec{k}) \equiv \pm\sqrt{3}\cos(k_x a/2)\sin(\sqrt{3}k_y a/2)$, $f_\pm(\vec{k}) \equiv f_x(\vec{k}) \pm i f_y(\vec{k})$, and $f_z(\vec{k}) \equiv \sin(k_z c)$. Both sets of notation in common use for the representations of D_{6h} are given. Commas separate degenerate functions, while semicolons separate nondegenerate functions belonging to a single representation.

Rep.	Illustrative	Complete, periodic
A_{1g} (Γ_1^+)	1; $k_x^2+k_y^2$; k_z^2; …	1; $f_x(\vec{k})^2+f_y(\vec{k})^2$; $f_z(\vec{k})^2$; …
A_{2g} (Γ_2^+)	$k_x k_y(k_x^2-3k_y^2)(k_y^2-3k_x^2)$	$\mathrm{Im}[f_+(\vec{k})^6]$
B_{1g} (Γ_3^+)	$k_z k_y(k_y^2-3k_x^2)$	$f_z(\vec{k})\,\mathrm{Im}[f_+(\vec{k})^3]$
B_{2g} (Γ_4^+)	$k_z k_x(k_x^2-3k_y^2)$	$f_z(\vec{k})\,\mathrm{Re}[f_+(\vec{k})^3]$
E_{1g} (Γ_5^+)	$k_z k_x, k_z k_y$	$f_z(\vec{k})\,\mathrm{Re}[f_+(\vec{k})]$, $f_z(\vec{k})\,\mathrm{Im}[f_+(\vec{k})]$; $f_z(\vec{k})\,\mathrm{Re}[f_-(\vec{k})^5]$, $f_z(\vec{k})\,\mathrm{Im}[f_-(\vec{k})^5]$
E_{2g} (Γ_6^+)	$k_x^2-k_y^2, 2k_x k_y$	$\mathrm{Re}[f_+(\vec{k})^2]$, $\mathrm{Im}[f_+(\vec{k})^2]$; $\mathrm{Re}[f_-(\vec{k})^4]$, $\mathrm{Im}[f_-(\vec{k})^4]$

type of interaction can lead to a triplet state (for $g<0$) as well as a singlet state (for $g>0$). The electron wave functions, as we have seen, are partly oriented by the crystal field, but no band has a definite value of $|j_z|$. Using this interaction shows that the crystal field tends to orient $\vec{d}(\vec{k})$ along the z axis, while spin-orbit coupling tends to orient $\vec{d}(\vec{k})$ along $\hat{k}$. The resulting state is a compromise in which $\vec{d}(\vec{k})$ wanders on the Fermi surface. If the pair potential depends strongly on momentum, $g \to V(\vec{k},\vec{k}')$, which is almost certainly the case in UPt_3, this expectation is only strengthened.

Detailed attempts to calculate the gap function from first principles have been made. They have been based on the theory of ^{3}He, in which, roughly speaking, the frequency- and wave-vector-dependent magnetic susceptibility (measured by neutron scattering) is used as an interaction in Eq. (10). Early attempts to implement this in UPt_3 (Norman, 1987; Putikka and Joynt, 1988, 1989) led to gap functions that did not have the proper translation symmetry. The other big complication, orbital degeneracy split by spin-orbit coupling and crystal fields, was treated crudely or not at all. In a series of papers, Norman (1990, 1993, 1994a, 1994b) has attempted to rectify this situation. The most recent of these papers is the first to really treat the channel dependence of the interaction properly. Norman proposes a model of on-U-site pairing which looks promising. The magnetic susceptibility for all frequencies and wave vectors is still needed as input, and further experimental work may be needed to push this approach further.

B. Gap functions and gap nodes

To discuss experiments, we must look at some actual gap functions belonging to the different representations. It has been customary to give examples of basis functions in discussions of the symmetry issue, without discussing how these functions are actually realized. This practice can create the misleading impression that these example basis functions themselves, or something very similar to them, are the alternatives for the superconducting state. This is not really true, as the examples usually given are dictated by simplicity of appearance and brevity of presentation. For example, tables of polynomial functions are given by Sigrist and Ueda (1991) and tight-binding-type functions are given by Putikka and Joynt (1988).

These tables, and all others so far given in the literature, have two flaws. They do not give a complete set of functions, which is needed if one wishes to understand all the possibilities, and the functions are not periodic in reciprocal space, as is required by translation symmetry. We shall attempt to rectify this situation in this section, first giving full tables, then explaining how they are constructed, and finally offering a guide to their use.

A set of complete periodic basis functions for singlet and triplet representations of D_{6h} is given in Tables I and II, respectively. The concept of completeness in this context is due to Yip and Garg (1993). It means that all possible functions in a given representation can be found in, or written as a combination of, the functions in the table. As an example, let us investigate the possible basis functions belonging to B_{1g}, ignoring the question of periodicity for the moment.

The listed function $f_z(\vec{k})\,\mathrm{Im}[f_+(\vec{k})^3]$ transforms according to B_{1g}. However, there is an infinite set of linearly independent functions that so transform and each therefore belongs to the representation B_{1g}. For example, the function $[f_z(\vec{k})]^3\,\mathrm{Im}[f_+(\vec{k})^3]$ belongs to this set, since multiplication by $[f_z(\vec{k})]^2$ does not change the transformation properties. Completeness is the statement that all of the basis functions for B_{1g} can be writ-

TABLE II. Illustrative polynomial functions and functions that form a complete periodic basis for the triplet representations of D_{6h}. For work involving the full Fermi surface, the final column should be used. $f_x(\vec{k}) \equiv \sin(k_x a) + \sin(k_x a/2)\cos(\sqrt{3}k_y a/2)$, $f_y(\vec{k}) \equiv \pm\sqrt{3}\cos(k_x a/2)\sin(\sqrt{3}k_y a/2)$, $f_\pm(\vec{k}) \equiv f_x(\vec{k}) \pm i f_y(\vec{k})$, $f_z(\vec{k}) \equiv \sin(k_z c)$, $k_\pm \equiv k_x \pm i k_y$, and $\hat{r}_\pm = \hat{x} \pm i\hat{y}$. Both sets of notation in common use for the representations of D_{6h} are given. Commas separate degenerate functions, while semicolons separate nondegenerate functions belonging to a single representation.

Rep.	Illustrative	Complete, periodic
A_{1u} (Γ_1^-)	$\hat{z}k_z$;	$\hat{z}f_z(\vec{k})$;
	$\hat{x}k_x + \hat{y}k_y$;	$\hat{x}k_x + \hat{y}k_y$;
	⋯	$\mathrm{Re}[f_+(\vec{k})^5\hat{r}_+]$;
	⋯	⋯
A_{2u} (Γ_2^-)	$\hat{x}k_y - \hat{y}k_x$	$\mathrm{Im}[f_-(\vec{k})\hat{r}_+]$;
		$\mathrm{Im}[f_+(\vec{k})^5\hat{r}_-]$;
		$\mathrm{Im}[f_+(\vec{k})^6]f_z(\vec{k})\hat{z}$;
B_{1u} (Γ_3^-)	$\hat{z}k_y(k_y^2 - 3k_x^2)$;	$\mathrm{Im}[f_+(\vec{k})^3]\hat{z}$;
	$k_z[\hat{x}(k_x^2 - k_y^2) - 2\hat{y}k_x k_y]$	$\mathrm{Im}[f_+(\vec{k})^2 f_z(\vec{k})\hat{r}_+]$;
		$\mathrm{Im}[f_+(\vec{k})^4 f_z(\vec{k})\hat{r}_-]$;
B_{2u} (Γ_3^-)	$\hat{z}k_x(k_x^2 - 3k_y^2)$	$\mathrm{Re}[f_+(\vec{k})^3]\hat{z}$;
	$k_z[\hat{y}(k_y^2 - k_x^2) - 2\hat{x}k_y k_x]$	$\mathrm{Re}[f_+(\vec{k})^2 f_z(\vec{k})\hat{r}_+]$;
		$\mathrm{Re}[f_+(\vec{k})^4 f_z(\vec{k})\hat{r}_-]$;
E_{1u} (Γ_5^-)	$\hat{z}k_x, \hat{z}k_y$;	$\mathrm{Re}[f_+(\vec{k})]\hat{z}$, $\mathrm{Im}[f_+(\vec{k})]\hat{z}$;
	$k_z\hat{x}, k_z\hat{y}$	$\mathrm{Re}[f_z(\vec{k})\hat{r}_+]$, $\mathrm{Im}[f_z(\vec{k})\hat{r}_+]$;
		$\mathrm{Re}[f_+(\vec{k})^2\hat{r}_-]f_z(\vec{k})$, $\mathrm{Im}[f_+(\vec{k})^2\hat{r}_-]f_z(\vec{k})$;
		$\mathrm{Re}[f_-(\vec{k})^5]\hat{z}$, $\mathrm{Im}[f_-(\vec{k})^5]\hat{z}$;
		$\mathrm{Re}[f_-(\vec{k})^4\hat{r}_-]f_z(\vec{k})$, $\mathrm{Im}[f_-(\vec{k})^4\hat{r}_-]f_z(\vec{k})$;
		$\mathrm{Re}[f_-(\vec{k})^6\hat{r}_+]f_z(\vec{k})$, $\mathrm{Im}[f_-(\vec{k})^6\hat{r}_+]f_z(\vec{k})$;
E_{2u} (Γ_6^-)	$\hat{x}k_x - \hat{y}k_y, \hat{x}k_y - \hat{y}k_x$	$\mathrm{Re}[f_+(\vec{k})\hat{r}_+]$, $\mathrm{Im}[f_+(\vec{k})\hat{r}_+]$;
	$\hat{z}(k_x^2 - k_y^2)k_z, \hat{z}k_x k_y k_z$	$\mathrm{Re}[f_+(\vec{k})^2]f_z(\vec{k})\hat{z}$, $\mathrm{Im}[f_+(\vec{k})^2]f_z(\vec{k})\hat{z}$;
		$\mathrm{Re}[f_+(\vec{k})^3\hat{r}_-]$, $\mathrm{Im}[f_+(\vec{k})^3\hat{r}_-]$;
		$\mathrm{Re}[f_-(\vec{k})^3\hat{r}_-]$, $\mathrm{Im}[f_-(\vec{k})^3\hat{r}_-]$;
		$\mathrm{Re}[f_-(\vec{k})^4]f_z(\vec{k})\hat{z}$, $\mathrm{Im}[f_-(\vec{k})^4]f_z(\vec{k})\hat{z}$;
		$\mathrm{Re}[f_-(\vec{k})^5\hat{r}_+]$, $\mathrm{Im}[f_-(\vec{k})^5\hat{r}_+]$;

ten as the listed basis function times a function that is completely invariant under all the operations of D_{6h}. There are no other functions which transform according to B_{1g}. The actual gap function is an infinite linear combination of all of them. Because of completeness, it suffices to examine only the functions listed in the tables in order to determine those properties. The number of functions belonging to A_{1g} is infinite. (The ellipsis in Table I under A_{1g} stands for all such functions.)

On the other hand, it is vitally important to look at *all* the functions in the final column when there is more than one listed. Nearly all published tables have the defect that they do not give a complete list, and this can lead to serious errors, since any one function may have special properties that are actually not generic. It can be shown (Yip and Garg, 1993) that the number of functions needed for a complete (in the special sense defined here) list for the representation is equal to the dimension of the representation in the singlet case and three times the dimension in the triplet case.

Periodicity is a separate issue. The actual gap function must be periodic in crystal momentum space (in the extended zone scheme), as the actual momenta are determined only up to reciprocal-lattice vectors. The usual polynomial basis functions do not have this property. It is not too difficult to remedy this problem, and this has been done in the tables. It is important to be careful about this if sheets of the Fermi surface intersect the Brillouin zone. This does occur in UPt_3. For example, the horizontal caps of the zone are at $k_z = \pm\pi/c$. Any gap function that contains $f_z(\vec{k}) = \sin(k_z c)$ as a factor clearly vanishes on these faces, resulting in a line of nodes on the "star" sheet of the Fermi surface, for example.

How does one use these tables? Let us imagine we have written down an infinite linearly independent set for a one-dimensional singlet representation and call these functions $F_i(\vec{k})$. Then the solution to the linearized gap equation belonging to the highest eigenvalue can be written as

$$\psi(\vec{k}) = \sum_{i=1}^{\infty} c_i F_i(\vec{k}). \tag{14}$$

Since all the symmetries have been taken into account already, the c_i are determined by dynamical considerations only. That is, they depend on the precise form of the starting crystal Hamiltonian and on the details of the pairing potential in Eq. (12). At present, we have no reliable way to calculate these coefficients in UPt_3. We can say, however, that there are no additional symmetries which will make any of the c_i turn out to be zero, and changing any parameter (by applying pressure, say) in the Hamiltonian will generically change all the c_i. The solution $\psi(\vec{k})$ will, however, have all the same transformation properties as the basis functions F_i because these properties are not altered by taking linear combinations.

In the two-dimensional singlet case, the gap function is

$$\psi(\vec{k}) = a_1 \sum_{i}^{2} c_{i1} F_i^{(1)}(\vec{k}) + a_2 \sum_{i}^{2} c_{i2} F_i^{(2)}(\vec{k}), \tag{15}$$

where $F_i^{(j)}$ is the jth member of the ith pair of functions in Table I. For E_{1g}, for example, $F_1^{(2)} = f_z(\vec{k})\,\mathrm{Im}[f_+(\vec{k})]$, up to multiplication by an invariant function. The complex coefficients a_1 and a_2 are determined by nonlinear effects, i.e., not by Eq. (12). Unlike the c_{ij}, a_1 and a_2 (or rather their ratio) may take on special values which are constrained by symmetry.

By far the most important characteristic of a gap is its nodal structure. We can now see how to deduce this for a singlet representation and an arbitrary Fermi surface. In E_{1g}, for example, all basis functions include $f_z(\vec{k}) = \sin(k_z c)$. Hence there are lines of nodes where the planes $k_z = 0$ and $k_z = \pm \pi/c$ intersect the Fermi surface. Also, the $F_i^{(1)}(\vec{k})$ are odd under reflection in the y-z plane. Thus, if $a_2 = 0$, then there are lines of nodes where $k_x = 0$ on the Fermi surface. If $a_1 = 0$, then there are lines of nodes where $k_y = 0$ instead. If a_1 and a_2 are nonzero and relatively real, $a_1/a_2 = \text{real}$, the plane of zeros in $\vec{k}$ space is rotated and the line of nodes is given by the intersection of the plane determined by the equation $a_1 k_x + a_2 k_y = 0$ and the Fermi surface. Finally if a_1/a_2 has an imaginary part, then the nodes lie at the intersection of these planes and the Fermi surface, which is at $k_x = k_y = 0$. These are point nodes. The symmetry of the low-temperature phase is not known until the a_1 and a_2 are known. For example, the $a_2 = 0$ state has a residual reflection symmetry in the x-z plane, and has time-reversal symmetry. The state with complex a_1/a_2 has neither of these symmetries. The angle dependence of the gap function for the $(1,i)$ state, i.e., where $a_1 = 1$ and $a_2 = i$, is shown on a single spherical Fermi surface in Fig. 11. This gap structure is called "hybrid I," characterized by a combination of an equatorial line node (at $k_z = 0$) and point nodes at the poles ($k_x = k_y = 0$). The gap grows linearly away from the nodes in both cases.

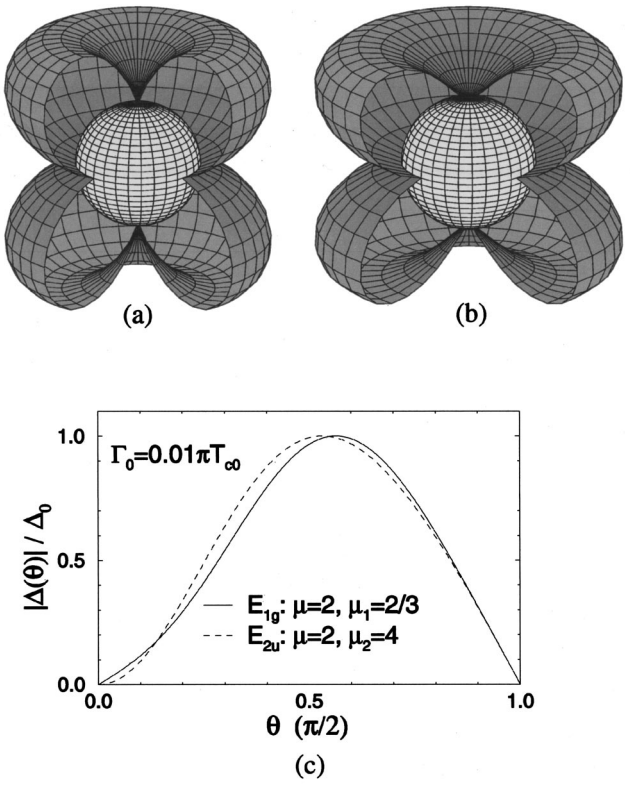

FIG. 11. Gap structure for a hybrid-I gap (a) and a hybrid-II gap (b), respectively appropriate for the E_{1g} and E_{2u} representations. The gap magnitude as a function of azimuthal angle θ is shown in (c). Note the linear rise from the equator in both cases and the linear vs quadratic rise from the pole for E_{1g} and E_{2u}, respectively. Note also that a general choice for the opening parameters (μ,μ_1,μ_2) would make the two gaps less similar than they appear here. From Graf, Yip, and Sauls, 1999.

The most complicated case is that of a two-dimensional triplet representation, E_{1u} or E_{2u}. The state of the system is given by

$$\vec{d}(\vec{k}) = a_1 \sum_{i=1}^{6} c_{i1} \vec{F}_i^{(1)}(\vec{k}) + a_2 \sum_{i=1}^{6} c_{i2} \vec{F}_i^{(2)}(\vec{k}), \tag{16}$$

where again the c_i are determined dynamically and, in the generic case, none of them are zero.

To determine the nodal structure of E_{2u}, we need to form the above sum, taking all 12 functions in the lower right square of Table II, and then compute $|\vec{d}(\vec{k})|$. First let $a_2 = 0$, so only the functions in the left column appear. Since $f_z(\vec{k})$ appears in only two of them, there is no line of nodes at $k_z = 0$. f_x and f_y appear in all functions, so the only nodes are where $f_x(\vec{k})$ and $f_y(\vec{k})$ *both* vanish, namely, at $k_x = k_y = 0$. Inspection of the second column then shows that this is independent of the choice of a_1 and a_2, so these point nodes are there for all E_{2u} states.

The fact that there are only point nodes for the two-dimensional triplet representations is an explicit realization of the general theorem due to Blount (1985) that, in the presence of spin-orbit coupling, singlet states may have either line nodes or point nodes, but triplet states have only point nodes. This has important consequences

for some candidate order parameters.

By setting $c_{1j}=c_{3j}=c_{4j}=c_{6j}=0$, we can construct a state in which $\vec{d}\sim f_z(\vec{k})$, so that there is a line of nodes in E_{2u} $(k_z=0)$. This has been proposed on phenomenological grounds (Choi and Sauls, 1991) and will be discussed in Sec. III.D.1. Since the c_i are not constrained by symmetry, they are functions of all the parameters of the underlying Hamiltonian. Nodes of the gap produced by such choices are therefore unstable in the sense that any change in the system (applying pressure, for example) will lift them.

The gap structure for this special choice of E_{2u} state is shown in Fig. 11, for the $(1,i)$ state where $a_1=1$ and $a_2=i$. This gap is called "hybrid II" and it is characterized by a combination of an equatorial line node where the gap vanishes linearly and point nodes at the poles where the gap vanishes quadratically.

C. Calculation methods

The effect of gap anisotropy and nodal structure on physical properties was investigated in the context of superfluid ^{3}He in the 1970s, as reviewed by Leggett (1975). For unconventional superconductors, the theoretical foundations were developed in the mid-1980s in the wake of the discovery of heavy-fermion superconductors, by authors such as Coffey, Rice, and Ueda (1985), Volovik and Gor'kov (1985), Hirschfeld, Vollhardt, and Wölfle (1986), Pethick and Pines (1986), Schmitt-Rink, Miyake, and Varma (1986), and Monien *et al.* (1987). Much of this early work is summarized by Sigrist and Ueda (1991). Properties such as specific heat, ultrasound attenuation, thermal conductivity, and NMR relaxation rate were calculated for various order parameters and compared to what experimental evidence there was at the time.

The three basic results that emerged from this work, and which remain today as the key elements in the analysis of thermal properties of any unconventional superconductor, including, for example, the high-T_c cuprates, are (1) there is a power-law dependence on temperature at $T\ll T_c$, instead of the conventional activated behavior (at least in the pure limit); (2) it is necessary to treat impurity scattering in (or near) the unitarity limit of strong (resonant) scattering (Pethick and Pines, 1986), described by a scattering phase shift $\delta_0\simeq\pi/2$; (3) a gapless regime appears at low energy, even for small concentrations of nonmagnetic impurities, giving rise to a residual normal fluid of zero-energy quasiparticles (Hirschfeld, Vollhardt, and Wölfle, 1986; Schmitt-Rink, Miyake, and Varma, 1986).

A fourth, more recent development was the recognition that, for some transport properties and certain gap structures, there can be asymptotic low-temperature behavior that is independent of the impurity concentration (universal), as first pointed out by Lee (1993).

All of these results depend on the fact that the gap has nodes, which is the reason we have consistently stressed this feature of the gap functions.

TABLE III. Density of states $\rho(\omega)$ at low energies for different nodal structures. The dispersion refers to the the change in energy $E_{\vec{k}}$ as $\vec{k}$ is varied away from the nodal point $\vec{k}_n$ but remains on the Fermi surface. In the case of a line node, the direction is perpendicular to the line.

Node type	Dispersion	Example gap $\lvert\Delta(\vec{k})\rvert$	$\rho(\omega)$
Line	linear	k_z	$\lvert\omega\rvert$
Point	linear	$\sqrt{k_x^2+k_y^2}$	ω^2
Line	quadratic	k_z^2	$\sqrt{\lvert\omega\rvert}$
Point	quadratic	$k_x^2+k_y^2$	$\lvert\omega\rvert$
Gapless	flat	0	constant

From a purely technical standpoint, the methods of calculating the response functions and thermodynamic functions of superconductors are generalizations of well-established techniques developed for the s-wave case of a nodeless gap function, where the agreement of theory and experiment is generally very good. In the case of UPt_3, many properties have been measured, and there are qualitative deviations from s-wave behavior, confirming the identification of this material as unconventional, in the sense of having an order parameter with a symmetry other than A_{1g}. This means that there are many possibilities for the gap function.

From these arguments, we can identify the most promising area of investigation to be the asymptotic low-temperature regime, as the qualitative behavior as $T\to 0$ may be independent of unknown parameters for a pure system, and even, in some cases, for a dirty system. Any discussion of low-temperature properties begins with the density of states $\rho(\omega)$, the number of states per unit energy range per unit volume for the quasiparticle excitations. We have seen that line nodes, point nodes, and no nodes are possible in the pure superconductors, and it turns out that gaplessness can occur as a result of impurity scattering. These lead to various results for the low-frequency behavior of $\rho(\omega)$. In the case of a unitary gap function, as defined in Sec. III.A, the density of states is given by $\rho(\omega)=2/V\,\Sigma_{\vec{k}}\delta(\omega-E_{\vec{k}})$, with $E_{\vec{k}}^2=\epsilon^2(\vec{k})+\lvert\Delta(\vec{k})\rvert^2$ or $E_{\vec{k}}^2=\epsilon^2(\vec{k})+\lvert\vec{d}(\vec{k})\rvert^2$. At sufficiently low ω, the sum over $\vec{k}$ may be restricted to the neighborhood of the nodes. The results are shown in Table III.

An example of a calculation for a point node at $\vec{k}_0$ with linear dispersion is

$$\rho(\omega)=\frac{1}{4\pi^3}\int_{\vec{k}\approx\vec{k}_0} d^3k\;\;\delta(\omega-E_{\vec{k}})$$

$$=\frac{1}{4\pi^3}\int dk_\parallel d^2k_\perp \times\delta[\omega-\sqrt{v_F^2k_\parallel^2+c^2(k_{\perp x}^2+k_{\perp y}^2)}] \tag{17}$$

$$=\frac{1}{4\pi^3 v_F c^2}\int dz\,dx\,dy\,\delta(\omega-\sqrt{z^2+x^2+y^2})$$

$$=\frac{\omega^2}{\pi^2 v_F c^2}. \tag{18}$$

TABLE IV. Power-law dependences for various quantities in the asymptotic low-temperature regime. These laws hold for a clean superconductor with linear dispersion of the gap at the nodes.

	Lines	Points
Specific heat C_V	T^2	T^3
NMR relaxation rate $1/T_1$	T^3	T^5
Thermal conductivity κ	T^2	T^3
Penetration depth $1/\lambda_{\parallel}^2$	T^3	T^2
Penetration depth $1/\lambda_{\perp}^2$	T	T^4

The origin for the integration is at $\vec{k}_0$, $k_{\parallel}$ is the direction normal to the Fermi surface, and $\vec{k}_{\perp}$ lies on the Fermi surface. c is the slope of the perpendicular dispersion.

Using Table III, which gives the power laws for the density of states, power laws for other measurable quantities may be derived by simple scaling arguments. See Barash and Svidzinsky (1996) for a good discussion. For example, the specific heat for $\rho(\omega)\sim\omega^{\alpha}$ is given by

$$C=-\frac{2}{T}\int_0^{\infty}\rho(E)E^2\frac{\partial f}{\partial E}dE$$

$$\sim-\frac{2}{T}\int_0^{\infty}E^{2+\alpha}\frac{\partial f}{\partial E}dE \tag{19}$$

$$\sim-\frac{2}{T}T^{2+\alpha}\int_0^{\infty}x^{2+\alpha}f'(x)dx\sim T^{1+\alpha}. \tag{20}$$

Here $f(E)=1/(1+e^{E/k_BT})$, and we made the substitution $x=E/k_BT$. Other quantities follow by the same sort of argument; Table IV results. Some gaps have more than one kind of node. As noted above, these are known as hybrid gaps. In this case, the lowest power dominates at sufficiently low temperature.

Beyond the low-temperature region, the response may still show qualitative signatures of unconventional superconductivity if there is directionality involved. The nodal points or lines may dominate the response to a low-frequency probe. The conduction of heat depends on the direction of current flow. The absorption of ultrasound depends on the propagation and polarization directions. We shall see examples in Secs. V.C and V.B.

One of the key differences between conventional and unconventional superconductors is the major impact impurities and defects have on the latter. Indeed, even an infinitesimal level of disorder will modify the density of states qualitatively if there are nodes. The gap fills in and the density of states at the chemical potential immediately becomes finite. If the scattering is at or near the unitarity limit, as is usually thought (Pethick and Pines, 1986), this conclusion is further strengthened: there can even be a peak in $\rho(\omega)$ at or near the chemical potential (Hirschfeld, Vollhardt, and Wölfle, 1986; Schmitt-Rink, Miyake, and Varma, 1986).

The subject of different types of impurity scattering in superconductors with strong spin-orbit coupling has not received much attention, possibly because it is somewhat vexatious. If we begin by ignoring spin-orbit coupling and assuming that the single-particle states are eigenfunctions of spin, then the division of scattering into the canonical three categories of potential scattering, spin-orbit scattering, and magnetic scattering still makes good sense. However, the consequences of the different kinds of scattering are not quite the same as in the case of s-wave pairing. Even potential scattering will reduce T_c. Formally, the anomalous self-energy Σ_2 vanishes and does not cancel the normal self-energy in the T_c equation. This vanishing is usually incorporated from the start in calculations. (This result follows from the usual assumption of isotropic scattering, which may be dangerous, according to Haas *et al.*, 1997.) T_c is a strongly decreasing function of concentration. This is as it must be, as the scattering mixes different momentum states. Since unconventional superconductivity depends for its pairing energy on constructive interference in momentum space, the mixing must reduce the strength of the pairing. Spin-orbit scattering and magnetic scattering also reduce the critical temperature for the same reason. If there is spin-orbit scattering, the anomalous self-energy also does not vanish, as the symmetry properties of the scattering operator do not allow this.

Once spin-orbit coupling in the lattice becomes important, even the classification of scattering types must change somewhat. An impurity produces scattering from a state $|\vec{k},\alpha\rangle$ to a state $|\vec{k}',\alpha'\rangle$. The pseudospin index α will not be conserved for general $\vec{k}$ and $\vec{k}'$ even if the scattering preserves spin. Thus there is no analog of potential scattering in heavy-fermion materials in general and in UPt_3 in particular. In view of the arguments in the preceding paragraph, this also implies that $\Sigma_{ss'}^{(2)}(\vec{k},i\omega_n)\neq 0$ for these materials. It would be interesting to see calculations of observable quantities which incorporate this fact. The Pauli part of the magnetic susceptibility should remain finite at zero temperature even for singlet pairing.

Magnetic scattering is distinguishable from spin-orbit scattering because the scatterer will generally have an internal degree of freedom. However, spin-orbit coupling and crystal-field effects must be taken into account. In UPt_3 the most interesting case is a magnetic scatterer which substitutes on the uranium site, which therefore feels a crystal field with hexagonal symmetry. As long as the splitting due to this field is much greater than the gap energy (as one would of course expect), the impurity level is twofold degenerate, not $2J+1$-fold degenerate. The relaxation time becomes independent of J. This is consistent with observations of Dalichaouch *et al.* (1995), but it does not depend on having triplet pairing, contrary to their conclusion.

D. Candidate theories

In the absence of a reliable microscopic account of the interaction that produces superconductivity, theoretical work has concentrated on the intermediate level of description. A parametrized order parameter is postulated,

without derivation from a microscopic Hamiltonian, in order to explain experiments. Success or failure is judged in a phenomenological fashion. This procedure is appropriate, since the identification of the order parameter would be a giant step in the construction of a complete theory. There are three points to be stressed in this connection. First, although we are not able to derive the order parameter from a Hamiltonian, it must nevertheless be consistent with the symmetry of the Hamiltonian. That is, it should fall into the classification scheme given above. Second, it should not involve fine-tuning of parameters. Third (and most obviously), a theory should explain, or at least be consistent with, *all* experiments. Historically most theories were motivated by one or a few experiments. In many cases, the broader consequences have not been sufficiently considered. One role of this review is to view the proposed theories with these three points in mind.

In this section, candidates for the order parameter in all three phases of UPt_3 are introduced and described. The theories and their original motivations are given in roughly chronological order. The most important features of any theory are the number of components and the nodal structure in the A and B phases, so these are given in detail.

1. Two-dimensional representations

Order parameters belonging to a two-dimensional representation may be thought of as vectors that are confined to the basal plane, so that they are characterized by the two coefficients (a_1,a_2) from Eqs. (15) and (16) multiplying independent basis functions for the gap. For brevity, we shall use the illustrative functions in this section.

All two-dimensional representation theories share important common features. The splitting of the critical temperatures for the A and B phases is due to a small coupling to the antiferromagnetism that splits the energies of the (1,0) and (0,1) states. The A phase is (1,0) and the C phase is (0,1). The state for the A phase is stabilized by the coupling to magnetism, whereas the state for the C phase is stabilized by the coupling to the external field. The B phase is the $(1,\pm i)$ state, a compromise between the two.

E_{1g} is a two-dimensional singlet (even-parity) representation. From Table I we see that the simplest illustrative example of degenerate basis functions is the pair (k_zk_x,k_zk_y). The state for the A phase is a (1,0) state, $\Delta(\vec{k})=\Delta_0(T)\,k_zk_x$, or a (0,1) state, $\Delta(\vec{k})=\Delta_0(T)\,k_zk_y$; which of the two is stable depends on small terms that split the energies, as discussed below. There are lines of nodes at the equator $(k_z=0)$ and on a "vertical" line $(k_x=0)$ or $(k_y=0)$. The B phase is proposed to be a complex combination: the $(1,i)$ state $\Delta(\vec{k})=\Delta_0(T)\,k_z[k_x+i\delta(T)\,k_y]$ or the $(1,-i)$ state $\Delta(\vec{k})=\Delta_0(T)\,k_z[k_y+i\delta(T)\,k_x]$. These states break time-reversal symmetry. Inspection of Table I shows that, generically, the energy gap $|\Delta(\vec{k})|$ in the B phase vanishes linearly $(\sim|k_z|)$ at the equator and also linearly at the poles $(k_x=k_y=0)$ where $|\Delta(\vec{k})|\sim\sqrt{k_x^2+k_y^2}=|\sin\theta|$, where θ is the polar angle. This nodal pattern, called *hybrid I*, is illustrated in Fig. 11. The position of the nodes and their linear nature follow from symmetry alone, as may also be verified from Table I.

This theory was originally proposed when it was found as the solution of a microscopic model (Putikka and Joynt, 1988, 1989). It was the first definite representation of D_{6h} to be given for the order parameter of the system. The B phase is similar in nodal structure to the earlier hybrid order parameter, "hybrid" indicating both line and point nodes. This nodal structure was first suggested by Hirschfeld, Vollhardt, and Wölfle (1986) based on a reasonable agreement between experiment and their calculations of thermal properties. The implications of the E_{1g} model for the phase diagram have received a detailed review (Park and Joynt, 1995).

E_{2u} is a two-dimensional triplet (odd-parity) representation. The degenerate basis functions from Table I are the pairs $[\hat{z}k_zk_xk_y,\hat{z}k_z(k_x^2-k_y^2)]$ and $(\hat{x}k_x-\hat{y}k_y,\hat{x}k_y-\hat{y}k_x)$. A general (1,0) state would have the form $\vec{d}(\vec{k})=c_1(T)\hat{z}k_zk_xk_y+c_2(T)(\hat{x}k_x-\hat{y}k_y)$, and the (0,1) state would be $\vec{d}(\vec{k})=c_1(T)\hat{z}k_z(k_x^2-k_y^2)+c_2(T)(\hat{x}k_y-\hat{y}k_x)$, following the notation of Sec. III.B. These states have point nodes at the poles. For the $(1,\pm i)$ states associated with phase B at low temperatures, the gap function is $\vec{d}=c_1(T)\,\hat{z}\,k_z(k_x\pm ik_y)^2+c_2(T)(k_x\pm ik_y)(\hat{x}\pm i\hat{y})^2$. This also has point nodes at $k_x=k_y=0$. Reference to Table II shows that the point nodal structure is generic in this representation. This is clearly inconsistent with experiment, as we shall see below. Consequently, proposals for E_{2u} have set $c_2(T)=0$, fixing $\vec{d}$ to be in the z direction. For the B phase we then get $\vec{d}\sim\hat{z}k_z(k_x^2-k_y^2+2ik_xk_y)$. This has linear line nodes and quadratic point nodes. This nodal structure, called *hybrid II*, is sketched in Fig. 11. The line of nodes is not dictated by symmetry and is unstable to any perturbation of the system (Blount, 1985).

The E_{2u} representation was originally proposed by Choi and Sauls (1991) in order to account for the anisotropy of the upper critical field, as discussed in Sec. IV.B below. It has been thoroughly reviewed by Sauls (1994).

An interesting version of this theory is that of Norman (1995b): on-uranium-site E_{2u} pairing. Then we may expect line nodes on the zone faces $k_z=\pm\pi/c$. This again corresponds to a particular choice of basis functions.

2. Spin triplet

This theory was originally proposed in order to explain the phase diagram in the H-T plane (Machida and Ozaki, 1991). The spin wave function of the pair has $S=1$, which transforms as a three-dimensional vector, so the $\vec{d}$ vector takes the form $\vec{d}=d_x\hat{x}+d_y\hat{y}+d_z\hat{z}$. As mentioned above, this theory depends on the questionable hypothesis that spin-orbit coupling is very small. The tables of Sec. III.B cannot be used directly, as they de-

pend on having spin-orbit energies which much exceed gap energies. However, the spatial form of the orbital wave function should still transform according to the D_{6h} group. It must be of odd parity. The spatial representation can be one or two dimensional and indeed any of the six odd-parity representations is possible. Hence many patterns of nodes are possible. Several specific possibilities have been considered (Machida and Ozaki, 1989, 1991; Machida, Ozaki, and Ohmi, 1989; Machida, 1992; Machida, Fujita, and Ohmi, 1993; Machida *et al.*, 1993; Ohmi and Machida, 1993, 1996a, 1996b). The most recent version posits an E_{2u} orbital state, which has a twofold orbital degeneracy: $\vec{d}=c_1\vec{d}_1(T)+c_2\vec{d}_2(T)$, etc. Together with the threefold spin degeneracy, this makes a six component order parameter (Machida and Ohmi, 1998; Machida, Nishira, and Ohmi, 1999).

The A phase is then a (1,0,0) state, i.e., $d_y=0$ and $d_z=0$. The forms of the B and C phases depend on the field direction, but could be, for example, (1,*i*,0) and (0,0,1) respectively, for a field in the z direction. As with the 2D theories, the phase diagram depends in an essential fashion on the coupling of superconductivity and magnetism.

3. Mixed representations

A number of theories involving two separate representations have been proposed. They share the characteristic feature that the two superconducting transitions involve gap functions that are not related by symmetry. The splitting of the phase transition is due to accidental degeneracy, not to coupling to the magnetism. Once two representations are involved, the possibilities for the form of the order parameter become numerous. As a class, such theories therefore have relatively little predictive power. It is correspondingly difficult to rule them out in a definitive fashion. However, some specific proposals can be evaluated.

- *Mixed A_{1u} and A_{2u}.* These two representations are degenerate if the in-plane spin-orbit interaction is zero (Joynt *et al.*, 1990). In this theory, the explanation of the two close transitions is that this coupling is small. This theory was used to explain the fact that $H_{c2}(T)$ is isotropic when $\vec{H}$ is rotated in the basal plane. The two representations are not mixed by the field for any such direction. The gap is generically nodeless, which creates difficulties with low-temperature properties.
- *Mixed A and B.* This proposal offers an explanation of the fact that the H-T phase diagram is rather similar for $\vec{H}$ along the c axis and $\vec{H}$ in the basal plane (Chen and Garg, 1993). This is due to the fact that the two representations A_i and B_j are not mixed by the external field for any direction of $\vec{H}$. In this theory, the two transitions are due to the separate T_c equations for A and B: the closeness of the two transitions is accidental. A number of nodal configurations are possible, but the B phase of this theory, in which the relative phase of the two representations is $\pi/2$, does not have a line of nodes (Sauls, 1994). This theory has received the most detailed treatment of any of the mixed-representation theories (Garg and Chen, 1994). It is the only one which will be considered seriously in detail later.
- *Mixed A_{1g} and E_{1g}.* This model is based on in-plane isotropy of the spin-orbit coupling for the near degeneracy of the two representations (Zhitomirskii and Ueda, 1997). Thus, while it has phenomenological virtues similar to the A-B theory for the phase diagram, it has additional theoretical motivation. However, the gap is generically nodeless.

4. Broken translation symmetry

In this picture, the Cooper pairs have a nonzero center-of-mass momentum (Heid *et al.*, 1995). This is a three-component theory, as the momentum is taken at the M point of the hexagonal Brillouin zone, which corresponds to three inequivalent crystal momenta. It is motivated microscopically by the idea of odd-frequency pairing (Balatsky and Abrahams, 1992), which is favored in two-channel Kondo models (Emery and Kivelson, 1992) that have been proposed for heavy-fermion systems (Cox, 1993). Phenomenologically, it was used to explain the same apparent out-of-plane isotropy in the H-T phase diagram as the spin-triplet and A-B theories. In fact, the free energy is the same as the spin-triplet theory at the Ginzburg-Landau level. The orbital wave function belongs to the A_{2g} representation, which can have vertical lines of nodes. Because of the nonzero pair momentum, a uniform field does not mix the different components of the order parameter.

5. Glass model

This model was proposed to explain the in-plane isotropy of the $H_{c2}(T)$ curve (Joynt *et al.*, 1990). It differs from the other models by taking into account the domain structure of the antiferromagnetism, which creates disorder on a scale comparable to the superconducting coherence length. Thus, even in zero field, the order parameter has spatial variation in the A phase. The scale of the variation is determined by a competition between the gradient energy of the superconducting order parameter and the interaction between superconductivity and magnetism. This scenario has been worked out only in the context of the E_{1g} representation. In this case, the B phase is actually the same as in the E_{1g} representation, with the same nodal pattern of line and point nodes with linear dispersion. The A phase may be thought of as an $(\hat{r}_x,\hat{r}_y)$ phase where $\hat{r}$ tries to follow the local magnetization direction. Graf and Hess (2001) have recently revisited this scenario and find that the properties of the superconducting state depend sensitively on the magnetic domain structure.

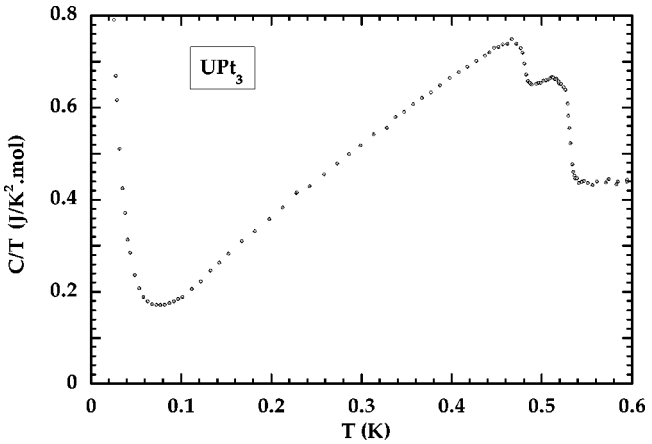

FIG. 12. Specific heat divided by temperature vs temperature. From Brison *et al.*, 1994b.

6. Other theories

A number of other proposals have been made but not worked out in much detail. Some of these have interesting features, but often too little is known about the theory to give a reasonable evaluation. Three examples are as follows: superconductivity is connected to a rotation of the magnetic moment (Blount, Varma, and Aeppli, 1990); the order parameter is nonunitary and belongs to the E_{1u} representation (Ohmi and Machida, 1996a, 1996b), or the order parameter belongs to the E_{2g} representation (Yin and Maki, 1994). There is also an interesting theory based on combining the odd-frequency pairing hypothesis with a novel picture of the normal-state quasiparticles to produce a magnetic superconducting ordering (Coleman, Miranda, and Tsvelik, 1994).

IV. SUPERCONDUCTING PHASE DIAGRAM

A magnetic field $\vec{H}$ has a profound effect on all superconductors. In conventional type-II systems there are two superconducting phases in the H-T plane: the low-field Meissner phase and the high-field vortex phase, separated by the $H_{c1}(T)$ curve. In UPt_3, by the same count, there are five phases: phase C, which is a vortex phase, and phases A and B, each divided into a Meissner phase and a vortex phase [below and above $H_{c1}(T)$].

A. Zero field and ambient pressure

1. Specific heat

The specific heat of UPt_3 is shown in Fig. 12 as C/T vs T. The data of Brison *et al.* (1994a), on a high quality single crystal annealed for 3 days at 1200 °C, nicely exhibits the main features: the onset of superconductivity at $\sim$0.5 K, the appearance of a second transition at a slightly lower temperature, the roughly linear decrease in C/T with temperature, and the large upturn below 0.1 K.

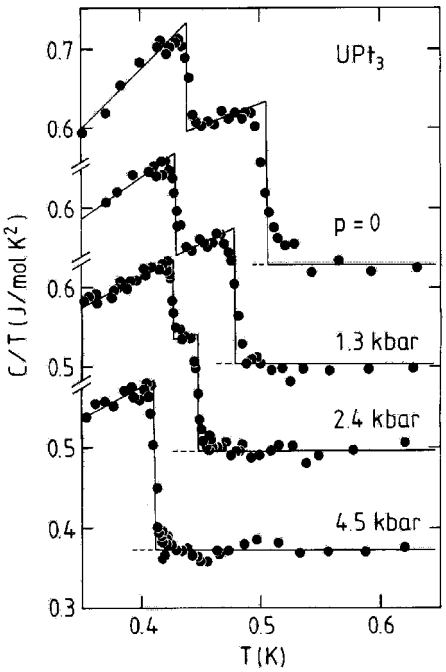

FIG. 13. Specific heat for different hydrostatic pressures plotted as C/T vs T. From Trappmann, Löhneysen, and Taillefer, 1991.

These features have been reproduced by several groups on different samples, provided these were of sufficient quality. As mentioned in Sec. II.E, improper heat treatment, for example, can cause the two superconducting transitions to be considerably broadened and suppressed.

The double transition was first resolved by Fisher *et al.* (1989) and there is now overwhelming evidence that it is an intrinsic property of UPt_3, a defining characteristic of the pure material. The main arguments against an extrinsic origin for the second transition, caused, for example, by inhomogeneities in the sample, are the following. All characteristics of the two transitions are found to converge on one and the same set of values for all crystals. For example, the difference ΔT_c between the two T_c's, commonly referred to as the "splitting," is remarkably invariable (wandering at most by $\pm 1\% T_c$). Both transitions can be very sharp, with a width $\simeq T_c/100$. No single transition has ever been observed with a width less than the splitting (50 mK). Finally, the transitions shift in subtle, nontrivial ways under applied magnetic field or pressure. For example, two sharp transitions at ambient pressure turn (reversibly) into a single, equally sharp transition upon applying hydrostatic pressure in excess of 4 kbar (Trappmann, Löhneysen, and Taillefer, 1991). The reader is referred to the excellent review on the specific heat of UPt_3 by Löhneysen (1994).

The specific heat in the vicinity of the superconducting transition is shown in Fig. 13 (for a high quality polycrystal). Using an idealized construction for C/T vs T shown by the straight lines (e.g., for the $P=0$ curve), we can define the following characteristics:

$$\gamma_N=(C/T)_{T>T_c^+},T_c^{\pm},$$

$$\Delta C^{\pm}/T_c^{\pm}=(C/T)_{T=T_c^{\pm}-\epsilon}-(C/T)_{T=T_c^{\pm}+\epsilon},$$

where + (−) refers to the upper (lower) transition. All published data on single crystals, analyzed in this way, are collected in Table V. This includes seven different crystals, grown using four different techniques. As can be seen, the values are all very close. For the sake of specificity, we adopt the following values as the defining parameters of C/T in UPt_3:

$$T_c^+=530, \quad T_c^-=480,$$

$$\Delta T_c=T_c^+-T_c^-=50 \quad (\text{in mK}), \tag{21}$$

$$\gamma_N=0.44, \quad \frac{\Delta C^+}{T_c^+}=0.24,$$

$$\frac{\Delta C^-}{T_c^-}=0.12 \quad (\text{in J K}^{-2}\ \text{mol}^{-1}). \tag{22}$$

We note that the splitting ΔT_c is only 10% of T_c. The proximity of the two T_c's is suggestive of a common origin, e.g., a lifted degeneracy. Note also that the specific-heat jumps at T_c^+ and T_c^- are large in absolute terms, i.e., in keeping with the huge value of γ_N. This shows that the heavy-fermion quasiparticles are involved in forming the superconducting state.

The application of a magnetic field decreases and merges the two transitions, without significant broadening, as established by Hasselbach, Taillefer, and Flouquet (1989, 1990), for a field direction both along and perpendicular to the c axis. This behavior was later confirmed by Jin, Carter, *et al.* (1992) and Bogenberger *et al.* (1993). Beyond a certain field, only one transition is seen in $C(T)$ vs T, with the critical point (H^*,T_H^*) in the H-T plane given by

$$(\vec{H}\perp\hat{c}): \quad H^*\simeq 0.4\ \text{T}, \quad T_H^*\simeq T_c^+-0.1\ \text{K}, \tag{23}$$

$$(\vec{H}\parallel\hat{c}): \quad H^*\simeq 0.8\ \text{T}, \quad T_H^*\simeq T_c^+-0.15\ \text{K}. \tag{24}$$

It has become clear from a variety of measurements, such as ultrasound attenuation (Adenwalla *et al.*, 1990; Bruls *et al.*, 1990), dilatometry (van Dijk *et al.*, 1993b), and magnetocaloric effect (Bogenberger *et al.*, 1993), that the critical point in the H-T diagram for both field directions is in fact a tetracritical point, where four lines (phases) meet, to within an accuracy of about 5 mK. The phase diagram obtained by Adenwalla *et al.* (1990) using sound velocity is shown in Figs. 14 and 15.

All measurements to date converge on very much the same H-T phase diagram. There are three distinct phases below the $H_{c2}(T)$ line, with phase B the stable one at low temperature, low field and low pressure. Again, phases A and B each have both a Meissner state [below $H_{c1}(T)$] and a vortex state [above $H_{c1}(T)$].

The very existence of multicomponent phase diagrams as in Figs. 14 and 15 (and an equivalent one for the P-T plane, shown in Fig. 16), in particular with their multicritical point, rules out an extrinsic origin to the lower transition. It also argues strongly in favor of a superconducting transition at T_c^-, i.e., one at which a new superconducting order parameter sets in, rather than a magnetic order or a change in structure. Further evidence for this comes from a sudden increase in the slope of $H_{c1}(T)$ at T_c^- (Vincent *et al.*, 1991), indicating an increase in condensation energy at that point (see Sec. V.D).

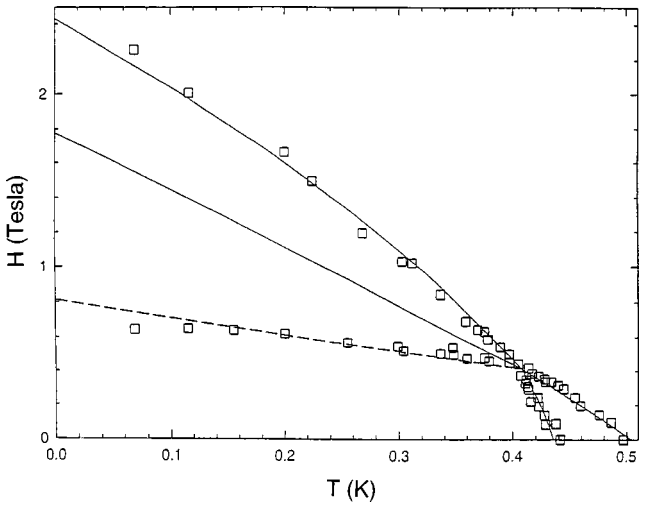

FIG. 14. Phase diagram for $\vec{H}$ in the *a*-*b* plane. Data (squares) are sound velocity measurements of Adenwalla *et al.* (1990) and the line is a theoretical fit from Park and Joynt (1995) using an E_{1g} gap structure.

2. Ginzburg-Landau theory

In the E_{1g} and E_{1u} representations, the order parameter transforms as a complex vector under in-plane rotations, and it makes good sense to write it as $\vec{\eta}=(\eta_x,\eta_y)$. [This was (a_1,a_2) above, but the η notation

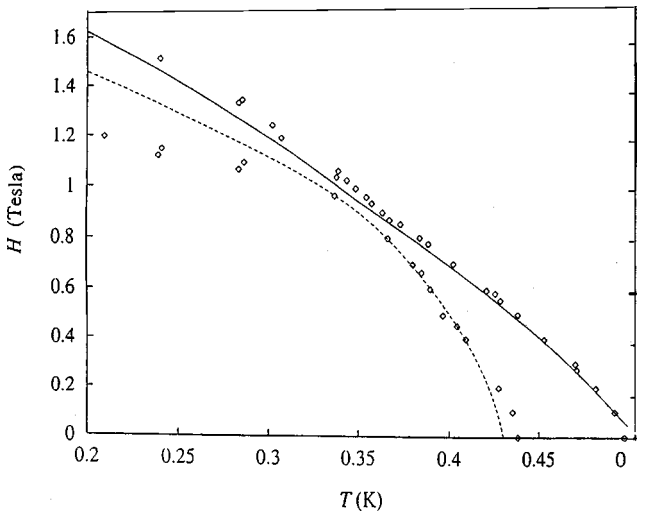

FIG. 15. Phase diagram for $\vec{H}$ along the c axis. Data (squares) are sound velocity measurements of Adenwalla *et al.* (1990) and the line is a theoretical fit from Park and Joynt (1995) using an E_{1g} gap structure.

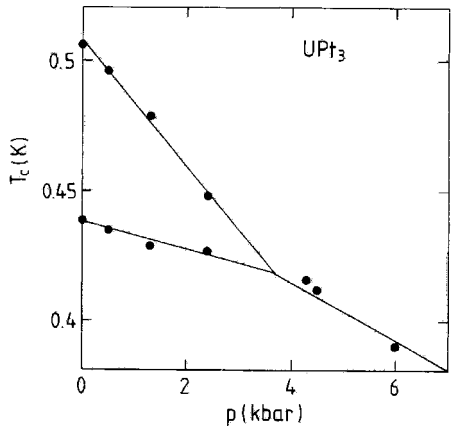

FIG. 16. Pressure-temperature phase diagram for hydrostatic pressure, as determined by specific heat. From Löhneysen, Trappmann, and Taillefer, 1992.

is conventional.] The free energy F therefore includes terms that are the usual two-dimensional scalars. The transformation properties of the E_{2g} and E_{2u} representations, exemplified by the functions in Table II, are less familiar, but the free energies of E_1 and E_2 are isomorphic in zero field and it makes sense to use the same notation for both. Because of this isomorphism, these two theories make the same predictions for the zero-field phase diagram.

At first, the presence of the staggered magnetization $\vec{M}_S$ will be ignored. Thus $F=\int f dV$ with

$$f(\vec{\eta})=\alpha_0(T-T_{c0})\,\vec{\eta}\cdot\vec{\eta}^*+\beta_1(\vec{\eta}\cdot\vec{\eta}^*)^2+\beta_2|\vec{\eta}\cdot\vec{\eta}|^2. \tag{25}$$

The parameters appearing in this expression are to be determined later, either by calculation from microscopic theory (difficult at the present stage of knowledge) or by comparison to experiment. The second quartic term arises because of the complex nature of $\vec{\eta}$, which makes f depend on the relative phase of η_x and η_y. Minimization of F gives two possible phases depending on the sign of β_2: $\beta_2>0$ gives $\vec{\eta}=\eta_+(T)(1,i)$ and $\beta_2<0$ gives $\vec{\eta}=\eta_-(T)(1,0)$, with $\eta_+(T)^2=\alpha_0(T_{c0}-T)/2\beta_1$ and $\eta_-(T)^2=\alpha_0(T_{c0}-T)/2(\beta_1+\beta_2)$. As emphasized above, these two phases have very different properties. It is important to note that symmetry operations may be performed on these phases to obtain equivalent, degenerate ones. For example, $\vec{\eta}=\eta(1,-i)$ is equivalent to $\vec{\eta}=\eta(1,i)$ by time-reversal symmetry. Sixfold anisotropy appears only at sixth order in $|\vec{\eta}|$ and is neglected in Eq. (25). At this level, $\vec{\eta}=\eta(1,0)$ is equivalent to $\vec{\eta}=\eta(0,1)$, but even with full crystal anisotropy any order parameter may be rotated by a multiple of $\pi/3$ in the x-y plane. These degeneracies may give rise to domains in real samples.

If we include the interaction between superconductivity and magnetism, we obtain

$$f(\vec{\eta})=\alpha_0(T-T_{c0})\,\vec{\eta}\cdot\vec{\eta}^*+\beta_1(\vec{\eta}\cdot\vec{\eta}^*)^2+\beta_2|\vec{\eta}\cdot\vec{\eta}|^2 - b|\vec{M}_S\cdot\vec{\eta}|^2+cM_S^2\vec{\eta}\cdot\vec{\eta}^*. \tag{26}$$

Here $\vec{M}_S$ is the staggered magnetization. In UPt_3, it is parallel to the a^* axis (and to the ordering wave vector $\vec{Q}$) and therefore it breaks the hexagonal symmetry.

We now introduce the effective-field method which will be used repeatedly below. In a situation in which there is more than one order parameter (here $\vec{\eta}$ and $\vec{M}_S$), but the respective critical temperatures are different, an effective free energy is written for the lower transition. The Néel temperature T_N is about ten times the superconducting critical temperature T_c. The magnetic order parameter is thus well established at T_c and $\vec{M}_S$ may be treated as an effective field which acts on $\vec{\eta}$. We choose coordinates such that $\vec{M}_S=M_S\hat{x}$ and set $b>0$, to find

$$f(\vec{\eta})=\alpha_0(T-T_c^+)|\eta_x|^2+\alpha_0(T-T_y)|\eta_y|^2 + \beta_1(\vec{\eta}\cdot\vec{\eta}^*)^2+\beta_2|\vec{\eta}\cdot\vec{\eta}|^2, \tag{27}$$

where $T_c^+=T_{c0}-cM_S^2/\alpha_0+bM_S^2/\alpha_0$ and $T_y=T_{c0}-cM_S^2/\alpha_0$.

There are now two transitions since the effective field breaks the symmetry between x and y. The prediction of two transitions in specific heat was the first successful prediction of the two-component theory (Joynt, 1988). The first transition to appear as the system is cooled is at T_c^+. For T just below T_c^+, $\eta_x^{eq}=[\alpha_0(T_c^+-T)/2(\beta_1+\beta_2)]^{1/2}$ is the equilibrium value of η_x. In the two-component theory, this is the (1,0) phase, identified with phase A. The specific-heat jump is $\Delta C_v^+=T_c^+\alpha_0^2/2(\beta_1+\beta_2)$. To find T_c^-, the temperature of the lower transition, we write an effective free energy for η_y, regarding η_x as an effective field which acts on η_y. We may take η_x real and write $\eta_y=|\eta_y|e^{i\phi}$, so that ϕ is the relative phase of the two components. This gives an effective free-energy density

$$f_{eff}(\eta_y)=\alpha_0(T-T_y)|\eta_y|^2+\beta_1|\eta_y|^4+2(\eta_x^{eq})^2|\eta_y|^2 + \beta_2|\eta_y|^4+2\beta_2(\eta_x^{eq})^2|\eta_y|^2\cos(2\phi). \tag{28}$$

If $\beta_2>0$, the last term is minimized by taking $\phi=\pm\pi/2$. On substituting for η_x^{eq}, we have

$$f_{eff}(|\eta_y|)=\alpha_0(1-\tilde{\beta})(T-T_c^-)|\eta_y|^2+(\beta_1+\beta_2)|\eta_y|^4, \tag{29}$$

with $\tilde{\beta}=(\beta_1-\beta_2)/(\beta_1+\beta_2)$ and $T_c^-=(T_y-\tilde{\beta}T_c^+)/(1-\tilde{\beta})$. The second transition occurs when the coefficient of the quadratic term changes sign, namely, at T_c^-. This is a lower temperature than T_y, which is the bare critical temperature for η_y. The second transition is pushed downwards because of the cross terms in η_y and η_x. This phenomenon is akin to a repulsion between the two transitions on the phase diagram. The lower phase in this theory is called the $(1,i)$ phase because of the relative phases of the two components, and it is identified with phase B. Note that the actual ratio of the two components is not $\sqrt{-1}$, but is a pure imaginary, temperature-dependent number. This number should approach i as $T\to 0$ as $\vec{M}_S$ can then be regarded as a perturbation.

The parameters in Eqs. (25) and (26) can only be cal-

TABLE V. Characteristics of the specific heat of UPt_3 in the vicinity of the superconducting transition in zero applied magnetic field and pressure, for all published data on single crystals. The annealing temperature is in °C, T_c in mK, and C/T in $J\,K^{-2}\,mol^{-1}$.

Reference	Annealing	T_c^-	T_c^+	ΔT_c	γ_N	$\Delta C^-/T_c^-$	$\Delta C^+/T_c^+$	ratio
Hasselbach *et al.* (1989)		434	490	56	0.45	0.10	0.21	0.48
Jin, Carter, *et al.* (1992)	950	464	515	51	0.41	0.12	0.24	0.50
Bogenberger *et al.* (1993)	1200	467	523	56	0.44	0.09	0.22	0.42
Brison *et al.* (1994b)	1200	480	530	50	0.44	0.12	0.23	0.52
Isaacs *et al.* (1995)	1230	460	510	50	0.44	0.11	0.23	0.48
Kimura *et al.* (1995)	1200	530	580	50	0.42	0.09	0.20	0.45
Taillefer, Ellman, *et al.* (1997)		431	492	61	0.43	0.09	0.22	0.41
Kycia (1997)	900	495	545	50	(0.44)	0.13	0.25	0.52

culated using microscopic theory, but some constraints from experiment can be noted. We must have $\beta_2>0$. If $\beta_2<0$, then the direction of $\vec{\eta}$ is always fixed relative to $\vec{M}_S$ and there is no second transition. As for c, superconductivity and magnetism are believed to be incompatible, as the two compete for the same Fermi surface. This argument would lead to $c>0$, although the sign of c does not affect any of the measurable quantities in this section. The same is true of b, but it is of greater physical relevance because it determines the relative orientation of $\vec{\eta}$ and $\vec{M}_S=M_S\hat{x}$, thus whether we get a (1,0) order parameter with ($b>0$) or a (0,1) order parameter with ($b<0$) in the A phase. Physically, the difference between (0,1) and (1,0) in the E_{1g} and E_{2u} phases is a gap structure which is rotated by 90° and 45° about the c axis, respectively. These structures lead to differences in ultrasonic attenuation (see Sec. V.C) and vortex lattice orientation (see Sec. V.D.1).

For a discussion of how to perform microscopic calculations of the parameters governing the coupling of magnetism and superconductivity, see Sigrist and Ueda (1991). For an analysis of phases in which $\vec{Q}$ and $\vec{M}_S$ are not parallel or perpendicular, see Joynt (1990).

The effective-field method is useful for finding the lower phase boundary. To get the total specific-heat jump relative to the normal state at the lower transition δC_v^-, one must keep in mind that both $|\eta_x(T)|^2$ and $|\eta_y(T)|^2$ have a kink at T_c^+. Thus the temperature dependence of both below T_c^+ is needed. A straightforward calculation (Sigrist, Joynt, and Rice, 1987; Hess, Tokuyasu, and Sauls, 1989; Machida, Ozaki, and Ohmi, 1989) gives $\delta C_v^- = T_c^-\,(\alpha_0^2/2\beta_1)$. This yields a dimensionless ratio between observable quantities of

$$\frac{\delta C_v^-}{\Delta C_v^+}=\frac{T_c^-(\beta_1+\beta_2)}{T_c^+\beta_1}. \tag{30}$$

Experimentally, the values for the specific heat ratios given in Table V yield $\beta_2/\beta_1=\frac{1}{2}$, using $\delta C_v^-/T_c^- \simeq \Delta C_v^-/T_c^- + \Delta C_v^+/T_c^+$. Weak coupling for two-component theories gives $\beta_2/\beta_1=1$. It is interesting to use the experimental value $\beta_2/\beta_1=\frac{1}{2}$ to investigate some other quantities of interest. The dimensionless quantity $\tilde{\beta}=(\beta_1-\beta_2)/(\beta_1+\beta_2)$ then becomes $\frac{1}{3}$. This allows us to fix the bare critical temperature T_y mentioned above:

$$T_y=(1-\tilde{\beta})T_c^- + \tilde{\beta}T_c^+ . \tag{31}$$

If we take the representative values $T_c^-=0.53$ K and $T_c^+=0.48$ K, then $T_y=0.497$ K. The interaction between η_y and η_x shifts the lower transition from 0.497 K down to 0.48 K, a shift of 17 mK. This in turn yields $bM_S^2/\alpha_0=33$ mK, which is a measure of the strength of the interaction between superconductivity and magnetism.

This is a convenient place to explain some of the differences in the predictions of various theories. The free energy of Eq. (26) applies to the E_{1g} and E_{2u} theories. The order parameter for the spin triplet is a three-component vector $\vec{\eta}'=(\eta_x',\eta_y',\eta_z')$ and the free-energy density is

$$f(\vec{\eta}')=\alpha_0(T-T_{c0})\,\vec{\eta}'\cdot\vec{\eta}'^{*}+\beta_1(\vec{\eta}'\cdot\vec{\eta}'^{*})^2 + \beta_2|\vec{\eta}'\cdot\vec{\eta}'|^2+cM_S^2\vec{\eta}'\cdot\vec{\eta}'^{*}-b\vec{M}_S^2|\eta_x'|^2. \tag{32}$$

As above, we have taken the interaction between $\vec{\eta}'$ and $\vec{M}_S$ to favor a parallel alignment in phase A. Since $\vec{M}_S=M_S\hat{x}$, we therefore have $\vec{\eta}'=\eta'(1,0,0)$ in this phase. At the lower transition, we enter the $(1,i,i)$ phase (in an obvious notation), which is identified with phase B. For the thermodynamic properties, however, the two-component theories and the three-component theory are equivalent. This may be seen by the mapping: $|\eta_x'|^2 \rightarrow |\eta_x|^2$ and $|\eta_y'|^2+|\eta_z'|^2\rightarrow|\eta_y|^2$. If we were to add spin-orbit coupling and a crystal field as a perturbation, the coefficient for $|\eta_z'|^2$ would be different from that of the other two components and the possibility of a third transition arises.

The order parameter for mixed-representation theories is $\Delta=\eta_aF_a(\vec{k})+\eta_bF_b(\vec{k})$ and the free-energy density is

$$f(\eta_a,\eta_b)=\alpha_a(T-T_a)|\eta_a|^2+\alpha_b(T-T_b)|\eta_b|^2 + \beta_a|\eta_a|^4+\beta_b|\eta_b|^4+\beta_{ab}|\eta_a|^2|\eta_b|^2 + \beta_{ab}'(\eta_a^2\eta_b^{*2}+\eta_a^{*2}\eta_b^2). \tag{33}$$

No coupling to the magnetization need be included, since it merely changes the value of the parameters that already appear. If we ignore the quartic cross-coupling terms, we get a specific-heat jump ratio of

TABLE VI. Experimental values of the change in various critical temperatures with pressure (for the four transition lines), as deduced from thermal expansion measurements (van Dijk, 1994).

	$\vec{H}\perp c$ $(H=0.6$ T) NC	$\vec{H}\perp c$ $(H=0.6$ T) BC	$\vec{H}\parallel c$ $(H=1.2$ T) NC	$\vec{H}\parallel c$ $(H=1.2$ T) BC
dT/dP_a (mK/kbar)	-6.5 ± 5	0 ± 50	-4.8 ± 5	0 ± 50
dT/dP_c (mK/kbar)	-0.5 ± 5	-170 ± 50	-3.0 ± 5	-210 ± 50
dT/dP (mK/kbar)	-13.5 ± 8	-170 ± 80	-12.2 ± 8	-210 ± 80

$$\frac{\delta C_v^-}{\Delta C_v^+}=\frac{T_c^-\alpha_b^2\beta_a}{T_c^+\alpha_a^2\beta_b}. \tag{34}$$

In this class of theories $\alpha_a\neq\alpha_b$ and $\beta_a\neq\beta_b$. Hence there is, from the phenomenological theory alone, no relation between the specific-heat jumps, nor even any reason to suppose that they are the same order of magnitude. In this sense, this theory offers no explanation of the fact that the two jumps are of similar height. It can be argued against this that, if $T_a\approx T_b$, then the other coefficients might well be close also when an actual microscopic calculation of the Ginzburg-Landau parameters is done. This would happen if the underlying theory were similar to BCS weak coupling in involving only one parameter (the coupling constant) per representation. The similarity in height of the specific-heat jumps is rather strong evidence against theories in which there is little relation between the nature of the two transitions in spite of their proximity, such as the mixed superconducting-magnetic theory of Blount, Varma, and Aeppli (1990).

In summary, the measured specific heat certainly suggests a superconducting order parameter with two, or possibly three, components which are nearly degenerate. The most apparent mechanism for the splitting of the degeneracy is a coupling to the antiferromagnetism. The evidence for and against this mechanism will be considered below. The comparable size of the jumps constitutes some evidence for the multidimensional representation theories. It does not rule out mixed-representation theories, but it limits their possible forms. It provides evidence that both transitions are due to superconductivity.

3. Other experiments

The superconducting transition at T_c^+ is immediately visible in many types of experiments, but the same is not true for the lower transition. Apart from specific heat, the transition at T_c^- between phase A and phase B was mainly seen in thermal expansion and ultrasound measurements. All measurements agree on the value of T_c^- relative to that of T_c^+. The coefficient of linear thermal expansion along the c axis, $\alpha_c\equiv(1/c)(\partial c/\partial T)$, shows a steplike positive anomaly $[\alpha_c(T_c^++\epsilon)>\alpha_c(T_c^+-\epsilon)]$ at the upper transition of about 0.6 parts per million and a negative anomaly $[\alpha_c(T_c^-+\epsilon)<\alpha_c(T_c^--\epsilon)]$ of about 0.2 parts per million at the lower transition. There is no corresponding signature of the transition in the thermal expansion in the basal plane. The longitudinal sound velocity v_s drops sharply at T_c^+ by a relative amount $\Delta v_s/v_s\approx2\times10^{-5}$ over a temperature range of about 10 mK (Adenwalla *et al.*, 1990; Bruls *et al.*, 1990). At T_c^-, a much smaller but still distinct anomaly is seen. (The lower transition is barely visible in transverse sound.) Sound velocity has been a key tool in mapping the phase diagram as a function of field and pressure, as shown in Figs. 14 and 15. Its relevance at zero field and pressure is mainly that the anomalies observed confirm the specific-heat results. As discussed in detail in Sec. V.C, the attenuation of transverse sound has revealed a clear signature of the transition between phase A and phase B and has provided a powerful probe of the nodal structure of each phase. Finally, note that even though the magnitude of T_c^+ can vary by up to 80 mK or so, the difference in critical temperatures is always roughly the same, $T_c^+-T_c^-=50$ mK (see Table VI). This suggests that disorder affects the two transitions in a similar way, which makes mixed-representation theories involving an s-wave and a d-wave part less attractive.

B. Phase diagram in a magnetic field

The most remarkable set of observations in UPt_3 is the phase diagram in a magnetic field with its three distinct phases. The data are shown for $\vec{H}\parallel\hat{a}$ in Fig. 14. They show the three superconducting phases and the normal phase meeting at a tetracritical point at $H_t=0.44$ T and $T_t=0.39$ K.

In this section we analyze this phase diagram in detail, beginning with a review of the experiments in the first subsection, then turning to the internal phase boundaries in the second. The third and fourth subsections are devoted to the anisotropy between the basal plane and c-axis field directions and the lower critical fields, respectively.

1. Upper critical fields and tetracritical point

The upper critical field $H_{c2}(T)$ of UPt_3 was first measured by Chen *et al.* (1984) and subsequently by many others. The data of Shivaram, Rosenbaum, and Hinks (1986) are shown in Fig. 17 for field directions parallel $(H_{c2}^{\parallel})$ and perpendicular $(H_{c2}^{\perp})$ to the c axis. Although $H_{c2}(T)$ is somewhat sensitive to sample quality, the following basic features have been reproduced in all recent measurements, on a variety of crystals: (1) the magnitude of $H_{c2}(T)$ is large relative to T_c, in keeping with the huge effective masses involved in the orbital response; (2) there is a reversal in the anisotropy $H_{c2}^{\parallel}/H_{c2}^{\perp}$

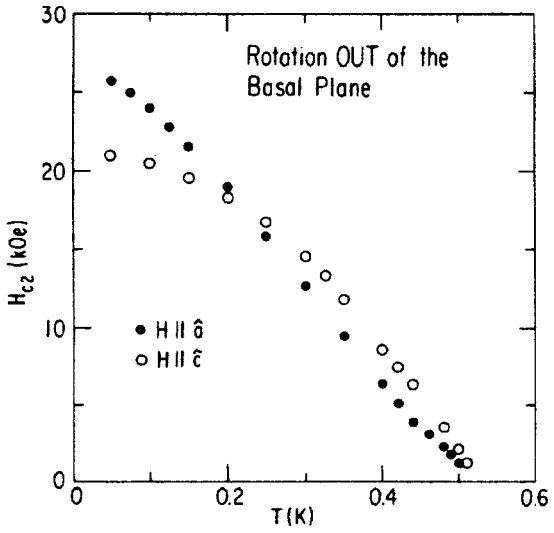

FIG. 17. Upper critical field for field directions parallel (open circles) and perpendicular (filled circles) to the c axis. From Shivaram, Rosenbaum, and Hinks, 1986.

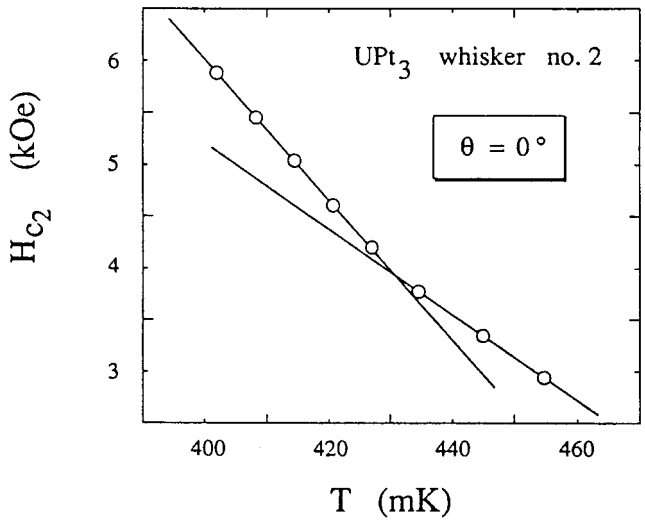

FIG. 18. Upper critical field for field in the basal plane, showing the sharp break in slope (kink) at about 4 Oe. From Taillefer *et al.*, 1990.

at $T\simeq 0.2$ K, with $H_{c2}^{\parallel}>H_{c2}^{\perp}$ near T_c and $H_{c2}^{\parallel}<H_{c2}^{\perp}$ at low temperature; (3) there is an abrupt increase of slope in $H_{c2}^{\perp}(T)$ at $T\simeq T_c^+-0.1$ K, $H\simeq 4$ kOe. The measured value of H_{c2} at $T\to 0$, a property of the C phase, increases with sample quality. In high quality single crystals (Shivaram, Rosenbaum, and Hinks, 1986; Keller *et al.*, 1995) one finds (in tesla)

$$\text{C phase:}\quad H_{c2}^{\parallel}(0)\simeq 2.1\text{ T};\quad H_{c2}^{\perp}(0)\simeq 2.8\text{ T}. \tag{35}$$

A rough estimate of the average coherence length at $T=0$ gives $\xi(0)\simeq\hbar\langle v_F\rangle/\pi\Delta(0)\simeq 120$ Å [using $\langle v_F\rangle=v_{bc}=5000$ m/s and $\Delta(0)\simeq 2k_BT_c$], and a corresponding average upper critical field $\langle H_{c2}(0)\rangle=\Phi_0/[2\pi\xi^2(0)]\simeq 2.3$ T, consistent with the measured values. Note that the coherence length is much shorter than a typical mean free path (in excess of 2000 Å in high quality crystals), so that UPt_3 samples are usually well into the "clean limit."

The slope of $H_{c2}(T)$ at $T_c=T_c^+$ is a property of the A phase, with

$$\text{A phase:}\quad \left(\frac{dH_{c2}^{\parallel}}{dT}\right)_{T_c^+}=-7.2\pm 0.6\text{ T/K};$$

$$\left(\frac{dH_{c2}^{\perp}}{dT}\right)_{T_c^+}=-4.4\pm 0.3\text{ T/K}. \tag{36}$$

Normally, one would be able to relate the value of $H_{c2}(T)$ at $T=0$ with its slope at T_c, but in UPt_3 this is suspect since the former is a property of the C phase. The change of phase is partly responsible for the anisotropy reversal, in addition to the presence of strong Pauli limiting for $\vec{H}\|\hat{c}$. This may be due either to the anisotropy of the susceptibility, as explained in Sec. II.D, or to anisotropy of the order parameter (see below). Figure 18 shows more clearly the "kink" in $H_{c2}^{\perp}(T)$, seen for all directions of $\vec{H}$ in the basal plane (Taillefer *et al.*, 1990).

In the Ginzburg-Landau regime (near T_c,) the a-c anisotropy is a combination of two effects: the angular dependence of the mass tensor (or Fermi velocity) and that of the gap $\Delta(\theta)$. It is striking that in UPt_3, characterized by a highly anisotropic gap structure (well established for the B phase and very likely for the A phase; see Secs. V.B and V.C), the anisotropy in $H_{c2}(T)$ near T_c^+ is precisely given by the mass tensor anisotropy, just as expected for an isotropic order parameter: $(dH_{c2}^{\parallel}/dT)_{T_c^+}/(dH_{c2}^{\perp}/dT)_{T_c^+}=1.64=\sqrt{m_r}$, where the mass ratio $m_r\equiv m_{\perp}/m_{\parallel}=\langle v_c^2\rangle/\langle v_b^2\rangle$. From Sec. II.B, the normal-state transport gives $m_r=2.7=(1.64)^2$. Moreover, the full dependence of H_{c2} on polar angle (near T_c^+) fits the standard mass tensor expression $H_{c2}(\theta)=\sqrt{m_r}H_{c2}(\pi/2)[m_r\sin^2\theta+\cos^2\theta]$. The slope of the thermodynamic critical field $H_c(T)$ in the A phase is dictated by the jump in specific heat ΔC at T_c^+: $(dH_c/dT)_{T_c^+}=-[4\pi\gamma_N(\Delta C/C_N)]^{1/2}\simeq -800$ Oe/K, using the value ΔC at the upper transition given in Table V.

Continuing to use s-wave theory with mass anisotropy for the moment, these data allow us to estimate the Ginzburg-Landau parameter $\kappa^{GL}\equiv\lambda/\xi$, where $\lambda=\lambda_i/\sqrt{m_i}$ and $\xi=\xi_i\sqrt{m_i}$. λ_i is the penetration depth for screening currents along the principal axis i (a, b, or c,) ξ_i is the coherence length describing the spatial variation of the order parameter along the i axis, and m_i is the i component of the normalized effective mass tensor ($m_am_bm_c\equiv 1$). Given that $m_r=m_{\perp}/m_{\parallel}=2.7$, with $m_a=m_b\equiv m_{\perp}$ and $m_c\equiv m_{\parallel}$, we have $\sqrt{m_{\perp}}=1.18$ and $\sqrt{m_{\parallel}}=0.72$, so that for the A phase: $\kappa^{GL}=44$, using data for either field direction: $(dH_{c2}^i/dT)_{T_c^+}=\sqrt{2}(\kappa^{GL}/\sqrt{m_i})(dH_c/dT)_{T_c^+}$ $(i=\parallel,\perp)$.

The large value of κ^{GL} places UPt_3 in the strong type-II limit of magnetic behavior, as for all heavy-fermion and cuprate superconductors. The fact that λ

$\gg\xi$ implies that the electrodynamic properties of UPt_3 can be treated in the local (or London) approximation. In this limit, the penetration depth is a simple and direct measure of the superfluid density. At $T=0$, the magnitude of λ is governed by the mass m and the conduction-electron density n: $\lambda(0)=(mc^2/4\pi ne^2)^{1/2}=c/\overline{\omega}_p$, where $\overline{\omega}_p$ is the average plasma frequency given, for example, by $\hbar\overline{\omega}_p=[2.2\times10^{-6}\ \text{eV}](m_i/\rho_{0,i}\tau_0)^{1/2}$ $(i=\|,\perp)$, with $\rho_{0,i}$ in $\mu\Omega$ cm and τ_0 in sec. Using the values derived from normal-state transport (Sec. II.B), we get $\hbar\overline{\omega}_p=0.37$ eV $(4.8\times10^{14}\ \text{sec}^{-1})$ and $\lambda(0)=6250$ Å, so that $\lambda_\|(0)=4500$ Å, $\lambda_\perp(0)=7400$ Å. These are the components of the penetration depth one would expect to measure in the B phase. If we assume that $\kappa^{GL}=44$ in the B phase as well as the A phase, then $\xi(0)=\lambda(0)/\kappa^{GL}\simeq140$ Å, and $\xi_\|(0)\simeq190$ Å, and $\xi_\perp(0)\simeq120$ Å. This Ginzburg-Landau estimate for $\xi(0)$ agrees well with our previous BCS estimate. A very rough independent estimate for κ^{GL} appropriate for low temperatures is obtained by ignoring gap anisotropy and using weak-coupling expressions for the condensation energy and the zero-temperature gap: $H_c^2(0)\simeq4\pi N_F\Delta^2(0)\simeq12\times(1.76)^2\gamma_N(k_BT_c)^2/\pi$, which gives $H_c(0)\approx550$ Oe, so that $\kappa^{GL}=\sqrt{m_\perp}H_{c2}^\perp(0)/[\sqrt{2}H_c(0)]\approx46$. This is an indication that UPt_3 is not too far from weak coupling.

For a review of upper critical fields in UPt_3 and other heavy-fermion superconductors, see Keller *et al.* (1995).

The first direct evidence of an additional phase boundary in UPt_3 came from measurements of the ultrasonic attenuation as a function of applied field (Müller *et al.*, 1986; Qian *et al.*, 1987). Early indications of a phase transition induced by a magnetic field also came from accurate measurements of $H_{c2}(T)$, which revealed a sudden change of slope near 0.4 T (Rauchschwalbe *et al.*, 1985; Taillefer, Picquemal, and Flouquet, 1988). The existence of a tetracritical point where the three superconducting phases meet was first proposed on the basis of specific-heat measurements in a magnetic field (Hasselbach, Taillefer, and Flouquet, 1989). The most complete tracing of the phase boundaries was done by locating the anomalies in the longitudinal sound velocity (Adenwalla *et al.*, 1990; Bruls *et al.*, 1990). The resulting phase diagram agrees with measurements of specific heat in applied fields (see Taillefer, 1990), with magnetostriction measurements (van Dijk *et al.*, 1993a), and with the magnetocaloric effect (Bogenberger *et al.*, 1993; Löhneysen, 1994) in the regions of temperature and field where there is overlap.

The tetracritical point is a rather remarkable structure that was analyzed from the purely thermodynamic point of view by Yip, Li, and Kumar (1991). If the four boundaries that meet at this point all correspond to second-order phase transitions, there are relations between the four specific-heat jumps across these lines and the slopes of the lines entering the point. This follows solely from the fact that the entropy is a continuous and single-valued function near the tetracritical point. These relations were verified by van Dijk *et al.* (1993b). They measured thermal expansion coefficients near the tetracritical point to determine the critical field slopes and used specific-heat measurements from Hasselbach, Taillefer, and Flouquet (1990). A violation would indicate that some of the transitions are first order. This conclusion that all boundaries are second order is also consistent with the fact that no hysteresis is ever observed. Other investigators (Adenwalla *et al.*, 1992) argued that the BC transition is weakly first order, but their analysis seems to imply that the ratio of specific-heat steps across the A-B boundary is zero, which is not consistent with experiment (see van Dijk *et al.*, 1993b, for details). It now seems safe to say that all four boundaries are really second order.

The rough analysis of upper critical fields using only mass anisotropy in a one-component theory gives insight into parameter magnitudes, but it obviously cannot produce multiple phases. Thus we now continue the development of multicomponent theories begun in Sec. IV.A. The application of a field produces a nonuniform order parameter and requires the introduction of gradient terms in the free energy. The minimization of the resulting functional is more complicated than the calculations done above for zero field. We shall focus on the case of $\vec{H}$ in the basal plane, as it is much simpler from the calculational point of view.

Unlike the zero-field calculations, there are substantial differences even between different two-component theories, so we subdivide the presentation.

a. E_{1g} theory

The uniform free-energy density is most conveniently written as

$$f_u=\alpha_0(T-T_c^+)|\eta_x|^2+\alpha_0(T-T_y)|\eta_y|^2+\beta_1(\vec{\eta}\cdot\vec{\eta}^*)^2+\beta_2|\vec{\eta}\cdot\vec{\eta}|^2, \tag{37}$$

and the gradient terms are

$$f_g=K_1\sum_{i,j=x,y}D_i\eta_jD_i^*\eta_j^*+K_2\sum_{i,j=x,y}D_i\eta_iD_j^*\eta_j^*+K_3\sum_{i,j=x,y}D_i\eta_jD_j^*\eta_i^*+K_4\sum_{i=x,y}|D_z\eta_i|^2. \tag{38}$$

The total free-energy density is $f=f_u+f_g$. Here we have defined the covariant derivatives: $D_i=\partial/\partial x_i+2ieA_i/\hbar c$, where $-e$ is the charge on the electron. The sixfold rotation axis is the z axis, and the direction of the order parameter is confined to the basal plane. Thus the sums run only over the in-plane coordinates x and y. The gradient terms in Eq. (38) are the most general allowed in two-component theories in the absence of magnetism. Some effect of $\vec{M}_S$ is implicitly contained in the uniform part of f in Eq. (37) by distinguishing between T_c^+ and T_y. The gradient terms of Eq. (38) do not include the breaking of hexagonal symmetry due to the appearance of $\vec{M}_S$. This means we have neglected the coupling of the magnetization to the supercurrent. We shall remedy this defect below by adding additional terms to Eq. (38). For the moment, this complication is neglected.

The first problem is to determine $H_{c2}(T)$. This is done in the usual fashion. One first minimizes the quadratic part of $F=\int f dV$ with respect to the functional form of $\vec{\eta}(\vec{r})$, which corresponds to finding the lowest eigenvalue of a linear operator. This determines the equilibrium form of $\vec{\eta}$. Once this form is substituted in the free energy, we can determine the location of the phase boundary by asking for what values of H and T the coefficient of the quadratic term changes sign. Details of calculations of this kind are given by Volovik (1988), Hess *et al.* (1989), Machida and Ozaki (1989), Sundaram and Joynt (1989), and Garg (1992).

We make the standard assumption that the order parameter is uniform along the direction of the field. Interestingly, this is not valid for all values of the parameters K_i (Garg, 1992). In fact, for $K_2+K_3>3.126K_1$, a nonuniform state is stable. However, this parameter range is not reached in UPt_3 (Park and Joynt, 1995). Nonuniform and even orbitally paramagnetic states have been investigated by Palumbo, Muzikar, and Sauls (1990) and Palumbo and Muzikar (1992a, 1992b), but there appears to be no evidence for them in UPt_3.

Minimizing the volume integral of the quadratic part of f with respect to the form of $\vec{\eta}(z)$ gives two Euler-Lagrange equations and two equations for the critical fields:

$$H_{c2x}(T)=\frac{\hbar c\alpha_0}{2e(KK_4)^{1/2}}(T_c^+-T),$$

$$H_{c2y}(T)=\frac{\hbar c\alpha_0}{2e(K_1K_4)^{1/2}}(T_y-T). \tag{39}$$

Here $K=K_1+K_2+K_3$. Given that $K>K_1$ and $T_c^+>T_y$, these two lines cross at the point (T_t,T_t). $H_{c2}(T)$ is given by the greater of the two, so $H_{c2}=H_{c2x}, H<H_t$, and $H_{c2}=H_{c2y}, H>H_t$, where

$$H_t=\frac{\hbar c\alpha_0}{2e(K_1K_4)^{1/2}}(T_c^+-T_y), \quad T_t=\frac{T_y\sqrt{K}-T_c^+\sqrt{K_1}}{\sqrt{K}-\sqrt{K_1}}. \tag{40}$$

In other words, H_{c2} has a kink at (H_t,T_t). Bear in mind that T_y is the bare lower critical temperature, not the actual one. Hence the NC phase boundary extrapolates back to the temperature axis to a point between T_c^+ and T_c^-. Therefore the very peculiar shape of the H_{c2} curve, with its very abrupt change in slope (Taillefer *et al.*, 1990), is well explained in the two-component theory, at least for $\vec{H}\perp\hat{c}$.

Computing the H_{c2} curve is analogous to finding the ground state of a particle in a magnetic field. The quantum-mechanical analog in the present case is a two-component spinor problem, with the components coupling in a different fashion to the external field, but not mixing. This leads to a level crossing and the kink. The reason for the crossing must be a symmetry. In this case the system is symmetric under reflection in the x-z plane.

The ratio of H_{c2} slopes $(\partial H_{c2}/\partial T)=H'$ below and above the kink is given by $H'_{NA}/H'_{NC}=(K_1/K)^{1/2}$. ($H_{XY}$ is the field at the boundary between phases X and Y.) This is one of the better measured quantities in UPt_3, as the upper critical field lines are rather linear for this direction of the applied field. Detailed measurements give values from 0.65 (Taillefer *et al.*, 1990) leading to $(K_1/K)\approx 0.42$.

In E_{1g} the in-plane stiffness constants K_1, K_2, and K_3 are generally of the same order of magnitude. Particle-hole symmetry and weak-coupling theory in fact lead to $K_2=K_3$ and $K_1=K_2+K_3$. This gives the above ratio as $K_1/K=0.5$, which is very reasonable agreement with experiment, which speaks strongly in favor of this theory. The same parameters give a reasonable fit to the less easily calculable AB and BC phase boundaries (Park and Joynt, 1995), to be discussed below.

b. E_{2u} theory

The free-energy density in the E_{2u} theory has the same structure as in Eqs. (37) and (38). However, it differs from E_{1g} in that $K_2\ll K_1$ and $K_3\ll K_1$. This arises from the fact that these two parameters are averages of the Fermi velocity over rather high in-plane angular harmonics in this theory (Sauls, 1994). According to Eq. (39), η_x and η_y have the same slope for the upper critical field. This would lead to no kink in H_{c2}, and in fact to a very different phase diagram than is observed. The E_{2u} theory relies on a different mechanism to produce the kink (Sauls, 1994), which we now discuss.

The idea is to introduce a coupling between the magnetism and the supercurrent which is allowed by symmetry. To the free-energy density in Eqs. (37) and (38), one adds a term

$$f_{ms}=K_{ms}\sum_{i=x,y}(|D_i\eta_x|^2-|D_i\eta_y|^2). \tag{41}$$

Here K_{ms} is proportional to $\vec{M}_S^2$. This gives a different slope to the two H_{c2} lines for the two components of $\vec{\eta}$. It leads then by precisely the same mechanism as above to the kink in the upper critical field:

$$H_{c2x}(T)=\frac{\hbar c\alpha_0}{2e[(K_1+K_{ms})K_4]^{1/2}}(T_c^+-T)$$

and

$$H_{c2y}(T)=\frac{\hbar c\alpha_0}{2e[(K_1-K_{ms})K_4]^{1/2}}(T_y-T). \tag{42}$$

In this theory, there is no natural explanation for the ratio of slopes, as there was in E_{1g}.

The physical upper critical field is given by $H_{c2}=H_{c2x}, H<H_t$ and $H_{c2}=H_{c2y}, H>H_t$, where

$$H_t=\frac{\hbar c\alpha_0}{2eK_4^{1/2}}\frac{1}{\sqrt{K_1+K_{ms}}-\sqrt{K_1-K_{ms}}} \tag{43}$$

and

$$T_t=\frac{T_y\sqrt{(K_1+K_{ms})}-T_c^+\sqrt{(K_1-K_{ms})}}{\sqrt{(K_1+K_{ms})}-\sqrt{(K_1-K_{ms})}} \tag{44}$$

are the formulas for the tetracritical point. In the E_{1g} theory, the current coupling term is also present, but for this direction of the field it changes only the effective values of K_1 and K. Note that the sign of the coupling K_{ms} is crucial for E_{2u}. Magnetism must favor one component of $\vec{\eta}$ in the uniform limit but relatively suppress gradients of this same component.

The identification of the A and C phases of UPt_3 for the field in the basal plane is the same for E_{1g} and E_{2u}. In the A phase, we have $\vec{\eta}=(\eta,0)$ in the A phase and $\vec{\eta}=(0,\eta)$ in the C phase. The physics of this is quite simple. At low applied fields, the orienting effect of the magnetization on $\vec{\eta}$ is the most important, while at high fields, $\vec{\eta}$ is aligned by the field. Furthermore, in the A and C phases, the free energy reduces to that of a one-component superconductor with mass anisotropy. Therefore the flux lattice in these phases is predicted to be of the centered rectangular form. The C phase has lines of nodes along both vertical and horizontal directions. This could lead to a $\sqrt{H}$ dependence in the specific heat at low temperatures (Volovik, 1988). This prediction is hard to test in UPt_3, as will be seen in Sec. V.A.

c. Mixed-representation theories

Mixed-representation theories can lead to very different results, depending on the choice of representations. The only one that has been worked out in any detail is the AB theory (Chen and Garg, 1993, 1994). We remind the reader that "AB" in this context refers to a mixture of an A_1 or A_2 representation with a B_1 or B_2 representation, not to the AB transition. For clarity in this section, we shall demote the letters for the theory to lower case. The free-energy density is of the form $f^{ab}=f_u^{ab}+f_g^{ab}$, with

$$\begin{aligned}f_u^{ab}=&\alpha_0(T-T_a)|\eta_a|^2+\alpha_0(T-T_b)|\eta_b|^2+\beta^a|\eta_a|^4\\&+\beta^b|\eta_b|^4+\beta_1^{ab}|\eta_a|^2|\eta_b|^2+\beta_2^{ab}[(\eta_a\eta_b^*)^2\\&+(\eta_b\eta_a^*)^2],\end{aligned} \tag{45}$$

and

$$\begin{aligned}f_g^{ab}=&K_a\sum_{i,j=x,y}|D_i\eta_a|^2+K_b\sum_{i,j=x,y}|D_i\eta_b|^2\\&+K_a'|D_z\eta_a|^2+K_b'|D_z\eta_b|^2.\end{aligned} \tag{46}$$

There are no terms for which the field mixes the two components η_a and η_b at this order. This is the reason for this choice of representations. This theory is therefore somewhat simpler than the two-component theories. For a fixed field direction in the basal plane, it is isomorphic to the two-component theories and cannot be distinguished on qualitative grounds. In terms of the parameters in Eqs. (45) and (46), the tetracritical point is at (H_t,T_t), with

$$H_t=\frac{\alpha_0\hbar c}{e}\,\frac{T_a-T_b}{2}\,\frac{1}{\sqrt{K_bK_b'}-\sqrt{K_aK_a'}}, \tag{47}$$

$$T_t=\frac{T_a-T_b}{2}-\frac{T_a+T_b}{2}\,\frac{\sqrt{K_bK_b'}-\sqrt{K_aK_a'}}{\sqrt{K_bK_b'}+\sqrt{K_aK_a'}}. \tag{48}$$

This theory also gives no natural explanation of the ratio of slopes.

d. Spin-triplet theory

The spin-triplet theory has qualitatively different behavior from the other theories in a field. The free-energy density can be written as $f^t=f_u^t+f_g^t$, with

$$\begin{aligned}f_u^t=&\alpha_0^t(T-T_{c0})\,\vec{\eta}\cdot\vec{\eta}^*+\beta_1(\vec{\eta}\cdot\vec{\eta}^*)^2+\beta_2|\vec{\eta}\cdot\vec{\eta}|^2\\&-\gamma M_S^2(2|\eta_x|^2-|\eta_y|^2-|\eta_z|^2),\end{aligned} \tag{49}$$

and

$$f_g^t=K_1^t\sum_{i=x,y;j=x,y,z}|D_i\eta_j|^2+K_2^t\sum_{j=x,y,z}|D_z\eta_j|^2 \tag{50}$$

(Machida and Ozaki, 1991; Machida, Ozaki, *et al.*, 1993). Here, we have again assumed that $\vec{M}_S$ is in the $\hat{x}$ direction. The A phase has the form $\vec{\eta}=(\eta,0,0)$. In this theory there is, at this level, no kink in the $H_{c2}(T)$ curve.

This theory originally postulated the following mechanism to produce the kink. Apart from the coupling of the applied field to the currents, which is linear in $\vec{H}$, there are paramagnetic terms which arise as soon as $H>H_{c1}$, i.e., as soon as the field penetrates the sample. These are quadratic in $\vec{H}$ and take the form

$$f_{2m}=a_zH_z^2\,\vec{\eta}\cdot\vec{\eta}^*+a_x(H_x^2+H_y^2)\,\vec{\eta}\cdot\vec{\eta}^*+a_d|\vec{H}\cdot\vec{\eta}|^2. \tag{51}$$

The three components, one having a high T_c, the other two having a lower T_c, have the same slope for the $H_{c2}(T)$ curve in the absence of these terms. When they are present at finite field, the second term will mean that the slopes are different. If a_d is positive, then the component of $\vec{\eta}$ parallel to $\vec{H}$ will be suppressed by the field. As long as this is the one belonging to the higher T_c, we can get a crossing of the H_{c2} curves. This happens not because the initial slopes of the curves are different, but because their curvatures are different. Thus, in this theory, the kink in H_{c2} is due to an effect that is nonlinear in the applied field. This is not obviously consistent with the experimental H_{c2} curve for this direction of the field, which is rather linear for $H\leqslant H_t$. Still, the linearity is somewhat sample dependent, and the spin-triplet theory gives a reasonable account of the phase diagram for this direction of the field. In a later version of this theory, the proposers note that the coupling of the current to the magnetization can also produce the tetracritical point (Machida, Ozaki, *et al.*, 1993), as in the E_{2u} theory.

We have thus far concentrated on the kink in H_{c2} and the AB tranisition. Theory does reasonably well in de-

scribing these features of the phase diagram. What about more global features of the diagram? Can we predict a real tetracritical point? What is the nature of the three phases at finite field?

These questions may be answered by focusing on the CB transition (Joynt, 1991). We start in the C phase, i.e., at a point (H,T) with $H>H_t$, $\vec{H}=H\hat{x}$, and $T<T_t$. At this point $\vec{\eta}=[0,\eta_y(x,z)]$, and $\eta_y(x,z)$ has a known analytic form if H is sufficiently close to H_{c2}, meaning in this case that (H,T) is sufficiently close to (H_t,T_t). We now fix T and reduce H. We again use the effective-field method, this time to write an effective free energy for η_x.

The Euler-Lagrange equation that results is

$$0=\frac{\delta F}{\delta \eta_x^*}=\alpha_0(T_c^- - T)\,\eta_x - KD_x^2\eta_x - K_4 D_z^2\eta_x + 2\beta_1|\eta_y|^2(x,z)\,\eta_x + 2\beta_2\eta_y^2(x,z)\,\eta_x^* + \mathcal{O}(\eta_y^3). \tag{52}$$

This is a Schrödinger equation for η_x. We see that the terms that result from the coupling of η_x and η_y now act as a potential in which the fictitious particle moves.

The lattice is commensurate with the field with one flux quantum passing through each unit cell. Our problem is therefore that of a particle in a periodic crystal potential with a commensurate magnetic field. This, together with fact that η_x must lie in the lowest Landau level near H_{c2}, allows one to solve for η_x. The general solution is

$$\eta_x=\eta_{x0}\sum_{n=-\infty}^{\infty} c_n e^{iz_0x/\ell^2}\exp\left(inq(z+z_0)/\ell - \frac{1}{2}(K_4/K)^{1/2}(x+x_0+nq\ell)^2/\ell^2\right). \tag{53}$$

This equation corrects two misprints which appeared in Eq. (5) of Joynt (1991). With the c_n and q parameters properly chosen, it represents a centered rectangular lattice for η_x with the origin of the coordinates at (x_0,z_0). When the eigenvalue corresponding to this solution passes through zero, η_x will appear and we are in the B phase via a second-order transition. $|\eta_x|^2$ has the same periodicity as $|\eta_y|^2$. Because the new lattice fits in the registry with the old, the CB transition does not change the structure of the lattice: in the B phase just below the CB boundary it is centered rectangular with the same aspect ratio as in the C phase. This is a consequence of Bloch's theorem and makes the designation of the CB boundary as the "flux lattice line," as it has sometimes been called, inappropriate. The actual evolution of the structure of the flux lattice will be discussed in more detail in Sec. V.D.1. Here we focus on the phase diagram itself.

The free energy which now results when the spatial forms of η_x and η_y have been substituted in is remarkably simple:

$$F=-\alpha_0[T-T_c^+(H)]\langle|\eta_x|^2\rangle-\alpha_0[T-T_y(H)]\langle|\eta_y|^2\rangle \tag{54}$$

$$+\tilde{\beta}_x\langle|\eta_x|^2\rangle^2+\tilde{\beta}_y\langle|\eta_y|^2\rangle^2+\tilde{\beta}_{xy}\langle|\eta_x|^2\rangle\langle|\eta_y|^2\rangle. \tag{55}$$

Here

$$T_y(H)=T_x-\frac{2e}{\hbar c\alpha_0}(K_1K_4)^{1/2}H,$$

$$T_c^+(H)=T_c^+-\frac{2e}{\hbar c\alpha_0}(KK_4)^{1/2}H \tag{56}$$

describe the bare H_{c2} curves and the $\tilde{\beta}_i$ are Abrikosov parameters. Details are given in Park and Joynt (1995). Inspection of the free energy of Eq. (55) for any fixed H reveals that it is essentially the same as the zero-field free energy. We need only make the replacements $|\eta_x|^2 \rightarrow\langle|\eta_x|^2\rangle$ and so on. The coupling constant β_1 is replaced by the renormalized constants $\tilde{\beta}_x,\tilde{\beta}_y$ and β_2 becomes $\tilde{\beta}_{xy}$.

The AB transition at finite field is computed in an exactly analogous fashion. In the above Eqs. (52)–(55) we need only interchange K and K_1 and η_x and η_y everywhere. The Abrikosov parameters also come out differently, since they are computed in the C lattice structure. These differences only amount to quantitative changes, however. Hence there is a beautiful symmetry between the BC transition and the AB transition.

This symmetry immediately implies that there are two transition as a function of T for any fixed H. The only exception is where $H=H_t$, when the two transitions become degenerate. The two-component theory leads unavoidably to the phase diagram observed for $\vec{H}$ in the basal plane, including the tetracritical point. A fit using parameters from an E_{1g} theory (Park and Joynt, 1995) produces very good phase boundaries, as shown in Fig. 14.

2. Lower critical field

We saw above that the magnitude of H_{c2} for different directions was consistent with the simple assumption of mass anisotropy in a one-component theory. We might expect that the lower critical field $H_{c1}(T)$ would be determined by the same parameters, λ, ξ, $m_\perp$, and $m_\parallel$. With the values arrived at above, we may use the relation $H_{c1}(T)=\ln(\kappa_{GL})H_c^2(T)/H_{c2}(T)$ to obtain the predicted values: $(dH_{c1}/dT)_{T_c^+}=-34(-45)$ Oe/K for $\vec{H}\|\hat{c}$ $(\vec{H}\perp\hat{c})$, and $H_{c1}(0)=55(41)$ Oe for $\vec{H}\|\hat{c}$ $(\vec{H}\perp\hat{c})$. As we shall see, these are much lower than the values extracted from existing experiments.

Attempts to measure the lower critical field $H_{c1}(T)$ of UPt_3 have been made by a few groups using different techniques (Shivaram *et al.*, 1989; Vincent *et al.*, 1991; Zhao *et al.*, 1991). This is a much more tricky measurement than that of $H_{c2}(T)$, and the results vary considerably. The data of Vincent *et al.* (1991), obtained in an M vs T measurement at fixed H, are shown in Fig. 19. The qualitative features are (1) a virtually isotropic $H_{c1}(T)$ over the whole temperature range, and (2) a sudden increase in slope occurring at a temperature T_0 approximately 50 mK below T_c. The slope near T_c^+ is

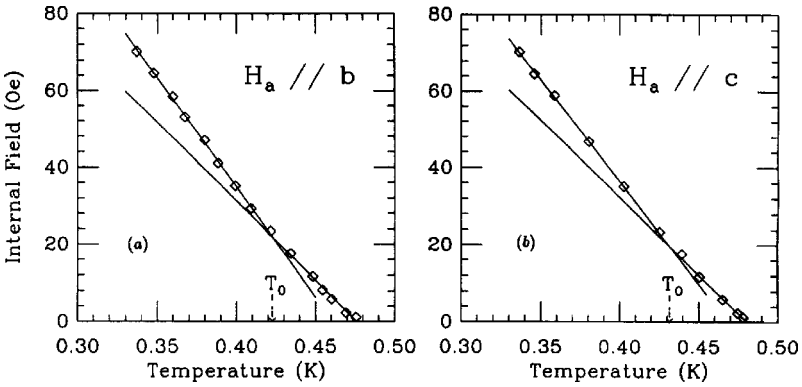

FIG. 19. Lower critical field for fields parallel and perpendicular to the c axis, obtained from magnetization data. From Vincent *et al.*, 1991.

$$\text{A phase:} \quad \left(\frac{dH_{c1}^{\parallel}}{dT}\right)_{T_c^+} \simeq -400 \text{ Oe/K};$$

$$\left(\frac{dH_{c1}^{\perp}}{dT}\right)_{T_c^+} \simeq -410 \text{ Oe/K}, \tag{57}$$

and the ratio of the slope above the kink (below T_0) to the slope below the kink is 1.4 (1.3) for $\vec{H}\perp\hat{c}$ ($\vec{H}\|\hat{c}$). See Sec. IV.B for a calculation which gives this value. These features were confirmed by Zhao *et al.* (1991) in an M vs H measurement at fixed T, but with different values: $T_c^+ - T_0 \simeq 100$ mK, the (isotropic) slope at T_c is 60% lower, and the ratios are 1.2 (1.3). Using an LC resonator technique, Shivaram, Gannon, and Hinks (1989) obtained much lower values, a large anisotropy, and a kink only for $\vec{H}\perp\hat{c}$. The most significant result is the observation of an increase in dH_{c1}/dT, evidence that the condensation energy increases at $T_0 \simeq T_c^-$, as it must if a second superconducting order parameter sets in at the lower transition. Quantitatively, however, the behavior of $H_{c1}(T)$ is unexpected given the upper critical field data. From the value of dH_{c1}/dT at T_c, an independent estimate of κ^{GL} can be made, and Vincent *et al.* (1991) obtain $\kappa^{GL} \simeq 2.5$.

While we do not expect the standard one-parameter Ginzburg-Landau description to hold quantitatively in UPt_3, the large discrepancy between estimates from H_{c2} and those from H_{c1} remains puzzling. It may also call into question the success of the various measurements in determining the true magnitude of H_{c1} in this system.

In summary, the measured $H_{c2}(T)$ of UPt_3 in the A phase exhibits exactly what is expected for an isotropic order parameter, given the known values of v_F, m_r, and T_c. The system is in the strong type-II limit, with $\kappa_{GL} \simeq 40$, so that the penetration depth is simply given by the London formula, with magnitude given by the plasma frequency and anisotropy governed by the mass ratio, which yields $\lambda_{\|}(0) = 4500$ Å and $\lambda_{\perp}(0) = 7400$ Å. On the other hand, measurements of the magnitude of $H_{c1}(T)$ seem to invalidate this simple picture, with values much larger than expected and much too small an anisotropy. Unfortunately, experiments disagree on the magnitude of H_{c1}, so that the situation is rather inconclusive. The transition to the high-field C phase is clearly detected in $H_{c2}^{\perp}(T)$, while the superconducting nature of the A to B transition is manifest in the increase of $H_{c1}(T)$ at T_c^-.

The theory of the lower critical fields in two-component theories has concentrated not on the magnitude, but rather on the kink in $H_{c1}(T)$. The calculations are simpler than those for the upper critical fields (Hess *et al.*, 1989).

In the Meissner state, the kinetic-energy density of the currents $H^2/8\pi$ is independent of the microscopic state. Hence, the free-energy balance of the various states is not affected by the application of the field. The transition temperature is calculated as in the zero-field case, and we find that it always occurs at T_c^+. Thus the AB phase boundary is vertical in the H-T plane for $H < H_{c1}$.

The $H_{c1}(T)$ curve must have a kink where it intersects the AB boundary. The standard formula for H_{c1} for a one-component superconductor depends only on the energy of a single vortex: $H_{c1} = (\Phi_0/4\pi\lambda_y\lambda_z)\ln\kappa$, where Φ_0 is the flux quantum and the $\ln\kappa$ factor is a correction for the core energy. This formula makes clear that the kinetic energy of the vortex is all that matters, up to logarithmic corrections. This in turn depends only on the superfluid density ($\propto 1/\lambda^2$), which is proportional to $|\eta_x|^2$ in the A phase, and H_{c1} is therefore linear near T_c^+. In the B phase the superfluid density is proportional to a sum of $|\eta_x|^2$ and $|\eta_y^2|$ weighted by the appropriate stiffness constants. Since both $|\eta_x^2|(T)$ and $|\eta_y^2|(T)$ have a kink at T_c^-, $H_{c1}(T)$ has a kink there as well. The relative magnitude of the kink may then be computed by simply combining Maxwell's equations with the expression for the current $\vec{j} \sim \delta F/\delta\vec{A}$ to get the penetration depths. Let us denote the slope of H_{c1} just above (below) T_c^- as $dH_{c1}/dT|_{+(-)}$. The result, ignoring core contributions, is then (Sarma *et al.*, 1992)

$$\frac{dH_{c1}/dT|_-}{dH_{c1}/dT|_+} = \frac{1}{4}\left(1+\frac{\beta_2}{\beta_1}\right)\left(3+\frac{K_1}{K}\right). \tag{58}$$

Combining data from various experiments now gives a rough consistency check on the two-component theory. The data of Vincent *et al.* (1991) give

$$\frac{dH_{c1}/dT|_-}{dH_{c1}/dT|_+} \approx 1.4, \tag{59}$$

while we had $\beta_2/\beta_1 \approx 0.5$ from specific-heat experiments and $K_1/K \approx 0.5$ from $H_{c2}(T)$. Substituting these two values into the right-hand side of Eq. (58), we obtain 1.31. This is very reasonable agreement considering the accuracy of the data and the fact that the experiments were performed on different samples.

3. In-plane anisotropy of the upper critical field

One of the simplest but most important of all experimental results is the observation that the in-plane anisotropy of H_{c2} is very small and that the anisotropy is sixfold, not twofold (Keller *et al.*, 1994, 1995). The magnitude of the anisotropy in the resistivity at fixed $|\vec{H}|$ from peak to valley is a maximum of 3% and changes sign at $T=437$ mK. These results can be explained by assuming that $\vec{M}_S$ rotates with the field so as to remain perpendicular to it (Sauls, 1996) and that $|\vec{M}_S|$ is thereby modulated. This is achieved by adding a term $\sim|\vec{M}_S|^6 \cos 6\theta_M$ (in an obvious notation) to the free energy.

The reason for the importance of these observations is that the hypothesis that the magnetization rotates with the field is absolutely central to all the theories of H_{c2} presented in this section except for the mixed-representation theories. Each depends on the same physical picture of the two in-plane components of the order parameter having different H_{c2} values depending on whether they are parallel or perpendicular to $\vec{H}$. The direction of the component that condenses at T_c^+, however, is fixed by the direction of the magnetization. In order for there to be in-plane isotropy of the phase diagram, which there is (to within 3%), the magnetization must rotate in field. If not, and the magnetization direction is fixed, the slopes of the NA and AB boundaries would be interchanged when the field is rotated by 90° in the plane. This would be in gross contradiction to the observations.

In fact, the hypothesis of magnetization rotation is in apparent contradiction with an experiment of Lussier, Taillefer, *et al.* (1996). An in-plane field of 3.2 T was applied, and the magnetic Bragg diffraction was observed. The sixfold symmetric pattern, interpreted as three equally populated domains, was unaffected by the field and interpreted as ruling out the idea of magnetization rotation. This interpretation has been called into question by Moreno and Sauls (2001). If it holds up, it would invalidate the overall theoretical analysis of the phase diagram. Mixed representation theories would become much stronger as candidates for the order parameter.

4. Magnetic field along the *c* axis

The phase diagram of UPt_3 when $\vec{H}$ is along the *c* axis shows interesting similarities and differences from that when $\vec{H}$ is in the basal plane. The data from Adenwalla *et al.* (1990) are shown in Fig. 15. The H_{c2} curve is much smoother. It is not entirely clear whether there is a kink or just a sudden change in curvature near the point $H_z = 0.9$ T and $T_z = 0.35$ K. The inner transition line is much smoother, shows no kink, and has considerable curvature even at low fields. The point (H_z, T_z) where the two lines meet (or come very close together) is rather far from the tetracritical point when $\vec{H}$ is in the basal plane, but ultrasonic measurements of the phase diagram at intermediate angles make it clear that the tetracritical point structure evolves in a continuous fashion from one to the other (Lin *et al.*, 1994a, 1994b). The lines meet to within an accuracy of about 5 mK for all directions. Still, when $\vec{H}$ is in the basal plane, four rather straight lines appear to meet, but this is not the case when $\vec{H}$ is along the *c* axis. Furthermore, there seems to be reciprocal curvature in the inner and outer boundaries reminiscent of level repulsion effects in quantum theory. An acceptable theory should explain both the similarities and the differences observed in the two directions.

a. E_{1g}

The Ginzburg-Landau theory of the phase diagram is similar in principle to that for the basal plane direction but in practice the calculations are more complex. Detailed analysis of the equations (Sundaram and Joynt, 1989; Zhitomirskii, 1989) leads to the conclusion that different Landau levels are coupled. All residual symmetries are broken when $\vec{H}\|\hat{c}$ and thus no level crossings are allowed. The E_1 theory is consistent with the data only if the two lines in Fig. 15 do not cross, with the consequence that there are only two superconducting phases: in this picture the A and C phases are not distinct and are connected by a narrow "neck" in the H-T plane, except when $\vec{H}$ is in the basal plane. The data of Fig. 15 can be fit within the E_{1g} theory (Park and Joynt, 1995).

The near crossing of the phase boundaries will occur only if $K_2 \approx K_3$ and then $H = -\hbar c(T_{c1} - T_y)/4eK_{ms}$ is an equation for the field at the near-crossing point. In a pure system with particle-hole symmetry, one does in fact find $K_2 = K_3$, as already noted. The fact that the crossing is narrowly avoided is therefore a consequence of higher-order terms in the underlying theory. The fit obtained by Park and Joynt (1995) is shown in Fig. 15.

There is very little theoretical work on the structure of the B phase near H_{c2} for $\vec{H}\|\hat{c}$. In the E_{1g} theory there are again two flux lattices just below the AB transition. They must be offset from one another in order that the AB transition be second order. The offset vector has not been computed. There is no guarantee that the structure is the same as for $\vec{H}$ in the basal plane, leaving open the interesting possibility of a transition in the vortex lattice as a function of angle.

b. E_{2u}

The E_{2u} picture has $K_2 \approx K_3 \approx 0$ but is nevertheless in some ways similar to the E_1 picture for $\vec{H}\|\hat{c}$, and a simi-

lar fit to the phase boundaries may be attempted. To obtain the near crossing appears to require that K_{ms} be negative. As we saw in the previous section, the E_{2u} theory for the other direction of $\vec{H}$ requires that K_{ms} be positive.

H_{c1} may also be calculated for this field direction (Hess, Tokuyasu, and Sauls, 1989) in the two-component picture. The ratio of slope above and below the kink is given by

$$\frac{dH_{c1}/dT|_-}{dH_{c1}/dT|_+}=\frac{1}{4}\left(1+\frac{\beta_2}{\beta_1}\right)\left(2+\frac{K_1}{K}+\frac{K}{K_1}\right). \tag{60}$$

Substituting $\beta_2/\beta_1=0.5$ and $K/K_1=2$ gives 1.56 for the ratio as compared with the experimental value of 1.3 (see Sec. IV.B.2). In general, the agreement of theory and experiment for the slope ratios for the two field directions is satisfactory, given the experimental difficulties outlined in Sec. IV.B.2. However, as was pointed out in that section, the overall values of H_{c1} are too large to be explained within Ginzburg-Landau theory with a single order parameter and mass anisotropy. In all multicomponent theories, one-component theory gives an adequate picture of the effectively one-component A phase (though of course not of the two-component B phase). Hence the mystery of the high H_{c1} values is not solved by invoking unconventional superconductivity.

c. Mixed-representation theories

This class of theories yields a phase diagram in agreement with experiment for the proper choice of representations. The AB theory was in fact first proposed for this purpose (Chen and Garg, 1993, 1994). If we take the free energy of Eqs. (45) and (55), there is a tetracritical point for all directions of the field. For this direction, this point is at (H_z, T_z), with

$$H_z=\frac{\alpha_0\hbar c}{e}\,\frac{T_a-T_b}{2}\,\frac{1}{K_b-K_a}, \tag{61}$$

$$T_z=\frac{T_a-T_b}{2}-\frac{T_a+T_b}{2}\,\frac{K_b-K_a}{K_b+K_a}. \tag{62}$$

The AB theory is distinguished by being essentially isotropic except for parameter changes. This has the minor drawback that one might have difficulty producing the shape changes in the phase boundaries as $\vec{H}$ is rotated from the basal plane to the c axis. However, no detailed fits have been attempted.

d. Spin-triplet theory

This theory also predicts a tetracritical point for $\vec{H}\|\hat{c}$ (Machida, Ohmi, and Ozaki, 1993). The difficulty is that, for this direction of the external field there may be too many phases (Joynt, 1992). For $\vec{H}$ in the basal plane, the AB phase boundary is formed by a line of points at which both η_y and η_z vanish continuously. The initial slopes of the AB and NA boundaries are identical, and the curvature terms eventually cause these boundaries to cross. The form of the curvature terms for $\vec{H}=H\hat{z}$ is

$$f_m=(a_z+a_d)H^2|\eta_z|^2+a_zH^2|\eta_x|^2+a_zH^2|\eta_y|^2, \tag{63}$$

which means that η_y and η_z are split by the external field in second order. Because the initial slopes are equal, the AB boundary must split into two, producing an additional phase. This has not been observed, in spite of the very careful investigation of this boundary using ultrasound. It has been suggested that this phase is suppressed by large a_d (Machida, Ohmi, and Ozaki, 1993), but the splitting is quadratic in field and only turns on at H_{c1}. The basic point is that the antiferromagnetic order produces an in-plane splitting and the field produces a splitting between the c axis and the plane. In a constant field just above H_{c1}, there must be three phase transitions as the temperature is changed. The difficulty of having too many phases is still present in later versions of the spin-triplet theory (Machida and Ohmi, 1998) and appears to be a major phenomenological problem for this picture.

C. Phase diagram under pressure

1. The pressure-temperature plane

The pressure-temperature (P-T) phase diagram of superconducting UPt_3 was first obtained by Trappman, Löhneysen, and Taillefer (1991) using specific-heat measurements under hydrostatic pressure, and is shown in Fig. 16. The two transition temperatures T_c^+ and T_c^- are suppressed by the application of pressure at an inital rate of approximately -20 mK/kbar and -5 mK/kbar, respectively. They eventually come together at a pressure between 3 and 4 kbar. The remarkable feature is that the two transitions do not cross at that point but merge and remain as a single transition thereafter (Löhneysen, Trappmann, and Taillefer, 1992). This degeneracy strongly suggests that the two transitions at ambient pressure are not accidentally close and, in our view, tends to rule out those theories that invoke accidental near degeneracy.

The total jump in the specific heat, i.e., the sum of the two separate jumps $\Delta(C^+/T_c^+)+\Delta(C^-/T_c^-)$, decreases gradually with pressure from about 0.3 J/K^2 mol at $P=0$ kbar to about 0.2 J/K^2 mol at $P=4.5$ kbar (Trappmann, Löhneysen, and Taillefer, 1991; Löhneysen, Trappmann, and Taillefer, 1992). This is consistent with the idea of two components, as it can be shown (Sigrist *et al.*, 1987) that each component continues to supply its own jump after merger, the result being the sum of the two.

Jin, Carter, *et al.* (1992) have shown that most of the pressure dependence of the critical temperatures comes from the stress along the c axis. These authors confirm that the two transitions merge and do not cross as a function of pressure. Stress in the basal plane broadens the transitions and moves them downwards, but does not merge them. The critical point is given by

$$P^*\simeq 3.7 \text{ kbar}, \quad T_P^*\simeq T_c^+-0.1 \text{ K}, \tag{64}$$

$$(\vec{S}\|\hat{c}): \quad S^*\simeq 1.4 \text{ kbar}, \quad T_S^*\simeq T_c^+-0.03 \text{ K}. \tag{65}$$

A variety of other measurements have confirmed the pressure dependence measured above. In a susceptibility measurement to detect T_c^+ as a function of uniaxial stress, Greiter, Lonzarich, and Taillefer (1992) obtain $dT_c^+/dP=-24\pm5$ mK/kbar with essentially all of the effect produced by stress along the c axis.

The pressure slopes of the critical temperatures can also be determined from measurements of the thermal expansion coefficient $\alpha(t)$ through the Ehrenfest relation (van Dijk *et al.*, 1994):

$$\frac{\partial T}{\partial P_i}=\frac{V_m\Delta\alpha_i}{\Delta(C/T)}, \tag{66}$$

where V_m is the molar volume, $\Delta\alpha_i$ is the change in the expansion coefficient, and $\Delta(C/T)$ is the change in specific heat divided by temperature. P_i, $i=a,c$ refers to the stress along the a or the c axis. The derivative must be taken at constant field. For hydrostatic pressure P, we have

$$\left.\frac{\partial T}{\partial P}\right|_H=2\left.\frac{\partial T}{\partial P_a}\right|_H=+\left.\frac{\partial T}{\partial P_c}\right|_H. \tag{67}$$

This method tends to find somewhat lower (and more uncertain) values for the slopes: $dT_c^+/dP=-13.5\pm10$ mK/kbar and $dT_c^-/dP=-1\pm15$ mK/kbar.

Neutron scattering (Aeppli, Bucher, Broholm, *et al.*, 1988; Aeppli, Bucher, Goldman, *et al.*, 1988) and resonant magnetic x-ray scattering (Isaacs *et al.*, 1995) have both been used to characterize the antiferromagnetism in UPt_3, as detailed in Sec. II.D. These experiments are of great importance because of the hypothesized connection between superconductivity and antiferromagnetism. Neutron scattering under pressure played a key role in establishing this connection. The intensity of various Bragg reflections (proportional to M_S^2) at a temperature $T=1.8$ K was found to be proportional to P_c-P, where $P_c\approx3.2$ kbar, as shown in Fig. 20 (Hayden *et al.*, 1992). The data may also be fit with a higher exponent and then $P_c\approx4$ kbar. The behavior of the critical temperature T_N under pressure was also measured by Hayden *et al.* (1992) in the same experiment. The striking finding was that this critical pressure for suppressing the moment to zero (or nearly zero) was very much the same pressure that was found to merge the two transitions T_c^+ and T_c^-. It is difficult to believe that this could be a simple coincidence—rather it argues strongly in favor of a model in which the two transitions at ambient pressure (and zero magnetic field) are the result of a doubly degenerate transition split by a coupling to the symmetry-breaking antiferromagnetic order.

The behavior of the critical temperature T_N was measured in the same experiment. Strangely, there was no observable pressure dependence of $T_N\approx5$ K, at least up to 2 kbar (which is still fairly far below P_c). The temperature dependence of M_S^2 appears to be accurately linear as long as $T>T_c^+$. The phenomenological form is therefore roughly

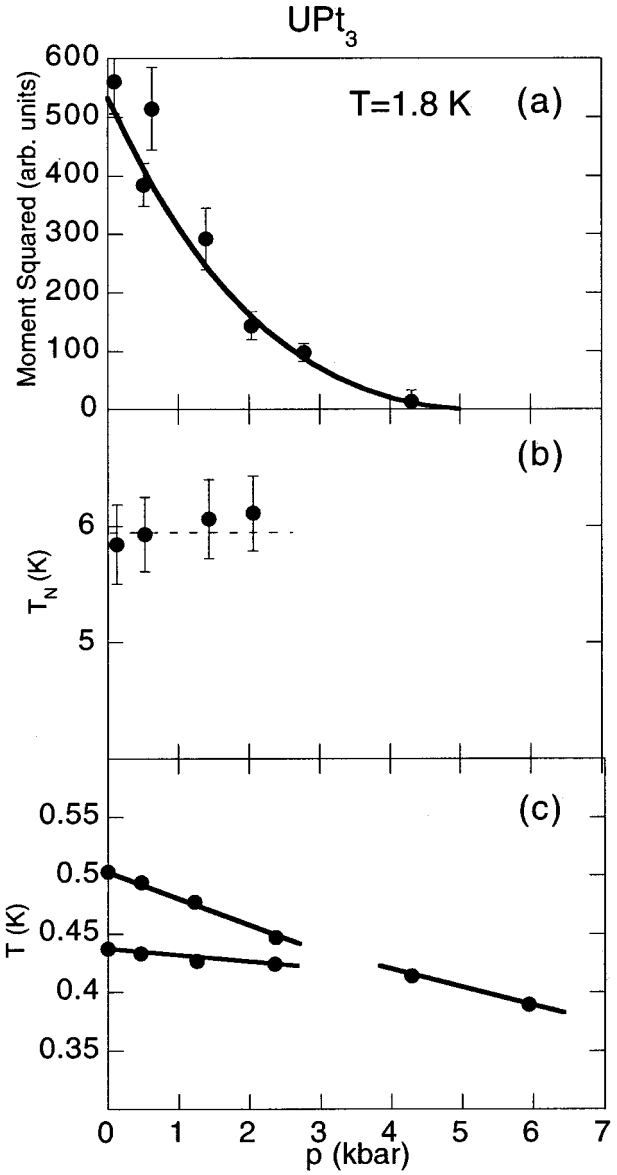

FIG. 20. The magnetic moment squared (a) and Néel temperature (b) as a function of pressure from neutron-scattering experiments. Also shown is the T-p phase diagram (Fig. 16). From Hayden *et al.*, 1992.

$$M_S(P,T)=M_{s0}\left(\frac{P_c-P}{P_c}\right)^{1/2}\left(\frac{T_N-T}{T_N}\right)^{1/2}, \tag{68}$$

where M_{s0} is the zero-temperature, zero-pressure value, $M_{s0}=0.02\mu_B$. Near T_c^+, there is a kink in $M_S(T)$ (Aeppli, Bucher, Broholm, *et al.*, 1988). The interpretation of the kink is not straightforward. It is present at roughly the same temperature even when $H=2.5T\gg H_{c2}$. It is therefore not entirely associated with superconductivity. Nevertheless, it appears to be more pronounced in the superconducting state. None of these effects is due to a rotation in the magnetic moment, which appears on more detailed examination to be absent (Hayden *et al.*, 1992; Isaacs *et al.*, 1995). This conflicts with theories that depend on a change in magnetic structure in the superconducting state (Blount *et al.*, 1990; Harán and Gehring, 1995).

The remarkable thing about these results is that they give us an unexpected and welcome tool for testing the theories of the phase diagram. Moderate pressures destroy antiferromagnetism, which restores the symmetry of the crystal structure. UPt_3 can be investigated in both the orthorhombic state below P_c and the fully hexagonal state above P_c.

Relatively little theoretical work has been done on the pressure dependence of the phase diagram. This dependence must be understood if we are to get at the superconducting order parameter. Fortunately, the relative simplicity of the data and the fact that the state of the system is spatially uniform make progress possible (Joynt, 1993; Park and Joynt, 1995; Harán and Gehring, 1995). The simplest free energy for the magnetism is

$$f_M = \alpha_M(P,T)M^2 + \beta_M M^4. \tag{69}$$

In order to reproduce the magnetic behavior above T_c^+ and zero pressure, we need to have

$$\alpha_M(P=0,T)/\beta_M = (1.6\times 10^{-4}\mu_B^2/K)(T-T_N), \tag{70}$$

while the pressure dependence is given by

$$\alpha_M(P,T) = \alpha_M^0(P-P_N)(T-T_N) \approx -\alpha_M^0 T_N(P-P_N), \tag{71}$$

with

$$\alpha_M^0/\beta_M = 5.3\times 10^{-5}\mu_B^2/(\mathrm{K\,kbar}). \tag{72}$$

These forms for the coefficients yield Eq. (68) immediately.

The superconducting part of the free energy is

$$f_S = \alpha_S(P,T)\,\vec{\eta}\cdot\vec{\eta}^* + \beta_1(\vec{\eta}\cdot\vec{\eta}^*)^2 + \beta_2|\vec{\eta}\cdot\vec{\eta}|^2, \tag{73}$$

where, for the first time, we must worry about the pressure dependence of α_S. Experiment again indicates that it is a linear function:

$$\alpha_S(P,T) = \alpha_{ST}(T-T_c^0) + \alpha_{SP}P. \tag{74}$$

For $P>P_c$, we have $M_S=0$ and the magnetic and superconducting parts of the free energy are independent. dT_c/dP is determined by the coefficients α_{ST} and α_{SP}: $\alpha_{SP}/\alpha_{ST} = 11$ mK/kbar.

In all the equations of this section, we have assumed that only the quadratic terms producing the phase transitions have pressure dependence. This is approximately consistent with experiment, but there is some evidence that the ratio β_2/β_1 increases slightly (10%) between 0 and 4 kbar (Löhneysen *et al.*, 1992).

The terms in the free energy that couple superconductivity and magnetism are

$$f_{SM} = -b|\vec{M}\cdot\vec{\eta}|^2 + b'M^2\,\vec{\eta}\cdot\vec{\eta}^*. \tag{75}$$

Now, considering $\vec{\eta}$ as an effective field acting on $\vec{M}_S$, we see that the theory does indeed produce a kink in $\vec{M}_S$ at T_c^+. The break in slope may be calculated from Eqs. (73), (69), and (75) as

$$\Delta\frac{dM^2}{dT} = -\frac{\alpha_S(b+b')}{4\beta_M(\beta_1+\beta_2)}. \tag{76}$$

Thus the Ginzburg-Landau theory is qualitatively consistent with the Aeppli, Bucher, Goldman, *et al.* (1988) data cited above. There are too many unknown parameters to make a quantitative comparison.

The P-T phase diagram is almost as unusual as the H-T phase diagram. Particularly striking is the fact that the two superconducting transitions merge at the critical pressure rather than crossing. Theory and experiment are in reasonably good agreement. Because the coupling terms are not very sensitive to the representation, as long as it is two dimensional, the observations do not distinguish between E_{1g} and E_{2u}. One possible discrepancy between the two-component theory and experiment is that the theory predicts (Harán and Gehring, 1995)

$$S \equiv \frac{T_c^+(P=0)-T_{ext}(P=0)}{T_c^-(P=0)-T_{ext}(P=0)} = 1. \tag{77}$$

Here $T_{ext}(P=0)$ is the temperature obtained by extrapolating $T_c(P)$ for $P>P_c$ back to the $P=0$ axis. This would be the zero-pressure critical temperature if there were no magnetism. This relation holds because, independent of magnetism, pressure should affect the critical temperatures of two degenerate components equally. $S>1$ for the data in Fig. 16. However, given the uncertainty in the measurements, there is rather large error in T_{ext}. It may be better to wait for more accurate determinations of S before drawing conclusions.

For the P-T phase diagram, the spin-triplet theory is equivalent to two-component theories and thus can account for the data.

The P-T diagram is evidence against mixed-representation pictures. In these theories, each component has its own pressure dependence. Thus the critical temperatures follow independent curves $T_c^+(P)$ and $T_c^-(P)$. These curves may or may not cross, but they should never merge.

2. The field-temperature-pressure space

Since both pressure and field measurements have been separately very informative, we may expect that the full mapping of the phase diagram in the three-dimensional H-T-P space would give further information about the underlying state of UPt_3. This turns out to be so.

The earliest work along these lines determined the initial pressure slopes of phase boundaries according to Eq. (66) (van Dijk *et al.*, 1993b, 1994). This extends the H-T plane infinitesimally into the third dimension without having to apply actual pressure. Since the effect of stress in the basal plane is not very informative, we concentrate on the effect of uniaxial stress along the c axis.

The C phase is not very sensitive to stress. The NC boundary moves down at rates of -0.5 ± 5 mK/kbar for $\vec{H}\perp\hat{c}$ and -3.0 ± 5 mK/kbar for $\vec{H}\parallel\hat{c}$. The B phase, by contrast, is rapidly suppressed. The BC boundary moves down at rates of -170 ± 50 mK/kbar for $\vec{H}\perp\hat{c}$ and -210 ± 50 mK/kbar for $\vec{H}\parallel\hat{c}$. The pressure dependences

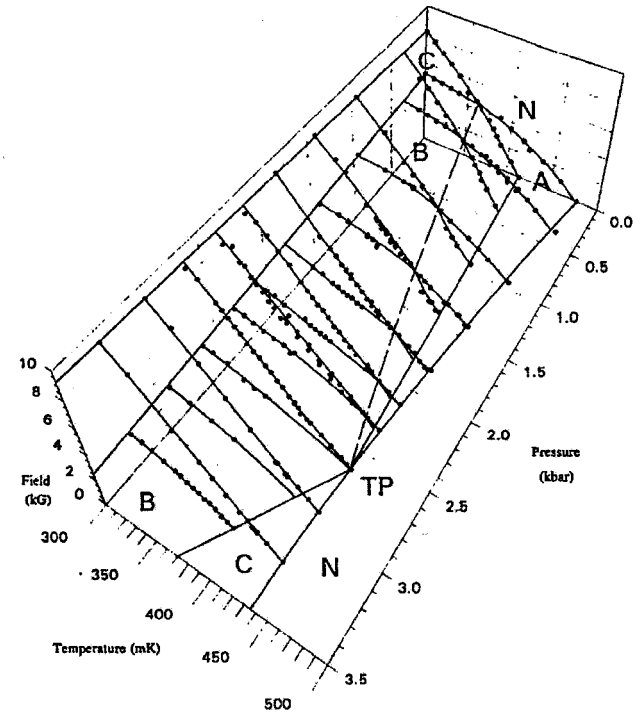

FIG. 21. Phase diagram in the H-P-T space as determined by ultrasound measurements of Boukhny *et al.* (1994).

of the NA and AB boundaries were not measured directly, but the end of the T_c splitting around $P \approx 3$ kbar means that the tetracritical point moves downward and the A phase disappears.

The positions of the phase boundaries in all three dimensions have been determined by measurements of the jump in sound velocities (Boukhny *et al.*, 1994). The phase diagram for $\vec{H} \perp \hat{c}$ which they deduce from their measurements is shown in Fig. 21. At low pressures their results are in agreement with those of van Dijk *et al.* for the NC and BC boundaries. However, there is a large discrepancy with other work for the AB boundary at zero applied field. The sound measurements give a value of $dT_{AB}/dP = +10$ mK/kbar, while the specific-heat data of Trappmann, Löhneysen, and Taillefer (1991) cited above give $dT_{AB}/dP = -5$ mK/kbar. Not even the sign is the same. The source of this difference is at present obscure.

Figure 21 shows the NC boundary to be very insensitive to pressure even at the highest pressure measured, 3.14 kbar. The BC phase boundary decreases with almost a constant slope, so there are no real surprises at higher pressures.

There are two main features that are noteworthy.

First, there are two phases when $P > P_c$, even at zero field. The B and C phases appear to have the same critical temperature at P_c, but the temperatures diverge again as pressure is increased further. This is also in apparent disagreement with the data of Trappmann, Löhneysen, and Taillefer (1991). These authors saw only one phase transition at zero field and high pressure. This may be due to the fact that the BC boundary at higher pressures is very flat as a function of temperature, making the specific-heat jump very broad when taken at constant pressure. These discrepancies at $P > P_c$ are absolutely central for the physical picture of superconductivity in UPt_3.

Second, the slope $(\partial H_{NC}/\partial T)_P$ of the NC phase boundary and the slope $(\partial H_{NA}/\partial T)_P$ of the NA phase boundary do not change much with pressure. The difference in these slopes is predicted to be proportional to $M_S^2 \sim (P - P_c)$ in E_{2u} theory and in some versions of the spin-triplet theory. This is in disagreement with experiment.

There is very little theory on the pressure dependence of the phase diagram at finite field. We summarize briefly the one paper on this topic (Joynt, 1993). Within the formalism presented in the previous section for the two-component theory, the pressure dependence in Ginzburg-Landau theory comes in the coefficients $\alpha(P,T)$ of the quadratic terms and the indirect effect of the magnetization. The pressure coefficients may then be determined from the experimental values of dT_c^+/dP and dT_c^-/dP. Once these are known, the analysis of H_{c2} and the BC boundary in Sec. IV.B can be repeated. Once again, the results hold, strictly speaking, only in the neighborhood of the critical point. Furthermore, they hold only in the low- (linear-) pressure regime, as no microscopic theory of the pressure effects exists.

The pressure derivatives of the phase boundaries can be expressed in terms of relations between observable zero-pressure quantities. For example,

$$\left(\frac{\partial H}{\partial P}\right)_{BC} = \left(\frac{\partial H}{\partial T}\right)_{NA} \times \left(\frac{\partial T_c^-}{\partial P}\right)_{H=0} \times \left(1 - u_y \frac{d_y}{d_x}\right)\left[1 - u_y \left(\frac{\partial H}{\partial T}\right)_{NA}\left(\frac{\partial H}{\partial T}\right)_{NC}\right]^{-1}, \tag{78}$$

where the $\partial H/\partial T$ are measured at zero pressure,

$$u_y \equiv \left(1 - \frac{\partial H/\partial T|_{BC}}{\partial H/\partial T|_{NA}}\right)\left(1 - \frac{\partial H/\partial T|_{BC}}{\partial H/\partial T|_{NC}}\right)^{-1}, \tag{79}$$

and

$$\frac{d_y}{d_x} \equiv \frac{(\partial T_c^+/\partial P)_{H=0}}{(\partial T_c^-/\partial P)_{H=0}}. \tag{80}$$

There are similar expressions for the other slopes. Taking data from van Dijk (1994) and van Dijk *et al.* (1993a, 1993b), $u \approx 0.88$ and $d_y/d_x < 0.2$, the results are as follows: $-\partial H/\partial P_{BC} = 0.135 \pm 0.055$ T/kbar (theory) as compared to 0.2 T/kbar (experiment) and $-\partial H/\partial P_{NC} < 0.006$ T/kbar (theory) as compared to 0.0 T/kbar (experiment). The theory also makes the prediction that $-\partial H/\partial P_{NA} = 0.09$ T/kbar; this quantity has yet to be measured.

If the values of u_y and d_y/d_x were taken from Boukhny *et al.* (1994), the theory results would be very different because of the difference in dT_{c2}/dP.

The fundamental question raised by the velocity data is this. Any theory in which the split transition is due to

the coupling to the magnetic order (E_{1g}, E_{2u}, spin triplet) contradicts the sound data above P_c. The symmetry is full D_{6h}, and the components of the order parameter must be degenerate. There is no room for a second transition as a function of temperature in zero field. Mixed-representation theories, on the other hand, would predict precisely this behavior. It is therefore crucial to obtain confirmation of the existence of this additional phase boundary by a different experiment, given the disagreement between sound-velocity and specific-heat measurements.

V. PROPERTIES OF THE SUPERCONDUCTING STATES

Since 1989, investigations into the superconducting behavior of UPt_3 can typically be divided into two distinct yet related efforts: an effort to elucidate the origin of phase multiplicity and an effort to identify the superconducting order parameter of the various phases. The present review is also divided along those lines. In Sec. IV, the superconducting phase diagram as a function of magnetic field, temperature, and pressure was discussed in detail, in the context of the various scenarios put forward to explain its various features. In this section, we review the main physical properties of UPt_3, with a view to identifying what is thought to be an unconventional order parameter. This discussion will focus almost exclusively on phase B—the low-temperature, low-field, zero-pressure phase. The other phases have so far remained largely inaccessible for experimental and/or theoretical reasons: the high-temperature phase (A) because of the very limited temperature range over which it exists, the high-field phase (C) because of the complicating presence of vortices, and the possible high-pressure phase for the obvious technical reason.

Information on the superconducting wave function can be obtained experimentally in a number of ways: (1) via the orbital part of the wave function by studying the temperature and field dependence of various physical properties, such as ultrasound attenuation and penetration depth; (2) via the spin part of the wave function by looking at the magnetic response, such as the Knight shift; (3) via direct gap spectroscopy, using electromagnetic absorption, various kinds of tunneling, photoemission, etc.; (4) via the phase of the wave function using the Josephson effect or other phase-sensitive experiments. While all of these approaches have been exploited in the study of high-T_c superconductors, with a few exceptions only the first two have been successfully applied to UPt_3 so far.

The use of directional probes (such as sound attenuation and thermal conductivity) is expected to be particularly powerful, as the presence of nodes in the gap for certain $\vec{k}$ directions will manifest itself as an enhanced thermal excitation of quasiparticles with velocities in those directions.

Power-law dependences in the thermal properties at low temperature derive from the asymptotic angular dependence of $\Delta(\vec{k})$ near the node, which translates as a certain power-law dependence of the density of quasiparticle states on energy E, as discussed in Sec. III.C. Let us stress two general points. First, these are asymptotic behaviors and so expected to apply only at $T \ll T_c$. How low in temperature one really needs to look is difficult to say; it depends on the property and a number of factors. A rough guide is $T < 0.3T_c$, so less than 150 mK in UPt_3. Second, these power laws hold only for perfectly pure systems. In real, impure samples, the gapless regime may mask them entirely. Theoretically, this regime is thought to extend at most to a temperature of about $(\hbar\Gamma\Delta_0)^{1/2}/k_B$, where Δ_0 is the maximum value of the gap. From our previous estimate of the elastic scattering rate for transport in high-quality crystals of UPt_3, $\Gamma = 1/2\tau_0 \simeq 10^{10}\,\mathrm{sec}^{-1}$ and $\hbar\Gamma \simeq 0.15 k_B T_c$, so that deviations from the pure behavior are expected below about $0.5T_c$ (using $\Delta_0 \simeq 2k_B T_c$). In practice, as we shall see in Sec. V.B, there is no sign of a residual normal fluid even down to much lower temperatures, and empirically the gapless regime therefore appears to be confined to below $\simeq 0.1T_c$ in crystals with $\rho_0 \simeq 0.2\ \mu\Omega$ cm. This means that the clean asymptotic behavior in UPt_3 is expected roughly below 150 mK or so, with possible deviations due to gaplessness at the low-temperature end. It should be said that a clear-cut power-law dependence on temperature is almost never seen. Experimentally, this is probably most often because the minimum temperature is not low enough, but also in some cases because excitations other than quasiparticles contribute to the quantity of interest. Theoretically, the prediction of a simple power law (where the power is not necessarily an integer) may not survive the inclusion of various effects, usually neglected, such as a multisheet Fermi surface, inelastic scattering, anisotropic scattering, a phase shift slightly away from $\pi/2$, or a range of phase shifts, not to mention a normal state not truly describable as a Fermi liquid. A widely known example of a clean power law in a superconductor is the observation of a linear dependence for the penetration depth below 25 K in the high-T_c cuprate $YBa_2Cu_3O_7$ ($T_c = 93$ K; Hardy *et al.*, 1993), viewed as strong evidence for a gap with line nodes characteristic of a $d_{x^2-y^2}$ pairing state.

With these points in mind, let us examine a number of quantities measured in phase B of UPt_3.

A. Specific heat

1. Temperature dependence

The specific heat of UPt_3 was shown in Figs. 12 and 13, and discussed in detail in Secs. IV.A.1, IV.B.1, and IV.C.1, in connection with the phase diagram. In this section we focus on an analysis of the data for phase B. The reader is referred to the excellent review of the specific heat by Löhneysen (1994).

The B phase exists at $H = 0$ and $P = 0$, and it sets in at $T_c^- = 0.48$ K. The presence of a huge anomaly in C/T below 0.1 K ($0.2T_c^-$) precludes the extraction of information from the specific heat in the range ($T \ll T_c$) where it would be most interesting and diagnostic for

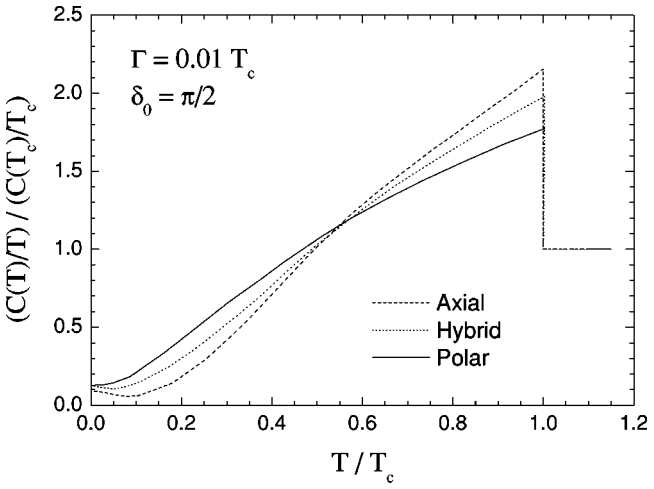

FIG. 22. Specific heat calculated for axial, polar, and hybrid gaps, plotted in reduced units as C/T vs T. The calculations assume resonant impurity scattering and an impurity scattering rate of $0.01k_BT_c$. From Hirschfeld, Wölfle, and Einzel, 1988.

order-parameter symmetry. Furthermore, nothing can really be said about the possible existence of a gapless regime. No satisfactory explanation has been given for the anomaly, which Schuberth, Strickler, and Andres (1992) showed to be a peak centered around 20 mK. In most reported studies, the data above 0.1 K are fit to $C/T=\gamma_0+aT$, usually in the range approximately between $0.3T_c^-$ and T_c^-, yielding a nonzero value for γ_0 which depends on sample quality (and the actual fitting interval). For high-quality crystals, a fit from 0.3 to $0.6T_c^-$ yields $\gamma_0\simeq 0.1-0.2\gamma_N$ (Bogenberger *et al.*, 1993; Brison *et al.*, 1994b; Taillefer, Ellman *et al.*, 1997), but an extrapolation of the data below 150 mK gives no intercept (Brison *et al.*, 1994b; see also Ott *et al.*, 1987). Such a fitting procedure is devoid of real meaning, not only because C/T is not really linear over any of that range, but also because a power law is not expected at such high temperatures. In particular, one cannot seriously argue in favor of a gap with a line node as opposed to a gap with point nodes on the basis of the asymptotic behavior given in Table IV: $C/T\propto T$ (line node), $C/T\propto T^2$ (point node). So the only two reliable facts are the following: (1) there is a large number of thermal excitations at low temperature (most probably quasiparticles), and (2) the jump at T_c^- is small compared with the isotropic BCS result ($\Delta C/\gamma_N T_c=1.43$). Indeed, at $T=T_c/4$, $C/\gamma_N T=0.5$ in UPt_3, compared to 0.13 in Al (Phillips, 1959), for example. This argues strongly for nodes in the gap (or at least a highly anisotropic gap), but again it does not really allow a distinction between line and point nodes. Theoretical calculations by Hirschfeld, Wölfle, and Einzel (1988) for a gap with point nodes, one with line nodes, and a hybrid gap are shown in Fig. 22. Note the presence of a gapless regime at very low temperature, where C/T saturates and gives a finite value at $T=0$, the signature of a residual normal fluid. Note also that above that regime, there is no clear power-law dependence, so that C/T is not linear for either the gap with line nodes or the hybrid gap. All three gaps can roughly account for the data of Fig. 12 (above $T_c/10$). At $T=T_c/4$, the calculation (with $\Gamma=0.01T_c$) gives $C/\gamma_N T=0.54$ (polar), 0.29 (axial) and 0.41 (hybrid). Whether the slightly better agreement found for the polar or hybrid gap can be viewed as evidence for line nodes is uncertain: it depends on the value used for Γ and on how one subtracts the low-T anomaly. The calculated jump at T_c is $\Delta C/\gamma_N T_c\simeq 0.7$ (polar), 1.2 (axial), and 1.0 (hybrid) (see also Monien *et al.*, 1987), all small relative to the value for an isotropic gap, and in rough agreement with the small measured values. It is difficult to be more quantitative about this aspect because of the presence of two transitions.

We conclude, more from the magnitude of C/T at low T and the jump at T_c than from any power-law analysis, that the specific heat of UPt_3 can be understood in terms of a highly anisotropic gap, most likely with nodes. A gap with line nodes or a hybrid gap is perhaps marginally favored over a gap with point nodes only.

At a pressure of 5 kbar, where antiferromagnetic order no longer exists (see Sec. IV.C.1), the C/T vs T curve (with only one transition) is very similar to that of the B phase at zero pressure (Sieck, Löhneysen, and Taillefer, 1995), e.g., $C/T=0.7\gamma_N$ at $T/T_c=1/3$ in both cases.

2. Vortex state

The application of a magnetic field H provides another way of studying the quasiparticle spectrum of unconventional superconductors and hence of probing their gap structure. In the vortex state, the quasiparticle energies are Doppler shifted by the superfluid flow around each vortex, so that quasiparticles near the nodes can be excited even at $T=0$ by applying small magnetic fields. Volovik (1993) was the first to show that, because the average Doppler shift is proportional to $\sqrt{H}$, a gap with a line of nodes (and therefore a density of states with a linear dependence on energy at low energies) would produce a dominant $\sqrt{H}$ contribution to the electronic specific heat. More generally, because the Doppler shift and the thermal energy k_BT have similar effects, one expects scaling relations for thermodynamic and transport properties with respect to the single scaling variable $x=T/T_c\sqrt{H_{c2}/H}$ (Kopnin and Volovik, 1996; Simon and Lee, 1997). For example, $C/T=\sqrt{H}F(x)$, where $F(x)$ is some unknown scaling function which tends to a constant for $x\ll 1$, so that at low temperature $C/T\propto\sqrt{H}$. In the high-temperature superconductors, the observation of this "Volovik" effect was first reported in specific-heat studies by Moler *et al.* (1994, 1997) and later others (Wright *et al.*, 1999; Junod *et al.*, 2000), as well as in low-temperature thermal conductivity measurements (Chiao *et al.*, 1999).

The field dependence of $C(T)$ in UPt_3 was first measured for $\vec{H}\|\hat{c}$ by Ellman *et al.* (1990) and then with greater resolution by Ramirez, Stücheli, and Bucher (1995) for both $\vec{H}\|\hat{c}$ and $\vec{H}\perp\hat{c}$. At their lowest temperature of 150 mK, the latter authors find $C(H)/T$ to be

well described by a fit to $a+b\sqrt{H}$, up to 1.9 T for $\vec{H}\perp\hat{c}$ and 0.75 T for $\vec{H}\|\hat{c}$. They offer this as evidence for a line node in the gap structure of the B phase. There are three reasons why this is more likely to be fortuitous than compelling. First, at 150 mK the specific heat is probably still contaminated to some extent by the huge anomalous peak at 20 mK, known, moreover, to grow with field (Schuberth and Fischer, 1994). Second, the authors neglected to consider possible hyperfine contributions in their field dependence, the like of which needed to be carefully subtracted from the data on $YBa_2Cu_3O_7$. Finally, 150 mK is not low enough to ensure that $F(x)$ is constant. In UPt_3 for $\vec{H}\perp\hat{c}$, $x\simeq 0.9$ at 150 mK and 0.4 T (the maximum field in the B phase), so that significant deviations from the simple $\sqrt{H}$ behavior are expected in the range investigated. In fact, it appears that in UPt_3 the regime where a simple scaling of the kind $C\propto TH^{1/2}$ for a line node might hold is not accessible by specific heat. Note, finally, that a $\sqrt{H}$ dependence is also found in conventional superconductors such as $NbSe_2$, with no nodes in the gap function (Sonier *et al.*, 1999).

In summary, specific-heat measurements on UPt_3 have proven invaluable in establishing the existence of phase multiplicity in this material and then in mapping out the phase diagram as a function of pressure and magnetic field. On the other hand, studies of the temperature and magnetic-field dependence of C/T in phase B have led to little in the way of firm information about the order parameter, largely because of the anomalous peak below 0.1 K. As we shall see, other properties have proven much more powerful in this respect.

B. Thermal conductivity

In this section, we show how the thermal conductivity $\kappa(T)$ has been used to gain insight into the details of the gap structure in UPt_3. The directional nature of transport properties makes them powerful probes of the superconducting state in unconventional superconductors with highly anisotropic gap structures. An additional advantage of heat conduction over specific heat is that only itinerant excitations are measured. This is particularly significant in UPt_3, since the large anomaly in C/T at low T is not present in κ/T (implying that it is due to localized excitations). In general, the main weakness of the technique is that it is often difficult to separate the contributions of phonons and electrons, and in most conventional superconductors phonons become the dominant carriers of heat at $T\ll T_c$. Conveniently, this is not the case for high-quality crystals of UPt_3 (with RRR$>$500), for which the phonon contribution can be neglected at all temperatures below T_c (see Lussier, Ellman, and Taillefer, 1994, 1996).

A number of groups have measured the thermal conductivity of UPt_3. The early measurements (Franse *et al.*, 1985; Jaccard *et al.*, 1985; Steglich *et al.*, 1985; Sulpice *et al.*, 1986; Ott *et al.*, 1987) were done on polycrystals and are therefore not able to shed light directly on the anisotropy of the gap. The electronic mean free path was also shorter in these early samples so that the phonon contribution may then have been nonnegligible. The first measurement on single crystals was performed by Behnia *et al.* (1991), who also studied the effect of a magnetic field in various directions, but not the anisotropy of the conduction for various directions of the heat current on the same crystal. That measurement was first performed by Lussier, Ellman, and Taillefer (1994, 1996); their findings were subsequently confirmed by Huxley *et al.* (1995) and extended to lower temperature by Suderow *et al.* (1997a, 1997b), who also studied the effect of a magnetic field (Suderow *et al.*, 1998).

1. Temperature dependence

Bardeen, Rickayzen, and Tewordt (1959) calculated the electronic contribution to the thermal conductivity of a superconductor with an isotropic s-wave gap, when the dominant scatterers are impurities. As a result of the coherence factor for an s-wave gap, they found that the relaxation time in the superconducting state τ_s acquires an energy dependence that is exactly canceled by that of the quasiparticle group velocity v_s in the product $v_s\tau_s$, so that the mean free path in the superconducting state is the same as in the normal state. A similar cancellation in the product of the density of states and velocity, $N_s(E)v_s=N(E_F)v_F$, leads to an expression for κ $[\propto N(E)v^2\tau]$ which is exactly equivalent to the normal-state expression except for the gap $[\Delta(T)]$ in the quasiparticle excitation spectrum:

$$\frac{\kappa_{es}}{\kappa_{en}}=\frac{\int_{\Delta(T)}^{\infty}dE\,E^2\frac{\partial f}{\partial E}}{\int_0^{\infty}dE\,E^2\frac{\partial f}{\partial E}}, \tag{81}$$

where $f(E)=(1+e^{E/k_BT})^{-1}$. The magnitude and temperature dependence of $\Delta(T)$ therefore completely determine $\kappa_{es}(T)$. The result is plotted in Fig. 23 for the standard BCS gap with $2\Delta(0)=3.52k_BT_c$. The characteristic exponential rise from $T=0$ is seen at low temperatures, such that κ_{es} is only 1–2 % of its normal-state value at $0.2T_c$. Equation (81) fits perfectly the measured $\kappa(T)$ in pure samples of conventional superconductors such as Al, Nb, and V in the range where phonons are negligible, with $2\Delta(0)/k_BT_c=3.52$ (Satterthwaite, 1962), 3.6 (Lowell and Sousa, 1970), and 3.39 (Tsai *et al.*, 1981), respectively.

It is instructive to compare the thermal conductivity of UPt_3, displayed in Fig. 7 for both κ_b and κ_c, with the standard theory. This is done in Fig. 23, where κ_b is plotted vs reduced temperature T_c^- (i.e., relative to the B-phase transition) and normalized by the normal state $\kappa_N=T/(a+bT^2)$. Because the theory does not include any inelastic scattering, the comparison should, strictly speaking, be limited to the elastic regime below about $T_c/4$. In that range, the thermal excitation of quasiparticles in UPt_3 is seen to be at least ten times faster than

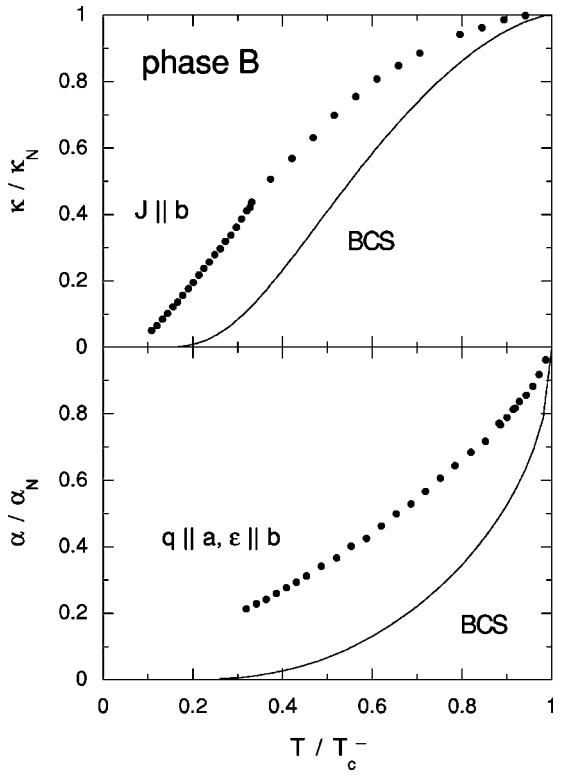

FIG. 23. Temperature dependence of heat (κ) and sound propagation (α) in the basal plane of UPt_3, normalized to the normal state, compared with the behavior expected of a standard BCS superconductor with an isotropic s-wave gap function.

the standard BCS model predicts. An additional discrepancy arises when one looks at the anisotropy, which we discuss below.

In the mid-1980s, several authors generalized the standard Bardeen-Rickayzen-Tewordt theory to apply it to unconventional order parameters, in particular with anisotropic gap structures with nodes (Hirschfeld, Vollhardt, and Wölfle, 1986; Schmitt-Rink, Miyake, and Varma, 1986; Arfi and Pethick, 1988; Arfi, Bahlouli, and Pethick, 1989). All of them neglected inelastic electron-electron scattering and assumed isotropic (s-wave) scattering off impurities, which is treated either in the Born limit of weak scattering (scattering phase shift $\delta_0 \simeq 0$) or in the unitarity limit of strong (resonant) scattering ($\delta_0 = \pi/2$). Two types of calculations were performed: self-consistent calculations which include the pair-breaking effect of impurity scattering (Hirschfeld, Vollhardt, and Wölfle, 1986; Schmitt-Rink, Miyake, and Varma, 1986) and those which neglect this effect (Arfi and Pethick, 1988; Arfi, Bahlouli, and Pethick, 1989). The effect of pair breaking shows up at temperatures below an energy scale γ, often called the impurity bandwidth, which depends on the normal-state scattering rate Γ_0. The value of γ depends strongly on the phase shift; it is highest for $\delta_0 = \pi/2$, where $\gamma \simeq \sqrt{\hbar \Gamma_0 k_B T_c}$ (Graf *et al.*, 1996; Hirschfeld and Putikka, 1996). For a high-purity crystal of UPt_3, where $\hbar \Gamma_0 = 0.05 k_B T_c$, this gives roughly $\gamma \simeq 0.2 k_B T_c$. The main feature of that regime, which we call the "gapless regime," is the novel presence of a residual normal fluid of zero-energy quasiparticles at $T=0$ (Hirschfeld, Vollhardt, and Wölfle, 1986; Schmitt-Rink, Miyake, and Varma, 1986).

Neglecting the pair-breaking effect of impurities and assuming isotropic (s-wave) scattering, Arfi and Pethick (1988) calculated the two components of κ, namely, $\kappa_{zz} \equiv \kappa_c$ and $\kappa_{xx} \equiv \kappa_a = \kappa_b$, for three generic gap structures: the polar ($\cos\theta$), the axial ($\sin\theta$), and the "d-wave" gap ($\sin\theta\cos\theta$), on a single spherical Fermi surface for a scattering phase shift close to 0 or $\pi/2$. Their results for κ/T versus T are shown in Fig. 24. Two basic features emerge: (1) heat conduction is always much better along the direction of nodes and (2) qualitative agreement with experimental data is not possible in the Born approximation, which is seen to lead to large values of κ/T at $T \to 0$ in the nodal directions, comparable in magnitude to the normal-state value. The necessity of invoking large phase shifts, close to $\pi/2$, to explain the fact that in heavy-fermion systems such as UPt_3 $\kappa/T \to 0$ as $T \to 0$ was first emphasized by Pethick and Pines (1986); it has since become a widespread assumption in the description of superconducting properties in all strongly correlated electron systems (e.g., high-T_c cuprates). For the three gaps considered in Fig. 24, the anisotropy of conduction is striking. For example, the ratio of heat conduction parallel and perpendicular to the c axis, $\kappa_{zz}/\kappa_{xx} \equiv \kappa_c/\kappa_b$, goes to zero for a polar gap and to infinity for an axial gap, as $T \to 0$. (See Barash and Svidzinsky, 1996, 1998 for the actual temperature dependence of the limiting behavior.) In each case, heat conduction in the direction where the gap is fully developed is quite similar to that of an s-wave gap (see Fig. 23). This implies that a measurement of transport anisotropy can be a powerful way of distinguishing between candidate gap structures.

In the mid-1990s, in the wake of measurements of the anisotropy of heat transport, further calculations were performed with the aim of using the new data to resolve the debate over the orbital symmetry of the order parameter. Fledderjohann and Hirschfeld (1995) showed that there is a distinct difference between the two hybrid gaps associated with phase B in the E_{1g} and E_{2u} scenarios, i.e., $\Delta(\theta) \sim \sin\theta\cos\theta$ and $\Delta(\theta) \sim \sin^2\theta\cos\theta$, respectively. Indeed, while the anisotropy ratio tends to zero as $T \to 0$ for the former (in the pure limit), it remains finite for the latter (in fact, it is unchanged below T_c for a spherical Fermi surface). This is a consequence of the topological difference in the gap at the point node between the two structures, namely, $\Delta(\theta) \sim \theta$ vs θ^2 [which leads to $N(E) \sim E^2$ vs E]. It appears that no other physical property is as sensitive to that subtle topological difference.

In general, $\kappa(T)$ is expected to depend on the complex topology of the Fermi surface and the microscopic pairing interaction, and one must go beyond a model with a spherical Fermi surface. However, as argued by Graf, Yip, and Sauls (1996, 1999) and Barash and Svidzinsky (1996, 1998), at sufficiently low temperature only a knowledge of the asymptotic topology of the gap at the

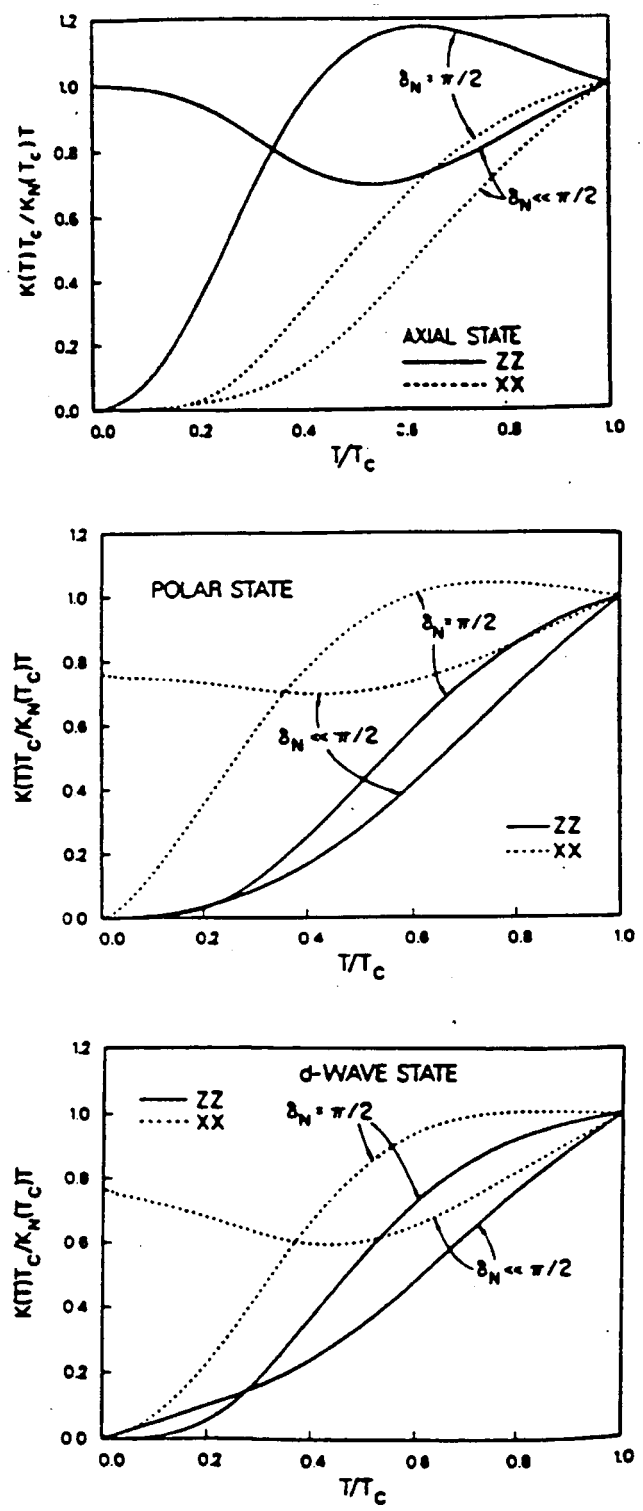

FIG. 24. Thermal conductivity calculated for axial, polar, and hybrid (d-wave) gaps, for directions of the heat current parallel (ZZ) and perpendicular (XX) to the c axis, plotted in reduced units as $\kappa_{ii}(T)/T$. From Arfi and Pethick, 1988. Impurity scattering is treated in the Born approximation ($\delta_N \ll \pi/2$) and in the unitarity limit ($\delta_N = \pi/2$).

nodes is needed. Within such an "asymptotic regime," it should be sufficient to approximate the Fermi surface by an ellipsoid and expand the gap structure at the nodes in terms of the lowest ellipsoidal harmonics. Both Norman and Hirschfeld (1996) and Graf, Yip, and Sauls (1996, 1999) have done this and fitted their calculations to the data of Lussier, Ellman, and Taillefer (1996), plotted in Fig. 25 as κ/T normalized to 1 at T_c^- versus reduced temperature. In the bottom panel, the anisotropy ratio is shown also normalized to 1 at T_c^-. Because at present the theory is somewhat simplistic in its treatment of electron-electron scattering, the most reliable comparison with experiment is in the "elastic regime." The data are therefore shown for $T<0.3T_c^-$, in which interval the effect of inelastic scattering on κ is less than 10%.

Two basic results emerge from the data. First, as pointed out earlier for κ_b, the rise in κ/T from $T=0$ is much more rapid than in conventional superconductors, and this is true for both current directions, indicating that there are nodes along both directions. This therefore rules out not only the nodeless gap of s-wave symmetry but also the axial and polar gaps, with nodes in only one of these directions. Second, the anisotropy κ_c/κ_b extrapolates to a finite, nonzero value at $T=0$, about half that of the normal state. As argued by Barash and Svidzinsky (1998), this special feature strongly favors a hybrid-II gap over a hybrid-I gap.

Let us compare the recent theoretical calculations with the experimental data of Lussier, Ellman, and Taillefer (1996) more quantitatively. The transport theory in its current state assumes isotropic scattering and is parametrized in terms of Γ_0 and δ_0. A rough estimate of the impurity scattering rate may be obtained from the normal-state conductivities given that we know γ_N and have a fair idea of $v_{F,i}$ from the dHvA effect:

$$\hbar\Gamma_0=\frac{\hbar}{6}\gamma_N\ v_{F,i}^2\left(\frac{1}{\kappa_{N,i}/T}\right)_{T\to 0}\simeq 0.1k_BT_c^-, \tag{82}$$

using $v_{F,i}\simeq 3800$ (6200) m/s and $\kappa_{N,i}/T=L_0/\rho_{0,i}$ with $\rho_{0,i}=0.61$ (0.23) $\mu\Omega$ cm, for $i=a$ ($i=c$). Within a factor of 2 either way, this should be about right. The phase shift is in principle unconstrained, but since significant deviations from the unitarity limit lead to gross disagreement with experiment, δ_0 is taken to be $\pi/2$. (For an account of the effect of arbitrary phase shifts, see Arfi, Bahlouli, and Pethick, 1989 and Hirschfeld and Putikka, 1996.) We discuss separately the temperature regimes above and below the onset of pair-breaking effects.

a. Asymptotic regime ($0.1<T/T_c^-<0.3$)

Within a simplified picture of a single ellipsoidal Fermi surface for UPt_3 with a mass ratio of 2.7 (see Sec. II.B) and assuming uniaxial symmetry about the c axis (i.e., leaving out states that break uniaxial symmetry), the magnitude of the gap depends only on the polar angle θ. A general gap will be a linear combination of ellipsoidal harmonics Y_{LM}, each of which vanishes for one or more values of θ (except Y_{00}). The nodes can therefore be points at the poles ($\theta=0$), a line around the equator ($\theta=90°$), two lines above and below ($\theta=90°\pm\theta_0$) the equator, or a combination of these three basic elements. The five lowest harmonics have the following structure: $Y_{00}\sim$const ("s-wave"),

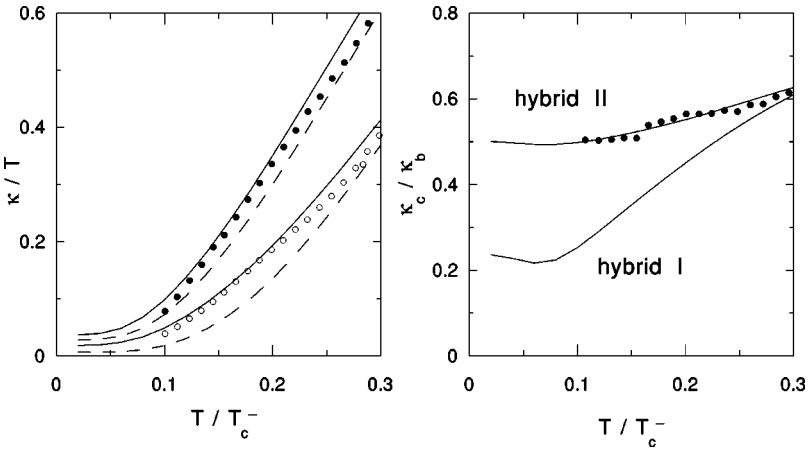

FIG. 25. Thermal conductivity and its anisotropy: (a) thermal conductivity along axes c (κ_c, open circles) and b (κ_b, filled circles) vs reduced temperature and normalized at T_c^-, for the asymptotic regime below ~150 mK. From Lussier, Ellmann, and Taillefer, 1996. (b) The anisotropy ratio κ_c/κ_b. The data are compared with calculations by Norman and Hirschfeld (1996) for a hybrid-I gap (dashed lines) and a hybrid-II gap (solid lines). The calculations use the parameters $\hbar\Gamma_0 = 0.05 k_B T_c^-$ and $\delta_0 = \pi/2$.

$Y_{10} \sim \cos\theta$ ("polar"), $Y_{11} \sim \sin\theta$ ("axial"), $Y_{20} \sim (\cos^2\theta - 0.15)$ ("tropical," as $\theta_0 = 23°$ for a mass ratio of 2.7), $Y_{21} \sim \sin\theta\cos\theta$ ("hybrid I"). The asymptotic behavior of the axial gap near the poles, for example, is linear ($\sin\theta \sim \theta$ for $\theta < 20°$ or so) and therefore the asymptotic regime corresponds approximately to $k_B T < \Delta(\theta = 20°)$, which translates roughly as $T/T_c < 0.3$.

A full calculation by Norman and Hirschfeld (1996), assuming $\hbar\Gamma_0 = 0.05 k_B T_c^-$ and $\delta_0 = \pi/2$, for the simplest hybrid gaps of E_{1g} and E_{2u} symmetry, namely, Y_{21} and Y_{32}, respectively, is compared to the data in Fig. 25. The fits have been fine tuned by adding a small amount of the next harmonic:

hybrid I (E_{1g}):

$$|\Delta_I(\theta)| \sim Y_{21} - 0.15 Y_{41} \sim \sin\theta\cos\theta \ (1 - 0.44\cos^2\theta); \tag{83}$$

hybrid II (E_{2u}):

$$|\Delta_{II}(\theta)| \sim Y_{32} + 0.25 Y_{52} \sim \sin^2\theta\cos\theta \ (1 + 0.65\cos^2\theta). \tag{84}$$

This slight admixture is a way of adjusting how fast the gap grows out of the point nodes in each case, while preserving the respective symmetries. The gap rises linearly from the line node at $\theta = \pi/2$, with a slope $S_{line} = |d\Delta(\theta)/d\theta| = 2.5\Delta_0$ for the hybrid-I gap and $2.1\Delta_0$ for the hybrid-II gap, where Δ_0 is the maximum value of the gap. From the point node at $\theta = 0$, the hybrid-I gap rises linearly with $S_{point} = 1.4\Delta_0$, while the hybrid-II gap rises quadratically with a curvature $S'_{point} \simeq 8\Delta_0$. Very similar results and values were obtained by Graf, Yip, and Sauls (1999). κ_b/T is well reproduced by the calculation for both gaps. It is along the c axis ($\theta \simeq 0$) that the gaps differ and the disparity in the behavior of the two gaps is clearly brought out by looking at the ratio of κ_c and κ_b. The data for κ_c/κ_b are almost flat and extrapolate to a value between 0.4 and 0.5 at $T = 0$, as also found by Huxley *et al.* (1995), something which the E_{2u} gap can easily reproduce. On the other hand, the E_{1g} gap above the gapless regime is qualitatively different, being characterized by a smooth extrapolation to zero. Indeed, if the gapless regime were suppressed by reducing Γ_0, the calculated ratio would eventually go to zero (see Norman and Hirschfeld, 1996), as expected on simple grounds of topology. We conclude that the anisotropy of heat conduction in the asymptotic regime favors a hybrid-II gap, of E_{2u} symmetry, over a hybrid-I gap, of E_{1g} symmetry, for phase B of UPt_3. We remind the reader that for a specified symmetry of the order parameter there are an infinity of possible gap structures. One is allowed by symmetry to multiply this basic gap structure by any function of θ with A_{1g} (or s-wave) symmetry: for example, by Y_{20} (the tropical gap), which introduces two extra lines of nodes at the tropics, in addition to the symmetry-imposed line around the equator. This will introduce additional nodes and therefore alter the transport properties at low temperature; in particular, a tropical gap leads to a nonzero extrapolated ratio κ_c/κ_b. In the same way, if one attempts to go beyond ellipsoidal harmonics and use more realistic basis functions reflecting the real Fermi surface and pairing potential, additional nodes may appear. What makes the simple approach used above reasonable is the basic idea that the condensation energy gained by going to the superconducting state is in general maximized by a gap function having the smallest number of nodes for a given symmetry. (See Norman and Hirschfeld, 1996, for a discussion of these issues.)

Quantitatively, the calculation for the hybrid-II gap agrees very well with the data, except at the lowest temperatures. For $\hbar\Gamma_0 = 0.05 k_B T_c^-$, deviations due to the gapless regime become noticeable below about $0.15 T_c^-$. They can be reduced by using a smaller Γ_0, but this would lead to an inconsistency when it comes to the normal state, which imposes the requirement that Γ_0 be within a factor of 2 or so of $0.1 T_c^-$. For a detailed theoretical discussion of thermal conductivity in the asymptotic regime, see Barash and Svidzinsky (1998).

b. Gapless regime ($T/T_c^- < 0.1$)

To leading order in $k_B T/\gamma$, the behavior in the gapless regime ($k_B T < \gamma$) is given by (Graf *et al.*, 1996)

$$\frac{\kappa_i}{T} = \frac{1}{3}\,\gamma_N v_{F,i}^2 \tau_i \left[1 + \frac{7\pi^2}{15}\, a_i^2 \left(\frac{k_B T}{\gamma}\right)^2\right] \quad (i = a,b,c), \tag{85}$$

where $v_{F,i}$ is the average Fermi velocity in the i direction. In the strong-scattering limit, the value of τ_i and a_i for the hybrid-II gap, for example, is

$$\text{hybrid II}(E_{2u}),\ \vec{J}\|b: \qquad \tau_b=\frac{3\hbar}{4S_{line}} \quad , \qquad a_b=\frac{1}{2}; \tag{86}$$

$$\text{hybrid II}\ (E_{2u}),\ \vec{J}\|c: \quad \tau_c=\frac{3\hbar}{2S'_{point}} \quad , \quad a_c=\frac{1}{2}, \tag{87}$$

where S'_{point} is the curvature of the gap at the quadratic point node.

The characteristic feature of gapless behavior is a residual linear term in $\kappa(T)$. The size of this linear term is dictated by the slope S (or curvature S') of the gap as it increases away from the node. Of particular interest is the prediction that for certain gap topologies and current directions—such as a current in the basal plane and a gap increasing as $\cos\theta$ (e.g., polar, hybrid I and hybrid II) or a current along $\hat{c}$ and a gap increasing as $\sin^2\theta$ (e.g., hybrid II), but not as $\sin\theta$ (e.g., axial and hybrid I)—the magnitude of $(\kappa/T)_{T\to 0}$ is independent of scattering rate. The possibility of such "universal" transport was first pointed out by Lee (1993) for a d-wave gap in two dimensions and confirmed in the high-T_c cuprate $YBa_2Cu_3O_7$ by Taillefer, Lussier, *et al.* (1997).

The calculated curves in Fig. 25 show clearly this residual linear term, which dominates κ for $k_BT<\gamma$. The gapless behavior is brought out by looking at the ratio κ_c/κ_b for the E_{1g} curve, where it sets in below $0.1T_c^-$. For the hybrid-II gap of Eq. (84), the *universal* limit of κ/T is approximately 1.4 (1.9) mW K^{-2} cm^{-1}, for the b axis (c axis). A smooth extrapolation of the data below $T_c^-/6$ clearly yields a much smaller value than these predicted limits. Suderow *et al.* (1997b) were able to extend the measurement of thermal conductivity down to $T_c/30$. They used two single crystals of a quality very similar to those used by Lussier, Ellman, and Taillefer (1994, 1996), characterized by $\rho_{0,i}=0.54$ (0.17) $\mu\Omega$ cm for $\vec{J}\|b$ ($\vec{J}\|c$), as compared to 0.61 (0.23) $\mu\Omega$ cm. (The slight difference in anisotropy ratio, 3.1 versus 2.7, leads one to suspect that the two crystals were not quite identical in at least one of the two studies, perhaps in both.) Their low-temperature data are plotted in Fig. 26 as κ/T versus T^2, with the inset focusing on the range below 30 mK. The measured $\kappa(T)$ below $0.1T_c^-$ is in sharp disagreement with the behavior expected theoretically for the gapless regime, and this for either of the two hybrid gaps. First, there is no sign of a residual linear term for $\vec{J}\|c$, and the residual linear term for $\vec{J}\|b$ is $\sim$10 times smaller than predicted based on the value of S_{line} determined from fitting κ_b/T in the asymptotic regime. Indeed, a linear fit below 30 mK yields $\kappa_i/T=\alpha_i+\beta_iT^2$, with $\alpha_i\simeq 0.15$ (0.0) mW K^{-2} cm^{-1} and $\beta_i\simeq$ 800 (1400) mW K^{-4} cm^{-1}, for the b axis (c axis). Note that this disagreement is independent of the chosen value for Γ_0. (In principle, it is also independent of δ_0, although if the phase shift were chosen to be less than $0.9\pi/2$ or so, a much larger linear term would be predicted at these temperatures; see Arfi, Bahlouli, and Pethick, 1989.) Moreover, the coefficients of the cubic term, β_c and β_b, are much too large to agree with Eq. (85). For example, the fitted value for κ_b/T yields $\gamma\simeq$15 mK (Suderow *et al.*, 1997b), a very small crossover temperature for $\delta_0=\pi/2$. Indeed, it implies $\hbar\Gamma_0/k_BT_c\simeq(\gamma/k_BT_c)^2\simeq 0.001$, i.e., an electronic mean free path of 50 μm.

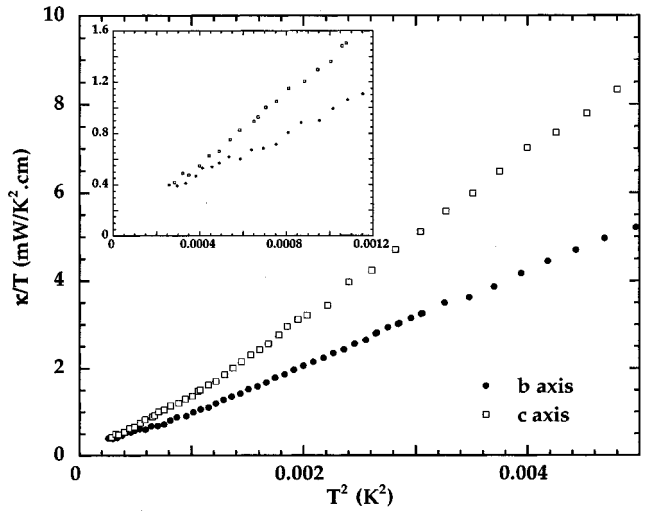

FIG. 26. Thermal conductivity along the c axis (open squares) and the b axis (filled circles) below 70 mK, plotted as κ_i/T vs T^2. The inset shows the data below 30 mK. From Suderow *et al.*, 1997b.

In summary, a comparison of recent theoretical and experimental results for the thermal conductivity of UPt_3 in phase B leads us to two basic conclusions. First, the behavior of both $\kappa_b(T)$ and $\kappa_c(T)$ in the asymptotic regime—the interval at low temperature where the nodal regions dominate the transport and neither gaplessness nor inelastic scattering is important—is in excellent agreement with a hybrid-II gap—with point nodes along the c axis from which the gap grows as θ^2 and a line node in the basal plane—and resonant impurity scattering ($\delta_0=\pi/2$). This is the simplest, lowest-order gap compatible with E_{2u} symmetry (when $\vec{d}\|\hat{c}$ is imposed). The strongest evidence in support of this identification, in particular as opposed to a hybrid-I gap (of E_{1g} symmetry) is the large value of the anisotropy ratio as $T\to 0$. In addition, the correct limiting temperature dependence (roughly $\kappa/T\sim T^2$) is observed below $\simeq$100 mK for both current directions (Suderow *et al.*, 1997b), and a good quantitative agreement is obtained with calculations using a scattering rate close to that extracted self-consistently from the normal-state data (i.e., $\hbar\Gamma_0=0.05k_BT_c$).

The second conclusion is that there is no such agreement when it comes to the gapless regime. For a hybrid-II gap, the theory predicts a residual linear term of about 1–2 mW K^{-2} cm^{-1} for both directions given the slope/curvature of the gap at the nodes obtained from fitting at higher temperature, and none is seen along the c axis while only a linear term ten times

smaller is resolved along the b axis. Disagreement is also obtained for the finite temperature corrections and the crossover temperature. It is not clear why this part of the theory appears to fail, but the simplified description of impurity scattering, in terms of a single isotropic relaxation rate and a single phase shift at $\pi/2$, may have to be reexamined.

2. Vortex state

The "Volovik effect" discussed in Sec. V.A.2 as the origin of the $\sqrt{H}$ dependence of the specific heat also applies to the heat conduction. The thermal conductivity study of Suderow *et al.* (1998) in UPt_3 represents the most detailed, accurate, and complete study of this phenomenon. Their central result is the observation of excellent scaling of both κ_b and κ_c as a function of the scaling parameter $x = T/T_c\sqrt{H_{c2}/H}$:

$$\frac{\kappa_b(H,T)}{T^{2.7}} = g_b(x), \tag{88}$$

$$\frac{\kappa_c(H,T)}{T^{3.1}} = g_c(x). \tag{89}$$

The scaling functions $g(x)$ flatten off at high x towards a constant so that the zero-field low-temperature power law of roughly T^3 is recovered. Barash and Svidzinsky (1998) have argued that precisely this kind of scaling is expected from a hybrid-II gap, while noticeable deviations from scaling are expected for the hybrid-I gap. Another way of seeing this is to note that at low temperature $\kappa \sim H$ for both current directions, suggesting that the density of states associated with the point nodes along $\hat{c}$ and that associated with the line node perpendicular to $\hat{c}$ has the same energy dependence, as is the case for the hybrid-II gap. In summary, both the weak temperature dependence of the anisotropy ratio κ_c/κ_b in zero field and the behavior in a magnetic field favor a state of E_{2u} symmetry over a state of E_{1g} symmetry for phase B of UPt_3.

C. Ultrasonic attenuation

The propagation of long-wavelength sound waves in a metal at low temperature is damped (or attenuated) primarily by electrons, so that a measurement of ultrasonic attenuation is a probe of the quasiparticle properties. Because sound can be made to travel in various well-defined directions in a single crystal, it is a directional probe very much as thermal conductivity was shown to be. For transverse (or shear) modes of vibration, the possibilities are multiplied because, in addition to the direction of the propagation vector $\vec{q}$, one can also vary the direction of particle motion, i.e., the polarization vector $\hat{\epsilon}$.

A basic consideration in the description of sound attenuation in metals is whether the wavelength λ of the sound wave is greater or shorter than the electronic mean free path l_0. In typical single crystals of UPt_3, with $l_0 < 5000$ Å, and at typical measurement frequencies (between 30 and 500 MHz), one always finds $l_0 < \lambda$, although in the best crystals at the highest frequencies the two lengths do become comparable. In this hydrodynamic (or "dirty") limit, the momentum dependence of the viscosity $\overline{\eta}$ is irrelevent and the attenuation is proportional to the square of the frequency:

$$\alpha_{\vec{q}\hat{\epsilon}} = \frac{\omega^2}{\rho v_s^3}\ \overline{\eta}_{\vec{q}\hat{\epsilon}}, \tag{90}$$

where $\omega = 2\pi f = v_s q = v_s/\lambda$, ρ is the density of the solid, and v_s is the sound velocity. An ω^2 dependence has indeed been observed in all experiments on UPt_3.

It is instructive to compare expressions for the thermal conductivity and the viscosity (in the hydrodynamic limit) for transverse sound (Arfi and Pethick, 1988; Moreno and Coleman, 1996):

$$\kappa_{ii} = \frac{1}{T}\sum_{\vec{k}} \left(-\frac{\partial f}{\partial E_{\vec{k}}} \right) \tau_{\vec{k}} v_{\vec{k}}^2 E_{\vec{k}}^2 [\hat{k}\cdot\hat{\imath}]^2, \tag{91}$$

$$\overline{\eta}_{\vec{q}\hat{\epsilon}} = \sum_{\vec{k}} \left(-\frac{\partial f}{\partial E_{\vec{k}}} \right) \tau_{\vec{k}} v_{\vec{k}}^2 |\vec{k}|^2 [\hat{k}\cdot\hat{q}]^2 [\hat{k}\cdot\hat{\epsilon}]^2, \tag{92}$$

assuming $\vec{v}_{\vec{k}} \| \vec{k}$. At low temperature, only those quasiparticles with $\vec{k}$ near nodal directions are thermally excited. Consider, for example, a node along $\hat{z}$ (or $\hat{c}$, i.e., at $\theta = 0$): κ_{zz} will be strongly enhanced over κ_{xx} because of the factor $[\hat{k}\cdot\hat{\imath}]^2 = \cos^2\theta$. On the other hand, the viscosity will remain almost as low for transverse sound propagating along $\hat{z}$ as it is for $\vec{q} \perp \hat{z}$, due to the extra factor $[\hat{k}\cdot\hat{\epsilon}]^2 = \sin^2\theta\sin^2\phi$. However, for configurations such that neither $\vec{q}$ nor $\hat{\epsilon}$ is perpendicular to the nodal direction, the thermally excited quasiparticles will be much more effective in attenuating the sound. Moreno and Coleman (1996) have emphasized the power of the technique, whereby a choice of $\vec{q}$ and $\hat{\epsilon}$ can make nodes either "active" or "inactive" in this way. This approach was applied to great effect in the case of UPt_3.

Before we consider anisotropic gap structures, it is instructive to compare the behavior of UPt_3 to standard BCS theory for an isotropic gap. This is done using the data of Ellman, Taillefer, and Poirier (1996) in Fig. 23 for α_{ba} in phase B (below T_c^-). For this particular polarization, the attenuation at low temperature rises much more rapidly than it does in conventional superconductors, for which $\alpha(T)$ agrees well with the BCS prediction [i.e., $\alpha(T) = f(\Delta)/f(0)$, where f is the Fermi function]. This is another indication of strong thermal excitation of quasiparticles.

The theory of ultrasonic attenuation in unconventional superconductors has developed in a way very similar to that of thermal conductivity. The same treatment of impurity scattering, assumed isotropic and close to the unitarity limit, and of pair-breaking was adopted. Note that, because the intrinsic zero of electronic attenuation is difficult to establish experimentally with accuracy, a measurement of α is not likely to be a good way of investigating the residual normal fluid predicted by the theory. The calculation of $\alpha_{\vec{q}\hat{\epsilon}}(T)$ is considerably

more involved that that of $\kappa_{ii}(T)$; in addition to the usual deformation potential, several other processes may be relevant, such as possible electric-field effects, collective modes of the order parameter (Wölfle, 1986), and Landau-Khalatnikov damping due to a modulation of the gap by the strain (Miyake and Varma, 1986). Furthermore, vertex corrections are important in the calculation of longitudinal sound attenuation (Hirschfeld, Wölfle, and Einzel, 1988). Finally, the $ql_0 \to 0$ approximation may not always be quite valid.

A number of authors have calculated $\alpha_{\vec{q}\hat{\epsilon}}(T)$ in the hydrodynamic limit for axial, polar, and/or hybrid-I gaps (Rodriguez, 1985; Coppersmith and Klemm, 1986; Hirschfeld, Vollhardt, and Wölfle, 1986; Scharnberg *et al.*, 1986; Schmitt-Rink, Miyake, and Varma, 1986; Monien *et al.*, 1987; Arfi and Pethick, 1988; Arfi, Bahlouli, and Pethick, 1989). All results are qualitatively similar; those of Arfi and Pethick (1988) are shown in Fig. 27, for axial, polar, and hybrid-I ("d-wave") gaps in the strong-scattering limit ($\delta_0 = \pi/2$) neglecting pair-breaking effects. All gaps give rise to pronounced anisotropies. Note the similarity between the polar and the d-wave states, in particular for transverse modes. This is a reflection of the fact that the point nodes at the poles in the d-wave gap are inactive for $\vec{q} \perp \hat{z}$. Note also how much larger $\alpha_{xy}(T)$ is relative to $\alpha_{xz}(T)$, as a result of (sections of) the equatorial line nodes being activated for $\hat{\epsilon} \perp \hat{z}$. A large anisotropy ratio $\alpha_{xy}(T)/\alpha_{xz}(T)$ is therefore a signature of a line node in the basal plane in uniaxial gaps.

1. Transverse sound

The attenuation of transverse sound in superconducting UPt_3 was measured by Müller *et al.* (1986) for $\vec{q} \| \hat{c}$ and by Shivaram, Jeong, *et al.* (1986), Thalmeier *et al.* (1992), and Ellman, Taillefer, and Poirier (1996) for $\vec{q} \| \hat{b}$ and both $\hat{\epsilon} \| \hat{a}$ and $\hat{\epsilon} \| \hat{c}$. In all cases, $\alpha \propto \omega^2$. From the magnitude of $\alpha(T_c) v_s^3 / f^2 \propto \tau(T_c)$, it appears that the various crystals used were of comparable quality (within a factor of 2), and it seems that the measurement of α_{bc} by Thalmeier *et al.* had problems (the size of the attenuation is 100 times too small). In their seminal study, Shivaram, Jeong, *et al.* (1986) found the viscosity ($\propto \alpha v_s^3$) to be isotropic in the normal state and to become distinctly anisotropic in the superconducting state, with $\alpha_{ba} \sim T$ and $\alpha_{ba} \sim T^3$ approximately. It was their study on UPt_3 that first provided definitive evidence for a highly anisotropic gap in heavy-fermion superconductors. Their data were soon shown to be in qualitative agreement with a gap structure with a line of nodes in the basal plane (Schmitt-Rink, Miyake, and Varma, 1986), such as a polar gap (Shivaram *et al.*, 1987). Ten years later, Ellman, Taillefer, and Poirier (1996) performed the same study on a crystal with two well-resolved transitions and were therefore able to measure transverse sound attenuation not only in phase B but also in phase A. Their results are shown in Fig. 28 (bottom panel). Early and recent data are in excellent agreement (for phase B).

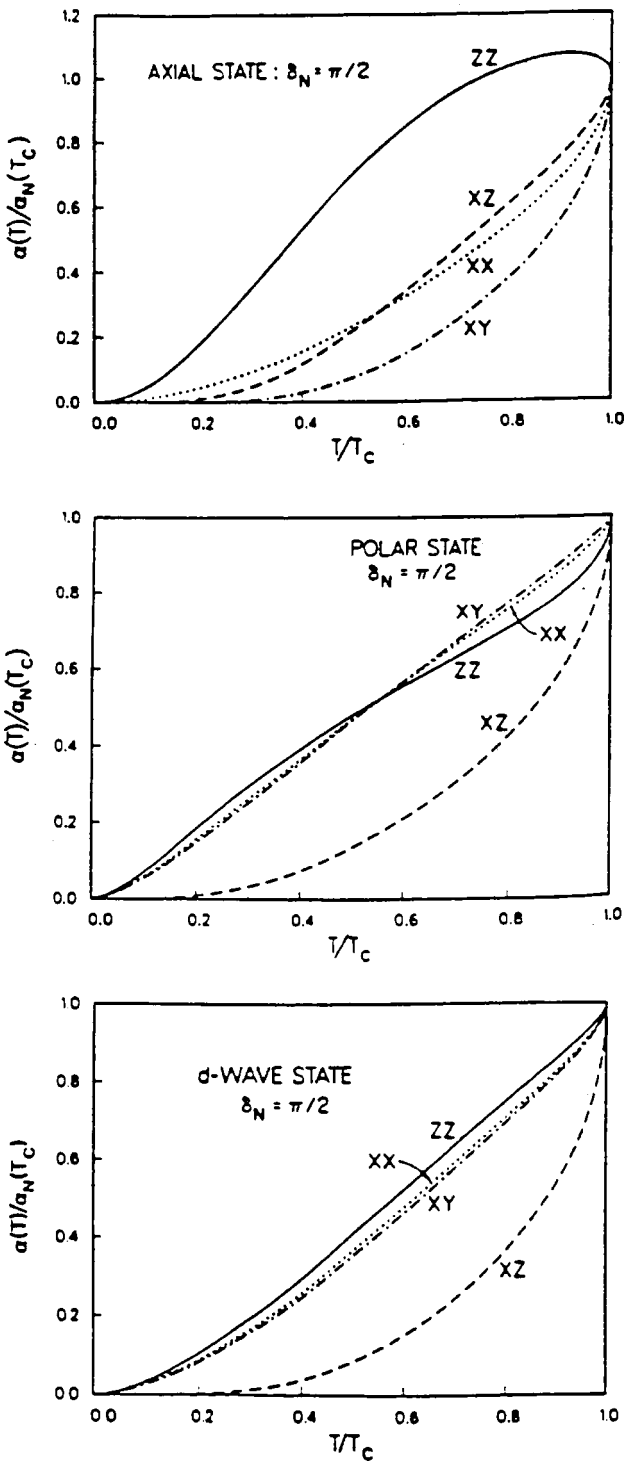

FIG. 27. Components of the ultrasound attenuation relative to their normal-state values at T_c calculated for the axial, polar, and hybrid-I (d-wave) gaps, assuming resonant impurity scattering and $\Gamma_0 \to 0$. From Arfi and Pethick, 1988.

As a result of its limited range in temperature, very little was known about phase A, and this study provided the first information on the quasiparticle spectrum in that phase. As may be seen, α_{ab} drops initially with decreasing temperature before becoming roughly constant, while α_{ac} has only a slight "bump" seemingly superimposed on the sharply falling attenuation observed in the

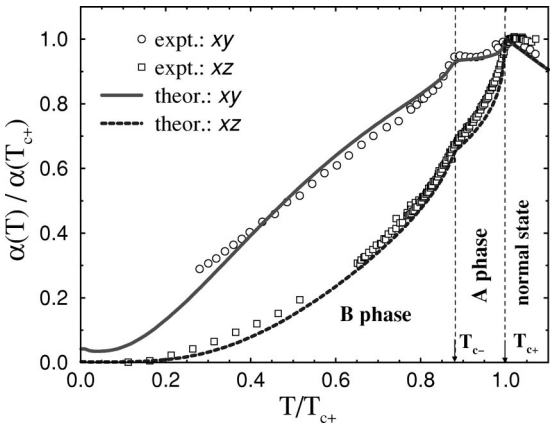

FIG. 28. Transverse ultrasound attenuation normalized at T_c^+ (data from Ellmann, Taillefer, and Poirier, 1996), compared to calculations by Graf, Yip, and Sauls (2000) for an E_{2u} gap.

B phase. Qualitatively, this implies that more quasiparticles exist in phase A than would be present if phase B extended up to the same temperature. Specifically, these extra excitations preferentially scatter sound when the polarization is in the basal plane. When the data are normalized to the attenuation at either T_c^+ or T_c^- and are plotted as a function of temperature normalized to the appropriate critical temperature, it is evident that α_{ab} is much enhanced in the A phase as compared to the B phase (see Taillefer, Ellman, *et al.*, 1997). In contrast, the data for the c-axis polarization, α_{ac}, are roughly equal in the two phases. From the observed difference in the anisotropy of the two phases, the authors conclude that the order parameter associated with phase A must change upon going into phase B, thereby providing additional evidence for a transition between two distinct superconducting states at T_c^-. There are more nodal lines in the gap structure of phase A than in that of phase B.

Graf, Yip, and Sauls (2000) have recently calculated the attenuation of transverse sound in both phases of UPt_3 for a number of gap structures and fitted these to the data of Ellman, Taillefer, and Poirier (1996), in an attempt to further discriminate between the possible scenarios for the phase diagram. Their results for the E_{2u} scenario are shown in Fig. 28. Specifically, the calculated curves are for a $(1,i)$ orbital state in phase B, with a $k_z(k_x^2+k_y^2)$ nodal structure, and a (1,0) state in phase A, with a $k_z(k_x^2-k_y^2)$ nodal structure. The agreement with experiment is excellent for both polarizations and for both phases, which leads the authors to conclude strongly in favor of the E_{2u} scenario. Indeed, equivalent calculations for E_{1g} and other scenarios fail to account for the behavior in the A phase (Graf, Yip, and Sauls, 2000). [Very recently, this conclusion has been challenged by Wu and Joynt (2002).] It should be stressed that this conclusion is weakened if one takes into account the multidomain structure that is likely to exist in phase A. For the calculated curves of Fig. 28, the authors have assumed a single domain over the whole crystal and, moreover, an optimum alignment of the nodal structure $k_z(k_x^2-k_y^2)$, i.e., such that the two mutually perpendicular planes of nodes containing the c axis are at 45° from the propagation vector $\vec{q}$. If the very existence of phase A is due to a coupling with the antiferromagnetic order, one expects the three equally populated magnetic domains (Lussier *et al.*, 1996) to generate a corresponding domain configuration for the superconducting order parameter, so that the nodal planes will be at $\pm 45°$ from the 0°, 120°, and 240°, directions. A more realistic calculation is to average over these three orientations. This averaging was shown to suppress the degree of anisotropy between α_{xy} and α_{xz} (Graf, Yip, and Sauls, 2000). Moreover, it eliminates the difference between E_{1g} and E_{2u}, and most probably means that one cannot tell whether it is the (1,0) state or the (0,1) state which is favored in phase A. For example, the (0,1) state in E_{2u} has $k_z k_x k_y$ nodal structure, i.e., the same three mutually orthogonal nodal planes as for (1,0) but rotated by an extra 45° about the c axis. Although this difference in orientation can lead to a large discrepancy in the attenuation arising in the two states in a single, suitably chosen monodomain, the discrepancy is averaged away in a multidomain configuration.

In summary, it is probably fair to say that the recent calculations of Graf, Yip, and Sauls (2000) confirm that the transverse sound attenuation measured in both phases A and B is compatible with the symmetry-breaking-field scenarios based on either E_{1g} or E_{2u} symmetry, but they do not allow one to distinguish between the two or allow one to determine whether it is the (1,0) or the (0,1) state which exists in phase A.

2. Longitudinal sound

The experimental situation for longitudinal sound attenuation in UPt_3 is somewhat confused. The first measurement, by Bishop *et al.* (1984), yielded a roughly T^2 dependence for α_{zz} between 0.15 and 0.4 K. Two years later, Müller *et al.* (1986) obtained $\alpha_{zz} \sim T^3$ in the same range, and also observed a lambda-shaped peak just below T_c. Then Schenstrom *et al.* (1989) obtained $\alpha_{zz} \sim T^{1.2}$; they also observed a very small anisotropy, with $\alpha_{xx} \sim T^{1.3}$. Thalmeier *et al.* (1992) also reported a virtually isotropic behavior, but this time with $\alpha_{zz} \simeq \alpha_{xx} \sim T^3$. Finally, in a high-resolution experiment down to much lower temperature (5 mK), Jin, Lee, *et al.* (1992) obtained $\alpha_{xx} \sim T^{1.5}$ for a fit between 5 and 400 mK. They also saw a sharp peak at T_c^+ and a "bump" at T_c^-. Unfortunately, they did not measure the anisotropy. It was taken on the same crystal as used previously by Schenstrom *et al.*, and the two sets of data for $\alpha_{xx}(T)$ agree well (the slightly different power laws come from the fact that Jin *et al.* included the range 5–100 mK, which by itself gives $T^{1.8}$). The data of Schenstrom *et al.* (1989) are shown in Fig. 29 for both modes.

One should not attach too much importance to the actual power law, but the fact that different measurements yield such different fits is intriguing. A number of

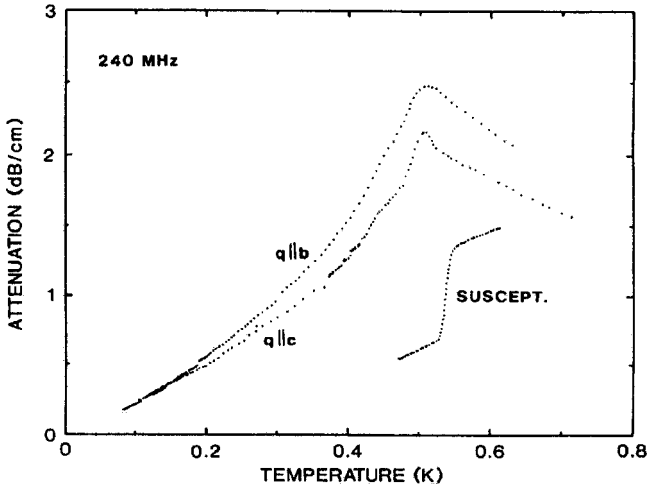

FIG. 29. Attenuation of longitudinal ultrasound propagating along the b axis and the c axis at 240 MHz as a function of temperature. From Schenstrom *et al.*, 1989.

factors would have to be examined in order to reconcile these disparate results. First, the frequency was different (it ranged from 92 MHz for Müller *et al.* to 508 MHz for Bishop *et al.*) and frequency effects have been observed (Müller *et al.*, 1986). Second, the relative importance of elastic and inelastic scattering was different for the different crystals. By itself, this effect could well account for most of the discrepancy. From the magnitude of the attenuation at T_c, one can see that the importance of inelastic scattering was about five times (three times) smaller in the experiment of Müller *et al.* (Bishop *et al.*) than it was in the case of Schenstrom *et al.* Of course, the possibility of heating the sample at the lowest temperature is perhaps an issue in some cases, giving rise to a false flattening off of α at low temperature. When comparing with the calculations in Fig. 27, the data of Fig. 29 below T_c^- are seen to be in fair agreement for either a polar or a hybrid-I gap. In order to say more, detailed calculations which include inelastic scattering and the presence of phase A are needed.

The peak at T_c in the longitudinal $\alpha(T)$, also seen in UBe_{13} (Golding *et al.*, 1985), has been attributed to a variety of mechanisms, including collective modes (Wölfle, 1986) and damping by domain walls (Joynt, Rice, and Ueda, 1986). For a discussion of this feature, see Sigrist and Ueda (1991) and Grewe and Steglich (1991).

In conclusion, the measured temperature dependence of both transverse and longitudinal ultrasonic attenuation in UPt_3 is in agreement with calculations assuming a hybrid gap in phase B and a gap structure with additional nodal planes in phase A. This is qualitatively consistent with both E_{1g} and E_{2u} scenarios.

We have not mentioned here studies in a magnetic field, for they have contributed little solid information on the nature of the superconducting phases. Note, however, that anomalies in the magnetic-field dependence of the longitudinal ultrasonic attenuation, first observed by Müller *et al.* (1987) and Qian *et al.* (1987), and investigated later by Schenstrom *et al.* (1989), provided the first clear indication of a phase transition between phase B and phase C.

D. London penetration depth

1. Vortex lattice

The subject of vortices is always interesting for theorists because of its intrinsic beauty. In UPt_3 alone, it has generated a literature of goodly size. Some other reviews of this topic have appeared. Salomaa and Volovik (1987) reviewed vortices in ^{3}He—this topic is the ancestor of all such work in UPt_3. Sigrist and Ueda (1991) included a summary of work on unconventional superconductors. We shall not recapitulate indvidual papers in detail, because there are, to date, few experiments that can test the theories. Only some conceptual developments will be mentioned. Schenstrom *et al.* (1989), Hess *et al.* (1989), and Tokuyasu *et al.* (1990) showed numerically that, for $\vec{H}$ along the c axis, the vortices become nonaxisymmetric. This could drive a transition in the flux lattice from hexagonal to honeycomb as a function of applied field. Similar effects have been found for all directions of $\vec{H}$ (Barash and Mel'nikov, 1991). The analytic groundwork for understanding the energetics of vortex lattices is contained in papers of Luk'yanchuk (1991) and Zhitomirskii and Luk'yanchuk (1992). For $\vec{H}$ along the c axis, one can even find a transition from a lattice consisting of single-quantum vortices to double-quantum vortices (Mel'nikov, 1992) in certain parameter ranges.

The only direct measurement performed to date on the vortex structure is low-angle neutron scattering (Kleiman *et al.*, 1992; Yaron *et al.*, 1997). In this experiment, the applied magnetic field is in the basal plane, say $\vec{H}=H\hat{x}$. It satisfies $H_{c1}\ll H<H_{c2}$. The neutrons are incident on the sample from the same direction. They scatter off the gradient in the magnetic field which is the result of the flux lattice. The scattering amplitude for a change in neutron wave vector $\vec{Q}$ is proportional to $h(\vec{Q})$, the Fourier component of the field. $\vec{Q}$ lies in the y-z plane, so the two crystal axes of the flux lattice are not equivalent. The scattering intensity is very low and falls off as λ^{-4}, where λ is a penetration depth. This means in practice that only Bragg scattering at the first shell of reciprocal-lattice vectors can be observed and only low temperatures (where λ is relatively small) are accessible. In the most recent experiment, the intensities have been measured at 50 mK and from 3 to 9 T. The A phase is not probed, but the BC transition is believed to occur at around 5–6 T in this sample, and signatures of it may be searched for. The experiment looked at the peak positions (lattice structure) and their intensities (form factor).

A conventional centered rectangular lattice is observed, i.e., a triangular lattice compressed in the c direction. The opening angle is $2\alpha_L=38°$ (at low field) instead of the standard $2\alpha_L=60°$ for a perfect triangular lattice. In the anisotropic London theory, the angle α is

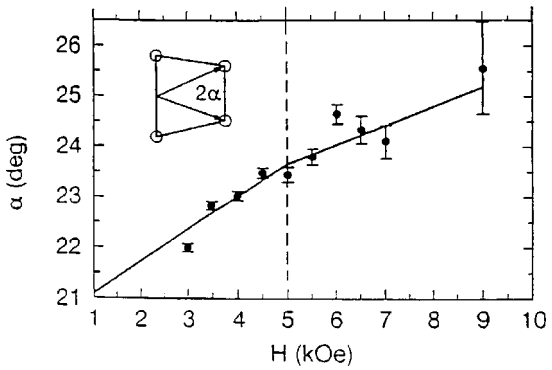

FIG. 30. The opening angle of the centered rectangular vortex lattice as a function of field from Yaron *et al.* (1997). The opening angle is defined in the inset. The fit is from Joynt (1997).

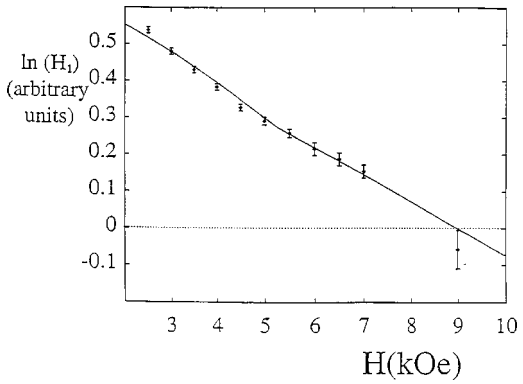

FIG. 31. The intensity of the first shell of Bragg peaks as a function of field from Yaron *et al.* (1997). The fit is from Joynt (1997).

governed by anisotropy in both the Fermi velocity and the gap, much as H_{c2} is. Describing both sources of anisotropy in terms of an effective mass tensor, Kleiman *et al.* find $m_\perp/m_\parallel=(3\tan^2\alpha_L)^{-1}=2.8$, a value very close to the normal-state mass ratio ($m_r=2.7$). Therefore, just as for our H_{c2} analysis of the A phase (see Sec. IV.B), we arrive at the conclusion that no additional anisotropy from the gap structure seems to show up in the B phase, measured this time by the distortion of the vortex lattice.

From a measurement of the form factors for the vortex-lattice Bragg peaks, Kleiman *et al.* (1992) obtain the following independent estimates for the coherence length and penetration depth: $\xi_\parallel(0)=157\pm4$ Å, $\xi_\perp(0)=93\pm3$ Å, $\lambda_\parallel(0)=4220\pm90$ Å, $\lambda_\perp(0)=7150\pm150$ Å. From these numbers we get a separate estimate of the average plasma frequency, namely, $\hbar\overline{\omega}_p=0.39$ eV, which is only 5% larger than we had evaluated from the resistivity and our estimate of $\tau_0=8\times10^{-11}$ sec (for $\rho_{0,c}=\rho_{0,\parallel}=0.23\ \mu\Omega$ cm), which is thereby nicely confirmed. Note that infrared reflectivity data also yield an average plasma frequency equal to 4.8×10^{14} sec^{-1}, or 0.32 eV (Sulewski *et al.*, 1988).

Let us now look at the effect of increasing the field (still applied in the basal plane). The structure remains centered rectangular through the BC transition. This is in agreement with a theorem of Zhitomirskii (1989) that this is the only possible structure for the vortex lattice of a two-component superconductor. At least for this direction of the field, there is no change from hexagonal to honeycomb. However, the opening angle α_L shows an overall increase as the field is increased (see Fig. 30). In the C or high-field phase, we should find conventional behavior, as only one component exists and the free energy of its spatial configurations is the same as that for a conventional superconductor (Barash and Mel'nikov, 1994; Fujita *et al.*, 1994). Thus we expect a field-independent α_L in this phase. Standard one-component theory gives $\tan^2(\alpha_L)=K_1/3K_4$. In the B phase, the second component grows as $\sqrt{(H_{BC}-H)}$. The second component has a different anisotropy in its stiffness coefficients (the K's). The anisotropy of the whole lattice is a combination of the two, leading to a field-dependent anisotropy. The angle is given by Joynt (1997),

$$\tan^2(\alpha_L)=\frac{K_1+r^2(H)(K_1+K_2+K_3)}{3[1+r^2(H)]K_4}, \tag{93}$$

with $r^2(H)$ the average ratio of $|\eta_x|^2$ to $|\eta_y|^2$, so that $r^2(H)\sim(H_{BC}-H)$. The stiffness coefficients are as defined in Eq. (38). The fact that α_L is found to be field dependent in UPt_3 at low fields is therefore consistent with a two-component picture. The prediction that it is field independent at higher fields is consistent with the data of Yaron *et al.* (1997), reproduced in Fig. 30, if their last data point at the highest fields, with large error bars, is ignored.

The second set of data is the intensity as a function of field. A form factor is usually measured by looking at the falloff of intensity at successively larger Bragg peaks. Here we are looking at the same Bragg peak but changing the lattice constant. The overall decrease in slope is due to the fact that the cores overlap more as the field increases, so the field distribution becomes smoother. Roughly, the intensity is $\sim\exp(-c\xi_0^2/a^2)$, where a is the intervortex separation, c is a constant, and ξ_0 is a coherence length.

A theory of this intensity in an unconventional superconductor, based on the picture of the B phase presented in Sec. IV.B, but assuming a double lattice with no offset, has been worked out (Joynt, 1997). The basic point is that the form factor should show a kink as H passes through H_{BC}. The kink is due to the fact that a second coherence length appears in the B phase. The data of Yaron *et al.* (1997), shown in Fig. 31, are consistent with this.

The theory of the neutron scattering is still at a simple level. Nonlocal effects may be important at the relatively low experimental temperatures (Takanaka, 1977). Also Yaouanc, Dalmas de Réotier, and Brandt (1997) have criticized the cutoff procedure implicit in the calculations. In addition, the theory is based on a generic two-component picture, so it gives no way to distinguish between different gap structures. The field needs more experimental input, possibly from other techniques for looking at vortices, such as decoration, scanning tunnel-

ing microscopy, and electron imaging, as well as more theoretical work.

Let us now turn to the A-B transition. This was investigated by Huxley *et al.* (2000), who used neutron scattering to look at the vortex lattice at $H=0.19$ T as a function of temperature for $\vec{H}\|\hat{c}$. They found that the lattice is accurately hexagonal in both phases. In the B phase, the nearest-neighbor vector is parallel to the a^* direction, while in the A phase it rotates by $\pm 15°$. They interpret this result as an alignment of the lattice to a gap of E_{2u} form, noting that a gap with $k_x k_y$ behavior in the plane should give rise to such an orienting effect, as it naturally introduces a 15° angle in the problem, unlike the k_x or k_y gaps appropriate for E_{1g}. The connection between the form of the gap and the lattice orientation is actually rather indirect, however, and a full Ginzburg-Landau analysis would be preferable. This has very recently been carried out by Moreno and Sauls (2001), who conclude that the data favor E_{2u}.

2. Temperature dependence

Because of the simple relation between the London penetration depth and the superfluid density tensor, $1/(\lambda_L^i)^2 \sim n_s^i$, a measurement of the penetration depth is a powerful probe of the superconducting state. There are two aspects to the measurement: (1) the absolute value $\lambda_i(0)$ and its anisotropy—which as we saw simply give the plasma frequency and the mass anisotropy—and (2) the temperature dependence $\delta\lambda_i(T)$ and its anisotropy—which give information about gap nodes and their configuration (see Sec. V; Gross-Alltag *et al.* 1991; Barash and Svidzinsky, 1996). As mentioned in Sec. V, the measurement of $\delta\lambda(T)$ in $YBa_2Cu_3O_7$ played a leading role in establishing the existence of line nodes in the gap structure of the high-T_c superconductor $YBa_2Cu_3O_7$ (Hardy *et al.*, 1993). For this material, microwave cavity techniques proved the most sensitive, and were successful because of the high degree of surface perfection achieved in as-grown single crystals (and helped by the large T_c). This issue of surface quality is a crucial one for most techniques attempting to measure the penetration depth, a concern we have not been faced with in the discussion of bulk probes. Indeed, because the magnetic field penetrates only about 1 μm into a sample of UPt_3 (0.2 μm in $YBa_2Cu_3O_7$), a large fraction of that depth must be free of defects which perturb the screening currents, and be representative of the bulk. The surface-sensitive techniques that have been applied to UPt_3 are mainly dc magnetization (see, for example, Gross-Alltag *et al.*, 1991) and ac susceptibility (see, for example, Signore *et al.*, 1994), as well as other high-frequency inductive techniques (see, for example, Shivaram, Gannon, and Hinks, 1990; Bruls, 1995).

The dc magnetization results of Gross-Alltag *et al.* (1991) for three single crystals and two field directions yield $\delta\lambda \sim T^2$ in all cases, with little anisotropy in the prefactor. (Note that similar supercurrent configurations may exist for different field directions.) Polishing leads to a 50% increase in $\delta\lambda$. This effect leads the authors to conclude that "because of the observed sensitivity of the crystal surfaces to mechanical working, a more sophisticated surface preparation would seem necessary to determine a $\delta\lambda$ anisotropy unambiguously." Much the same conclusion may be reached from the studies of Signore *et al.* (1994). Another cause for concern is the large value extracted at low temperature: $\lambda(0)=19\,000 \pm 5000$ Å, a factor of 3 larger than expected.

In recent years, muon spin relaxation (μSR) has become a prime method for the study of type-II superconductors, because it is largely insensitive to surface effects (muons penetrate ~ 100 μm) and it allows for an absolute measurement of λ. The inhomogeneity of the field profile inside the sample when permeated by vortices leads to a relaxation of the muon spin, which can be detected and used as a measure of the field distribution. The weak point of this technique is that in order to extract $\lambda(T)$ from the observed relaxation, a convoluted analysis and some assumptions about the vortex lattice are necessary. Broholm *et al.* (1990) were the first to use transverse-field μSR to probe the internal field distribution of a crystal of UPt_3 along both high-symmetry directions. The penetration depth for the B phase they extract from their analysis has the following characteristics. The absolute value of the London penetration depth at $T=0$ is $\lambda_\|(0)=6920\pm 40$ Å, $\lambda_\perp(0)=7200 \pm 100$ Å. While $\lambda_\perp(0)$ is in excellent agreement with estimates from either normal-state transport or neutron diffraction, $\lambda_\|(0)$ is considerably larger then these estimates (by a factor of 1.6). The temperature dependence of $\lambda_\perp(T)$, which reflects that of the superfluid density in the basal plane, obeys

$$\frac{\lambda_\perp^2(0)}{\lambda_\perp^2(T)} = \left(1+\frac{\delta\lambda_\perp(T)}{\lambda_\perp(0)}\right)^{-2} \simeq 1 - a\frac{T}{T_c}, \tag{94}$$

all the way from 0.1 to $0.6T_c$, with $a \simeq 1$ (Broholm *et al.*, 1990). The fact that a is so large means that thermal excitation of quasiparticles with velocity in the basal plane is strong, as was previously established by transverse ultrasonic attenuation. Assuming that this dependence extrapolates down to low temperature implies $\delta\lambda \sim T$, as expected for a line node in the basal plane. The other component, $\lambda_\|(T)$, is somewhat flatter at low temperature. The authors argue that a proper fit is only possible with a hybrid-type gap (with both a line node at the equator and point nodes at the poles) and is not consistent with a polar gap.

Yaouanc *et al.* (1998) have recently performed the same μSR experiment on a single crystal with a clear double transition. Their data are shown in Fig. 32. They obtain values of $\lambda(0)$ that are in better agreement with the neutron and H_{c2} results: $\lambda_c(0)=4260\pm 150$ Å, $\lambda_a(0)=6040\pm 130$ Å. The temperature dependence agrees qualitatively with that of Broholm *et al.* Yaouanc *et al.* were able to fit their data using either a hybrid-I gap, proportional to $Y_{21}-0.1Y_{41}$, or a hybrid-II gap, proportional to $Y_{32}-0.1Y_{52}$. As can be seen from Fig. 32, both gaps fit the low-temperature data reasonably well. (Note that the best fit for hybrid I is obtained using

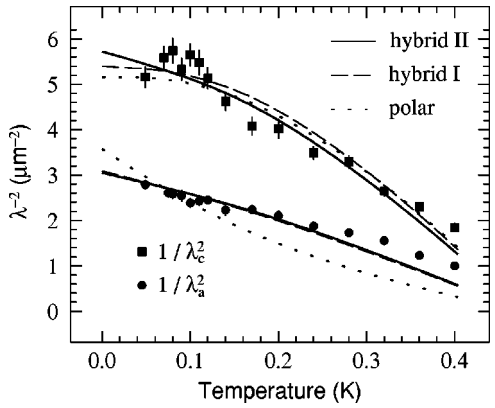

FIG. 32. Temperature dependence of the penetration depth for principal directions parallel (λ_c) and perpendicular (λ_a) to the c axis, plotted as $\lambda_i^{-2}(T)$ vs T. Lines are fits assuming the three different gap structures as shown. From Yaouanc *et al.*, 1998.

the very same orbital dependence that gave the best fit to the thermal conductivity data in Fig. 25.)

In summary, the μSR data of Yaouanc *et al.* (1998) are in remarkably good agreement with the picture developed until now for the superconducting state of UPt_3. The anisotropy in $\delta\lambda(T)$ supports the assignment of a hybrid gap to the B phase and the magnitude of $\lambda(0)$ is just right.

E. Other properties

There are a host of properties measured in UPt_3 not mentioned in this review, which in principle also contain information about the symmetry of the order parameter. We have elected to focus on those properties which we felt were at a sufficiently advanced stage of development to warrant a meaningful confrontation between theory and experiment. Furthermore, there are areas of investigation that have not yet been, or are just beginning to be, exploited in the case of UPt_3, such as electron tunneling and electromagnetic absorption—which played such a prominent role in our understanding of conventional superconductors—or Josephson junctions and angle-resolved photoemission, which have produced some of the most decisive information in the high-T_c cuprates.

In this section, we discuss briefly two techniques that have shed some light on the order parameter of UPt_3 from a different angle to that of thermodynamic and transport properties discussed until now: nuclear magnetic resonance and point-contact spectroscopy. The former can access information about the spin part of the wave function (via the Knight shift), as was done so beautifully in superfluid ^{3}He, and it is an example of case-II coherence factors (nuclear-spin relaxation rate), as opposed to the case-I coherence factors applicable to κ and α. The latter technique is one of several spectroscopic probes of superconductors, measuring the energy gap directly rather than indirectly via the temperature and field dependence, and one of the few actually applied with some success to UPt_3.

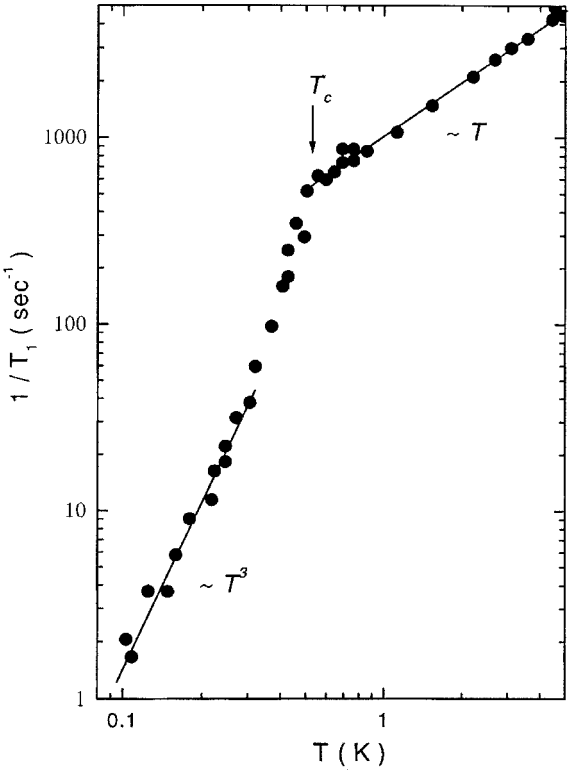

FIG. 33. Temperature dependence of the nuclear magnetic relaxation rate ($1/T_1$) measured on a powdered sample. From Kohori *et al.*, 1988.

1. Nuclear magnetic resonance

a. Nuclear-spin relaxation

Nuclear spins precessing in a magnetic field will relax as a result of their interaction with conduction electrons. The relaxation process involves the flipping of spins so that the relevant coherence factor (case II) which accounts for the pair correlations in the superconducting state is different from that relevant to κ and α where no spin flip occurs (case I). For an s-wave order parameter, this difference shows up dramatically as a peak in $1/T_1$ just below T_c, reflecting the divergent density of states at the gap edge (see, for example, Tinkham, 1996). For unconventional order parameters, case-I and case-II coherence factors are the same and contribute no extra energy dependence relative to the matrix elements in the normal state, so they do not lead to any enhancement (Sigrist and Ueda, 1991). Therefore the presence of a so-called Hebel-Slichter peak in $1/T_1$ is a signature of a conventional s-wave order parameter.

The nuclear magnetic relaxation rate of ^{195}Pt in UPt_3 was measured by Kohori *et al.* (1988), using powders of 70–200 μm (to maximize surface area). Their data are plotted in Fig. 33 on a log-log plot. In the normal state, from 0.5 to 4.2 K, a Korringa law ($1/T_1 \sim T$) is observed, consistent with the Fermi-liquid behavior seen in other properties (although seldom to quite as high a temperature). The relaxation rate drops precipitously just below T_c, in a way that is reminiscent of $\alpha_{xy}(T)$. The absence of any Hebel-Slichter peak is unambiguous. At low tem-

perature, between 0.1 and 0.3 K, $1/T_1 \propto T^3$, just as expected for a gap with a line node or, more precisely, for a quasiparticle density of states that grows linearly in energy (Sigrist and Ueda, 1991). This is true of the E_{1g}, E_{2u} with $\vec{d} \| \hat{z}$, and polar gaps. It is an intriguing fact that a T^3 dependence of $1/T_1$ at low temperature is observed in virtually all unconventional superconductors: heavy fermions (UPt_3, UBe_{13}, $CeCu_2Si_2$, UPd_2Al_3), high-T_c cuprates (e.g., $YBa_2Cu_3O_7$), Sr_2RuO_4, and organics. Kohori *et al.* (1988) were able to fit their data assuming a polar gap $\Delta_0 \cos\theta$ and neglecting gapless effects due to impurity scattering. From a best fit to the entire T dependence, they get $\Delta_0 = 5.3 k_B T_c$. In the usual way, the coefficient of the T^3 term at low temperature is dictated by the regions in the gap near the nodes, in this case by the slope of the gap at the line node, and the fit therefore yields $S_{line} = 5.3 k_B T_c$. Note that the value obtained in Sec. V.B from fitting $\kappa(T)$ with an E_{1g}-type gap in the asymptotic regime was $S_{line} = 5.3 k_B T_c$, using the weak-coupling value for the maximum gap, $\Delta_{\max} = 2.1 k_B T_c$. (A very similar value is obtained for the E_{2u} gap.) This clearly calls for a full calculation of $1/T_1$ vs T using both the E_{1g} and E_{2u} gaps.

We note *en passant* that there is no indication of a linear term in $1/T_1$ at low temperature. Just as in the results for $\kappa(T)$ down to 0.1 K, the residual normal fluid predicted by theory for UPt_3 with $\hbar\Gamma_0 \simeq 0.1 k_B T_c$ (Hirschfeld, Wölfle, and Einzel, 1988) remains elusive.

b. Knight shift

The Knight shift is important because it gives the actual spin polarization at a nuclear site. Thus the spin susceptibility χ_s can be measured, although absolute measurements require the independent determination of hyperfine coupling constants. In superfluid ^{3}He, the susceptibility of the isotropic B phase drops by 1/3 on cooling from T_c to 0, while in the equal-spin-paired A phase, there is no change in the measured χ_s as long as the order parameter is free to rotate. In an s-wave superconductor, χ_s drops to zero. It is possible to make bulk measurements on strongly type-II materials such as UPt_3 in the range $H_{c1} \ll H < H_{c2}$ because the field in the sample is essentially uniform.

Measurements in the normal state confirmed that the temperature dependence of the Knight shift tracks the temperature dependence of the measured uniform susceptibility (Kohori *et al.*, 1987, 1990). The shift is large, reflecting the heavy-fermion nature of UPt_3, and negative, reflecting negative hyperfine couplings between the d and the s electrons of the Pt atom. Near T_c, the shift is about -8% for $H \perp c$ and about -2% for $H \| c$ (Lee *et al.*, 1993). In the superconducting state, some temperature dependence of the Knight shift has been detected (Tou *et al.*, 1996, 1998). However, the reduction of the shift is very small. If we denote the shift for $H \| c$ as K_c, and those for H along the a and b directions as K_a and K_b, and their changes on reducing the temperature from T_c to 0 as δK_i, then the observations are that $\delta K_a \approx 0$, $\delta K_b = 0.07\%$, and $\delta K_c = 0.08\%$. Furthermore, the latter two changes occur only at low fields. If $H_b \geqslant 3.37$ kOe or $H_c \geqslant 2.30$ kOe, then $\delta K_b = 0$, and $\delta K_c = 0$. No change at all, or possibly a very small rise, in the shift is observed if H is along a, at all field strengths. Even the largest changes are not much bigger than the error bars.

Tou *et al.* interpret their results in terms of the spin-triplet theory (Ohmi and Machida, 1996a, 1996b) with very small spin-orbit coupling, which gives results similar to the A phase of ^{3}He. The in-plane anisotropy is then attributed to coupling of the superconducting order parameter to $\vec{M}_S$. The picture requires, in addition, a reorientation of $\vec{d}$ as a function of H for H along the c axis at around $H_c = 2.3$ kOe. This explanation has the virtue of explaining the isotropy of δK_i at high fields. However, it has several drawbacks. It does not explain the foremost puzzle about the results, which is why the changes, when they do occur, are very small. It takes no account of the Van Vleck part of the susceptibility, which is large but not affected by superconductivity, as pointed out in Sec. II.C.1. Finally, there is no independent evidence for a reorientation transition at $H_c = 2.3$ kOe from other measurements. While the Knight-shift results are not conclusive in favor of any theory, they speak against singlet models such as the E_{1g} model, which should have a reduced susceptibility at zero temperature. Even in this case, however, no theory of the Knight shift that takes into account spin-orbit coupling and Van Vleck contributions has been offered so far.

2. Point-contact spectroscopy and Josephson tunneling

The current-voltage characteristics of a point contact between a normal electrode (or tip) and a superconductor can yield spectroscopic information on the energy gap via the mechanism of Andreev reflection. For a recent review of point-contact spectroscopy in heavy-fermion superconductors, the reader is referred to the excellent article by Löhneysen (1996). We will only summarize here the main results and conclusions.

A typical point-contact spectrum on UPt_3 is shown in Fig. 34, for an electron injection preferentially along the c axis. A gap is unambiguously observed, with a maximum amplitude of about 100 μV, or $\approx 2 k_B T_c$. The V-shaped feature is at variance with the prediction for a standard s-wave gap which leads to a flat region near zero bias (see Fig. 34). [More conventional gap features of this kind have been seen in $CeCu_2Si_2$ and URu_2Si_2 for current directions also along $\hat{c}$ (De Wilde *et al.*, 1994).] The fits in Fig. 34 are as follows: curve 0, $\Delta = \Delta_0$ (isotropic gap); curves 1 and 3, $\Delta = 2\Delta_0 \hat{k}_z (\hat{k}_x + i\hat{k}_y)$; curve 2, $\Delta = \Delta_0 \hat{k}_z$; curve 4, $\Delta = (s\sqrt{3}/2)\Delta_0 \hat{k}_z (\hat{k}_x^2 + \hat{k}_y^2)$, with $\Delta_0 = 75$ μV and $m_\perp / m_\| = 2.25$ for curves 0, 1, 2, 4 and $\Delta_0 = 75$ μV and $m_\perp / m_\| = 10$ for curve 3. The V shape is thus seen as evidence for a point node along $\hat{c}$, as supported by the various fits in Fig. 34. The fit for gaps with a point node yields a gap maximum $\Delta_0 = 75$ μV $= 2.0 k_B T_c$ ($T_c = 0.44$ K). In UPt_3, unlike in $CeCu_2Si_2$ and URu_2Si_2, the gap feature disappears rap-

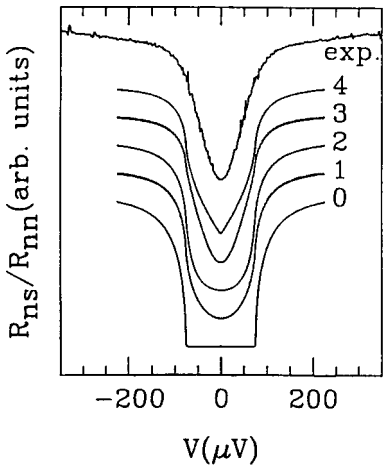

FIG. 34. Point-contact spectroscopy: normalized differential resistance vs voltage of a silver tip pressed on the basal plane of a UPt_3 single crystal (exp.), compared with calculations for various gap structures described in the text. From De Wilde *et al.*, 1994.

idly with increasing magnetic field or temperature (De Wilde *et al.*, 1994), in keeping with the strong thermal excitation of quasiparticles along $\hat{c}$. Point-contact spectra for injection in the basal plane in most cases show no feature (Goll *et al.*, 1993), a fact used as evidence for a line node in the basal plane, possibly broadened into a "belt" by impurities. Goll *et al.* (1995) have observed a double-minimum structure typical of Andreev reflection. These authors argue that such a structure is only possible if the order parameter does not change sign as $k_z \rightarrow -k_z$. In other words, a gap given, for example, by $|k_z|(k_x+ik_y)$ (of E_{1u} symmetry) can account for the double minimum, but $k_z(k_x+ik_y)$ (of E_{1g} symmetry) cannot.

The Josephson effect was observed for the first time in UPt_3 by Sumiyama *et al.* (1998). They clearly observed a supercurrent in UPt_3-Cu-Nb junction in an SNS configuration. Some differences in the critical current were seen between current flow in the *b* and *c* directions. The authors ascribed this to an underlying anisotropy in the order parameter. However, the Fraunhofer pattern was chaotic, suggesting nonuniform current flow. Furthermore, the measurements for different directions were taken on different faces with correspondingly different Cu interlayers. This makes it difficult to normalize the results with respect to one another. In the SNS configuration, there is no $eI_cR_n/\Delta \sim 1$ to help with this. If one is to draw conclusions about anisotropy, the barrier itself must not break translation symmetry along the face. Thus it would probably be premature to conclude anything about the order parameter at the present stage of these experiments. If the junction quality improves, and particularly if *SIS* junctions are made, then phase-sensitive experiments, for example, corner junction experiments, would become possible. This could yield a wealth of valuable information about the order parameter. The possibilities have received a comprehensive review by Sauls (1994).

VI. CONCLUSIONS AND FUTURE DIRECTIONS

There are three types of evidence to indicate that UPt_3 is an unconventional superconductor. These are the anisotropic transport properties in the superconducting state, most notably the ultrasonic attenuation and the thermal conductivity; the multiplicity of phases, most notably seen in specific-heat and ultrasonic measurements; and the absence of activated temperature dependence in any physical property. This is a combination of very disparate physical phenomena. Together, they make an exceedingly powerful case that superconductivity in UPt_3 is unconventional. Any attempt to explain the behavior of UPt_3 using *s*-wave superconductivity would involve multiple *ad hoc* features. Qualitatively, the three types of evidence are naturally explained in the framework of unconventional superconductivity.

This does not narrow down the range of possibilities as much as we might wish, however. Even within the usual group-theoretical framework, there are numerous forms for the superconducting order parameter. Let us try to analyze this issue briefly, but systematically, pulling together all of what has gone before.

The two-dimensional representation and spin-triplet scenarios have traditionally dominated the field, as they give a natural explanation for the split transition. Within this picture, the splitting is caused by the coupling to magnetism. This was very strongly supported by the pressure data, in which the superconducting transitions coalesce just when the magnetism disappears. It seems difficult to believe that this beautiful result could be accidental. Yet, as we have seen, there is also evidence from sound velocities that the coalescence is illusory and may actually be a crossing. The latter would support the mixed-representation hypothesis. Related to this is the in-plane near isotropy of the critical fields. To produce this result, two-component theories must invoke the hypothesis that the magnetization is rotated by the field. This has been called into question by neutron-scattering experiments.

If one assumes that somehow these problems can be solved, the two-dimensional picture also gives very nice agreement of theory and experiment for the entire *H-T-P* phase diagram, but only if the *K* parameter, which represents coupling of the order parameter direction to the field direction, is appreciable, as it is in E_{1g}. A large class of theories, most importantly E_{2u}, in which *K* vanishes or is small, have difficulty with the behavior of the normal-superconducting phase boundaries under pressure.

Can these problems be solved? It is perhaps suggestive that they all revolve around a single question, the coupling of superconductivity and magnetism. Do we understand the nature of the magnetic ordering? Does the small moment mean that it is a secondary order parameter? Why is the magnetic ordering so poor, and does this fact affect its coupling to superconductivity? If there are no answers, or if these are not the right questions, then the alternative is that the coupling of superconductivity and magnetism is not the origin of the split transition.

If the split transition is due to an accidental degeneracy, as in the mixed-representation picture, equally many questions remain to be answered. Most such scenarios have a difficult time producing a gap nodal structure consistent with experiment. Perhaps the most difficult problem is one of credibility: how is it that the first truly unconventional superconductor would just happen to have this very unlikely feature?

In the other category of phenomena, that of low-temperature and anisotropic properties, we have an equally tantalizing situation. The specific heat suggests that there are gap nodes but sheds little light on the nodal structure. Ultrasonic attenuation clearly shows that there is a line of nodes in the basal plane, which narrows down the possibilities more than any other single observation. The presumption is now strong that the gap is odd under reflection in the x-y plane.

It is thermal conductivity, however, which is probably the only tool for actually probing in detail what is happening at the gap nodes. Based on experiments to date, we can state that gap nodes at the poles with quadratic dispersion appear to be favored by the data in the asymptotic regime. This type of gap is associated with the E_{2u} theory, but this is somewhat arbitrary: this gap structure is not symmetry related in this representation and could occur only by a fortuitous accident. In the gapless regime, no theory appears at present to account for the data all that well.

Early hopes that the order parameter of UPt_3 would be sorted out quickly, as quickly as the problem of ^{3}He or high-T_c superconductivity, have been dashed. It is a much more complicated system. We require new probes of the gap structure and the vortex structure. We need to understand the theory of the low-temperature behavior better, including the behavior of the residual normal fluid in the presence of impurities and interactions. We need to resolve the important questions remaining about the phase diagram, especially regarding the coupling of superconductivity and magnetism, and we need definitive answers about what is going on at high pressure. There appears to be plenty for everyone to do.

REFERENCES

Abell, J. S., 1989, in *Handbook on the Physics and Chemistry of Rare Earths*, edited by K. A. Gschneidner, Jr. and L. Eyring (Elsevier, Amsterdam), Vol. 12, p. 1.

Adenwalla, S., J. B. Ketterson, S. K. Yip, S. W. Lin, M. Levy, and B. K. Sarma, 1992, Phys. Rev. B **46**, 9070.

Adenwalla, S., S. W. Lin, Q. Z. Ran, Z. Zhao, J. B. Ketterson, J. A. Sauls, L. Taillefer, D. G. Hinks, M. Levy, and B. K. Sarma, 1990, Phys. Rev. Lett. **65**, 2298.

Aeppli, G., E. Bucher, C. Broholm, J. K. Kjems, J. Baumann, and J. Hufnagl, 1988, Phys. Rev. Lett. **60**, 615.

Aeppli, G., E. Bucher, A. I. Goldman, G. Shirane, C. Broholm, and J. K. Kjems, 1988, J. Magn. Magn. Mater. **76-77**, 385.

Albers, R. C., A. M. Boring, and N. E. Christensen, 1986, Phys. Rev. B **33**, 8116.

Anderson, P. W., 1984, Phys. Rev. B **30**, 4000.

Arfi, B., H. Bahlouli, and C. J. Pethick, 1989, Phys. Rev. B **39**, 8959.

Arfi, B., and C. J. Pethick, 1988, Phys. Rev. B **38**, 2312.

Aroński, M. C., R. Clarke, B. G. Demczyk, B. R. Coles, J. L. Smith, A. de Visser, T. Vorenkamp, and J. J. M. Franse, 1993, Physica B **186-188**, 788.

Balatsky, A., and E. Abrahams, 1992, Phys. Rev. B **47**, 513.

Barash, Yu. S., and A. S. Mel'nikov, 1991, Zh. Eksp. Teor. Fiz. **100**, 307 [JETP **73**, 170 (1991)].

Barash, Yu. S., and A. S. Mel'nikov, 1994, Phys. Lett. A **186**, 259.

Barash, Yu. S., and A. A. Svidzinsky, 1996, Phys. Rev. B **53**, 15 254.

Barash, Yu. S., and A. A. Svidzinsky, 1998, Phys. Rev. B **58**, 6476.

Bardeen, J., L. Cooper, and J. R. Schrieffer, 1957, Phys. Rev. **108**, 1175.

Bardeen, J., G. Rickayzen, and L. Tewordt, 1959, Phys. Rev. **113**, 982.

Behnia, K., L. Taillefer, J. Flouquet, D. Jaccard, K. Maki, and Z. Fisk, 1991, J. Low Temp. Phys. **84**, 261.

Bernhoeft, N. R., and G. G. Lonzarich, 1995, J. Phys.: Condens. Matter **7**, 7325.

Bishop, D. J., C. M. Varma, B. Batlogg, E. Bucher, Z. Fisk, and J. L. Smith, 1984, Phys. Rev. Lett. **53**, 1009.

Blount, E., 1985, Phys. Rev. B **32**, 2935.

Blount, E. I., C. M. Varma, and G. Aeppli, 1990, Phys. Rev. Lett. **64**, 3074.

Bogenberger, B., H. v. Löhneysen, T. Trappmann, and L. Taillefer, 1993, Physica B **186-188**, 248.

Boukhny, M., G. L. Bullock, B. S. Shivaram, and D. G. Hinks, 1994, Phys. Rev. Lett. **73**, 1707.

Brison, J. P., N. Keller, P. Lejay, J. L. Tholence, A. Huxley, N. Bernhoeft, A. Buzdin, B. Fak, J. Flouquet, L. Schmidt, A. Stepanov, R. A. Fisher, N. Phillips, and C. Vettier, 1994a, Physica B **199-200**, 70.

Brison, J. P., N. Keller, P. Lejay, J. L. Tholence, A. Huxley, N. R. Bernhoeft, A. Buzdin, B. Fak, J. Flouquet, L. Schmidt, A. N. Stepanov, R. A. Fisher, N. E. Phillips, and C. Vettier, 1994b, J. Low Temp. Phys. **95**, 145.

Brodale, G. E., R. A. Fisher, N. E. Phillips, G. R. Stewart, and A. L. Giorgi, 1986, Phys. Rev. Lett. **57**, 234.

Broholm, C. L., 1989, Ph.D. thesis (University of Copenhagen).

Broholm, C., G. Aeppli, R. N. Kleiman, D. R. Harshman, D. J. Bishop, E. Bucher, D. L. Williams, E. J. Ansaldo, and R. H. Heffner, 1990, Phys. Rev. Lett. **65**, 2062.

Bruls, G., 1995, Physica B **206-207**, 580.

Bruls, G., D. Weber, I. Kouroudis, H. Weinfurter, K. Clausen, M. Yoshizawa, B. Lüthi, and E. Bucher, 1993, Physica B **186-188**, 258.

Bruls, G., D. Weber, B. Wolf, P. Thalmeier, B. Lüthi, A. de Visser, and A. Menovsky, 1990, Phys. Rev. Lett. **65**, 2294.

Bullock, G. L., B. S. Shivaram, and D. G. Hinks, 1993a, Europhys. Lett. **21**, 357.

Bullock, G. L., B. S. Shivaram, and D. G. Hinks, 1993b, Physica B **186-188**, 245.

Buyers, W. J. L., 1996, Physica B **223-224**, 9.

Chen, D.-C., and A. Garg, 1993, Phys. Rev. Lett. **70**, 1689.

Chen, D.-C., and A. Garg, 1994, Phys. Rev. B **49**, 479.

Chen, J. W., S. E. Lambert, M. B. Maple, Z. Fisk, J. L. Smith, G. R. Stewart, and J. O. Willis, 1984, Phys. Rev. B **30**, 1583.

Chiao, M., R. W. Hill, Ch. Lupien, B. Popic, R. Gagnon, and L. Taillefer, 1999, Phys. Rev. Lett. **82**, 2943.

Choi, C., and J. Sauls, 1991, Phys. Rev. Lett. **66**, 484.

Coffey, L., T. M. Rice, and K. Ueda, 1985, J. Phys. C **18**, L813.
Coleman, P., E. Miranda, and A. M. Tsvelik, 1994, Phys. Rev. B **49**, 8955.
Coppersmith, S. N., and R. A. Klemm, 1986, Phys. Rev. Lett. **56**, 1870.
Cox, D. L., 1993, Physica B **186-188**, 312.
Dalichaouch, Y., M. C. de Andrade, D. A. Gajewski, R. Chau, P. Visani, and M. B. Maple, 1995, Phys. Rev. Lett. **75**, 3938.
Dalmas de Réotier, P., A. Huxley, A. Yaounc, J. Flouquet, P. Bonville, P. Imbert, P. Pari, P. C. M. Gubbens, and A. M. Mulders, 1995, Phys. Lett. A **205**, 239.
de Visser, A., 1986, Ph.D. thesis (University of Amsterdam).
de Visser, A., J. Flouquet, J. J. M. Franse, P. Haen, K. Hasselbach, A. Lacerda, and L. Taillefer, 1991, Physica B **171**, 190.
de Visser, A., J. J. M. Franse, and J. Flouquet, 1989, Physica B **161**, 324.
de Visser, A., J. J. M. Franse, and A. Menovsky, 1984, J. Magn. Magn. Mater. **43**, 43.
de Visser, A., J. J. M. Franse, and A. Menovsky, 1985, J. Phys. F: Met. Phys. **15**, L53.
de Visser, A., F. E. Kayzel, A. A. Menovsky, J. J. M. Franse, K. Hasselbach, A. Lacerda, L. Taillefer, J. Flouquet, and J. L. Smith, 1990, Physica B **165-166**, 375.
de Visser, A., F. E. Kayzel, A. A. Menovsky, J. J. M. Franse, J. van den Berg, and G. J. Nieuwenhuys, 1986, Phys. Rev. B **34**, 8168.
de Visser, A., R. J. Keizer, A. A. Menovsky, M. Mihalik, F. S. Tautz, J. J. M. Franse, B. Fak, N. H. van Dijk, J. Flouquet, J. Bossy, and S. Pujol, 1997, Physica B **230-232**, 49.
de Visser, A., E. Louis, J. J. M. Franse, and A. Menovsky, 1986, J. Magn. Magn. Mater. **54-57**, 387.
de Visser, A., A. Menovsky, and J. J. M. Franse, 1987, Physica B **147**, 81.
de Visser, A., A. Menovsky, J. J. M. Franse, K. Hasselbach, A. Lacerda, L. Taillefer, P. Haen, and J. Flouquet, 1990, Phys. Rev. B **41**, 7304.
de Visser, A., N. H. van Dijk, K. Bakker, and J. J. M. Franse, 1993, Physica B **186-188**, 212.
De Wilde, Y., J. Heil, A. G. M. Jansen, P. Wyder, R. Deltour, W. Assmus, A. Menovsky, W. Sun, and L. Taillefer, 1994, Phys. Rev. Lett. **72**, 2278.
Ellman, B., M. Sutton, B. Lussier, R. Brünig, L. Taillefer, S. M. Hayden, and G. Shea-McCarthy, 1997, preprint, cond-mat/9704125.
Ellman, B., L. Taillefer, and M. Poirier, 1996, Phys. Rev. B **54**, 9043.
Ellman, B., J. Yang, T. F. Rosenbaum, and E. Bucher, 1990, Phys. Rev. Lett. **64**, 1569.
Ellman, B., A. Zaluska, and L. Taillefer, 1995, Physica B **205**, 346.
Emery, V. J., and S. Kivelson, 1992, Phys. Rev. B **46**, 10 812.
Evans, S. M. M., and G. A. Gehring, 1989, J. Phys.: Condens. Matter **1**, 10 487.
Fisher, R. A., S. Kim, B. F. Woodfield, N. E. Phillips, L. Taillefer, K. Hasselbach, J. Flouquet, A. L. Giorgi, and J. L. Smith, 1989, Phys. Rev. Lett. **62**, 1411.
Fisher, R. A., B. F. Woodfield, S. Kim, N. E. Phillips, L. Taillefer, A. L. Giorgi, and J. L. Smith, 1991, Solid State Commun. **80**, 263.
Fisk, Z., and J. P. Remeika, 1989, in *Handbook on the Physics and Chemistry of Rare Earths*, edited by K. A. Gschneidner, Jr. and L. Eyring (Elsevier, Amsterdam), Vol. 12, p. 53.
Fledderjohann, A., and P. J. Hirschfeld, 1995, Solid State Commun. **94**, 163.
Franse, J. J. M., A. Menovsky, A. de Visser, C. D. Bredl, U. Gottwick, W. Lieke, H. M. Mayer, U. Rauchschwalbe, G. Sparn, and F. Steglich, 1985, Z. Phys. B: Condens. Matter **59**, 15.
Frings, P.H., 1984, Ph.D. thesis (University of Amsterdam).
Frings, P. H., J. J. M. Franse, F. R. de Boer, and A. Menovsky, 1983, J. Magn. Magn. Mater. **31-34**, 240.
Fulde, P., J. Keller, and G. Zwicknagl, 1988, Solid State Phys. **41**, 1.
Garg, A., 1992, Phys. Rev. Lett. **69**, 676.
Fujita T., W. Aoyama, K. Machida, and T. Ohmi, 1994, J. Phys. Soc. Jpn. **63**, 247.
Garg, A., and D-C. Chen, 1994, Phys. Rev. B **49**, 479.
Geibel, C., *et al.*, 1991a, Z. Phys. B: Condens. Matter **84**, 1.
Geibel, C., *et al.*, 1991b, Z. Phys. B: Condens. Matter **83**, 305.
Golding, B., B. J. Bishop, B. Batlogg, W. H. Haemmerle, Z. Fisk, J. L. Smith, and H. R. Ott, 1985, Phys. Rev. Lett. **55**, 2479.
Goll, G., C. Bruder, and H. v. Löhneysen, 1995, Phys. Rev. B **52**, 6801.
Goll, G., H. v. Löhneysen, I. K. Yanson, and L. Taillefer, 1993, Phys. Rev. Lett. **70**, 2008.
Gor'kov, L., 1987, Sov. Sci. Rev., Sect. A **9**, 1.
Graf, M. J., and D. W. Hess, 2001, Phys. Rev. B **63**, 134502.
Graf, M. J., S.-K. Yip, and J. A. Sauls, 1996, J. Low Temp. Phys. **102**, 367; **106**, 727(E).
Graf, M. J., S.-K. Yip, and J. A. Sauls, 1999, J. Low Temp. Phys. **114**, 257.
Graf, M. J., S.-K. Yip, and J. A. Sauls, 2000, Phys. Rev. B **62**, 14 393.
Graf, M. J., S. K. Yip, J. A. Sauls, and D. Rainer, 1996, Phys. Rev. B **53**, 15 147.
Greiter, M., G. G. Lonzarich, and L. Taillefer, 1992, Phys. Lett. A **169**, 199.
Grewe, N., and F. Steglich, 1991, in *Handbook of Physics and Chemistry of Rare Earths*, edited by K. A. Gschneidner, Jr. and L. Eyring (Elsevier, Amsterdam), Vol. 14, p. 343.
Gross-Alltag, F., B. S. Chandrasekhar, D. Einzel, P. J. Hirschfeld, and K. Andres, 1991, Z. Phys. B: Condens. Matter **82**, 243.
Haas, S., A. V. Balatsky, M. Sigrist, and T. M. Rice, 1997, Phys. Rev. B **56**, 5108.
Harán, G., and G. A. Gehring, 1995, J. Phys.: Condens. Matter **7**, 8151.
Hardy, W. N., D. A. Bonn, D. C. Morgan, R. Liang, and K. Zhang, 1993, Phys. Rev. Lett. **70**, 3999.
Hasselbach, K., L. Taillefer, and J. Flouquet, 1989, Phys. Rev. Lett. **63**, 93.
Hasselbach, K., L. Taillefer, and J. Flouquet, 1990, Physica B **165-166**, 357,313.
Hayden, S. M., L. Taillefer, C. Vettier, and J. Flouquet, 1992, Phys. Rev. B **46**, 8675.
Heffner, R. H., D. W. Cooke, A. L. Giorgi, R. L. Hutson, M. E. Schillaci, H. D. Remp, J. L. Smith, J. O. Willis, D. E. Maclaughlin, C. Boekema, R. L. Lichti, J. Oostens, and A. B. Denison, 1989, Phys. Rev. B **39**, 11 345.
Heffner, R. H., and M. R. Norman, 1996, Comments Condens. Matter Phys. **17**, 361.
Heid, R., Ya. B. Bazaliy, V. Martisovits, and D. L. Cox, 1995, Phys. Rev. Lett. **74**, 2571.

Hess, D. W., P. Riseborough, and J. L. Smith, 1993, *Encyclopedia of Applied Physics* (VCH, Weinheim), Vol. 7, p. 435.
Hess, D. W., T. A. Tokuyasu, and J. A. Sauls, 1989, J. Phys.: Condens. Matter **1**, 8135.
Hewson, A. C., 1993, *The Kondo Problem to Heavy Fermions* (Cambridge University Press, Cambridge).
Hirschfeld, P. J., and W. O. Putikka, 1996, Phys. Rev. Lett. **77**, 3909.
Hirschfeld, P. J., D. Vollhardt, and P. Wölfle, 1986, Solid State Commun. **59**, 111.
Hirschfeld, P. J., P. Wölfle, and D. Einzel, 1988, Phys. Rev. B **37**, 83.
Huxley, A. D., P. Rodière, D. McK. Paul, N. van Dijk, R. Cubitt, and J. Flouquet, 2000, Nature (London) **406**, 160.
Huxley, A. D., H. Suderow, J. P. Brison, and J. Flouquet, 1995, Phys. Lett. A **209**, 365.
Isaacs, E. D., P. Zschack, C. L. Broholm, C. Burns, G. Aeppli, A. P. Ramirez, T. T. M. Palstra, R. W. Erwin, N. Stücheli, and E. Bucher, 1995, Phys. Rev. Lett. **75**, 1178.
Jaccard, D., J. Flouquet, P. Lejay, and J. L. Tholence, 1985, J. Appl. Phys. **57**, 3084.
Jaccard, D., and E. Vargoz, 1998, J. Magn. Magn. Mater. **177**, 294.
Jin, C., D. M. Lee, S. W. Lin, B. K. Sarma, and D. G. Hinks, 1992, J. Low Temp. Phys. **89**, 557.
Jin, D. S., S. A. Carter, B. Ellman, T. F. Rosenbaum, and D. G. Hinks, 1992, Phys. Rev. Lett. **68**, 1597.
Joynt, R., 1988, Supercond. Sci. Technol. **1**, 210.
Joynt, R., 1990, J. Phys.: Condens. Matter **2**, 3415.
Joynt, R., 1991, Europhys. Lett. **16**, 289.
Joynt, R., 1992, J. Magn. Magn. Mater. **108**, 31.
Joynt, R., 1993, Phys. Rev. Lett. **71**, 3015.
Joynt, R., 1997, Phys. Rev. Lett. **78**, 3189.
Joynt, R., V. Mineev, G. Volovik, and M. E. Zhitomirskii, 1990, Phys. Rev. B **42**, 2014.
Joynt, R., T. M. Rice, and K. Ueda, 1986, Phys. Rev. Lett. **56**, 1412.
Julian, S. R., P. A. A. Teunissen, and S. A. J. Wiegers, 1992, Phys. Rev. B **46**, 9821.
Julian, S. R., G. J. McMullan, N. Dorion-Leyraud, A. D. Huxley, M. P. Ray, M. R. Norman, J. Floquet, and G. G. Lonzarich, 2000, *The Fermi Surface of UPt_3* (University of Cambridge, Cambridge).
Junod, A., B. Revaz, Y. Wang, and A. Erb, 2000, Physica B **284-288**, 1043.
Kadowaki, K., and S. B. Woods, 1986, Solid State Commun. **58**, 507.
Keller, N., J. P. Brison, P. Lejay, J. L. Tholence, A. Huxley, L. Schmidt, A. Buzdin, and J. Flouquet, 1995, Physica B **206-207**, 568.
Keller, N., J. L. Tholence, A. Huxley, and J. Flouquet, 1994, Phys. Rev. Lett. **73**, 2364.
Kimura, N., R. Settai, Y. Onuki, H. Toshima, E. Yamamoto, K. Maezawa, H. Aoki, and H. Harima, 1995, J. Phys. Soc. Jpn. **64**, 3881.
Kleiman, R. N., C. Broholm, G. Aeppli, E. Bucher, N. Stücheli, D. J. Bishop, K. N. Clausen, K. Mortensen, J. S. Pederson, and B. Howard, 1992, Phys. Rev. Lett. **69**, 3120.
Kleiman, R. N., P. Gammel, E. Bucher, and D. Bishop, 1989, Phys. Rev. Lett. **62**, 328.
Kohori, Y., T. Kohara, H. Shibai, Y. Oda, T. Kaneko, Y. Kitaoka, and K. Asayama, 1987, J. Phys. Soc. Jpn. **56**, 395.
Kohori, Y., T. Kohara, H. Shibai, Y. Oda, Y. Kitaoka, and K. Asayama, 1988, J. Phys. Soc. Jpn. **57**, 395.
Kohori, Y., M. Kyogaku, T. Kohara, K. Asayama, H. Amitsuka, and Y. Miyako, 1990, J. Magn. Magn. Mater. **90-91**, 510.
Kopnin, N. B., and G. E. Volovik, 1996, JETP Lett. **64**, 690.
Kycia, J. B., 1997, Ph.D. thesis (Northwestern University).
Kycia, J. B., B. M. Davis, J. I. Hong, M. W. Meisel, D. N. Seidman, and W. P. Halperin, 1995, J. Low Temp. Phys. **101**, 623.
Kycia, J. B., J. I. Hong, M. J. Graf, J. A. Sauls, D. N. Seidman, and W. P. Halperin, 1998, Phys. Rev. B **58**, 603.
Lawrence, J. M., and D. L. Mills, 1991, Comments Condens. Matter Phys. **15**, 163.
Lee, M., G. F. Moores, Y.-Q. Song, W. P. Halperin, W. W. Kim, and G. R. Stewart, 1993, Phys. Rev. B **48**, 7392.
Lee, P. A., 1993, Phys. Rev. Lett. **71**, 1887.
Lee, P. A., T. M. Rice, J. W. Serene, L. J. Sham, and J. W. Wilkins, 1986, Comments Condens. Matter Phys. **12**, 99.
Leggett, A. J., 1975, Rev. Mod. Phys. **47**, 331.
Leggett, A. J., 1987, J. Magn. Magn. Mater. **63-64**, 406.
Libero, V. L., and D. L. Cox, 1993, Phys. Rev. B **48**, 3783.
Lin, S. W., C. Jin, H. Zhang, J. B. Ketterson, D. M. Lee, D. G. Hinks, M. Levy, and B. K. Sarma, 1994a, Physica B **194-196**, 2024.
Lin, S. W., C. Jin, H. Zhang, J. B. Ketterson, D. M. Lee, D. G. Hinks, M. Levy, and B. K. Sarma, 1994b, Phys. Rev. B **49**, 10 001.
Löhneysen, H. v., 1994, Physica B **197**, 551.
Löhneysen, H. v., 1996, Physica B **218**, 148.
Löhneysen, H. v., T. Trappmann, and L. Taillefer, 1992, J. Magn. Magn. Mater. **108**, 49.
Lonzarich, G. G., and S. R. Julian, 1994, private communication.
Lowell, J., and J. B. Sousa, 1970, J. Low Temp. Phys. **3**, 65.
Luke, G. M., A. Keren, L. P. Le, W. D. Wu, Y. J. Uemura, D. A. Bonn, L. Taillefer, and J. D. Garrett, 1993, Phys. Rev. Lett. **71**, 1466.
Luk'yanchuk, I., 1991 J. Phys. I **1**, 1155.
Lussier, B., B. Ellman, and L. Taillefer, 1994, Phys. Rev. Lett. **73**, 3294.
Lussier, B., B. Ellman, and L. Taillefer, 1996, Phys. Rev. B **53**, 5145.
Lussier, B., L. Taillefer, W. J. L. Buyers, T. E. Mason, and T. Peterson, 1996, Phys. Rev. B **54**, R6873.
Machida, K., 1992, Prog. Theor. Phys. Suppl. **108**, 229.
Machida, K., T. Fujita, and T. Ohmi, 1993, J. Phys. Soc. Jpn. **62**, 680.
Machida, K., T. Nishira, and T. Ohmi, 1999, J. Phys. Soc. Jpn. **68**, 3364.
Machida, K., and T. Ohmi, 1998, J. Phys. Soc. Jpn. **65**, 4018.
Machida, K., T. Ohmi, and M. Ozaki, 1993, J. Phys. Soc. Jpn. **62**, 3216.
Machida, K., and M. Ozaki, 1989, J. Phys. Soc. Jpn. **58**, 2244.
Machida, K., and M. Ozaki, 1991, Phys. Rev. Lett. **66**, 3293.
Machida, K., M. Ozaki, T. Fujita, and T. Ohmi, 1993, Physica B **186-188**, 218.
Machida, K., M. Ozaki, and T. Ohmi, 1989, J. Phys. Soc. Jpn. **58**, 4116.
Mathur, N. D., F. M. Grosche, S. R. Julian, I. R. Walker, D. M. Freye, R. K. W. Haselwimmer, G. G. Lonzarich, 1998, Nature (London) **394**, 39.
Mel'nikov, A. S., 1992, Zh. Eksp. Teor. Fiz. **101**, 1978 [JETP **74**, 1059 (1992)].

Menovsky, A., J. J. M. Franse, and A. C. Moleman, 1984, J. Cryst. Growth **67**, 31.
Midgley, P. A., S. M. Hayden, L. Taillefer, B. Bogenberger, and H. v. Löhneysen, 1993, Phys. Rev. Lett. **70**, 678.
Mineev, V. P., and K. V. Samokhin, 1999, *Introduction to Unconventional Superconductivity* (Gordon and Breach, Amsterdam).
Miyake, K., and C. M. Varma, 1986, Phys. Rev. Lett. **57**, 1627.
Moler, K., D. J. Baar, J. S. Urbach, R. Liang, W. N. Hardy, and A. Kapitulnik, 1994, Phys. Rev. Lett. **73**, 2744.
Moler, K., D. L. Sisson, J. S. Urbach, M. R. Beasley, A. Kapitulnik, D. J. Baar, R. Liang, and W. N. Hardy, 1997, Phys. Rev. B **55**, 3954.
Monien, H., K. Scharnberg, L. Tewordt, and D. Walker, 1987, Solid State Commun. **61**, 581.
Moreno, J., and P. Coleman, 1996, Phys. Rev. B **53**, 2995.
Moreno, J., and J. A. Sauls, 2001, Phys. Rev. B **63**, 024419.
Müller, T., W. Joss, and L. Taillefer, 1989, Phys. Rev. B **40**, 2614.
Müller, V., D. Maurer, E. W. Scheidt, Ch. Roth, K. Lüders, E. Bucher, and H. E. Bömmel, 1986, Solid State Commun. **57**, 319.
Müller, V., Ch. Roth, D. Maurer, E. W. Scheidt, K. Lüders, E. Bucher, and H. E. Bömmel, 1987, Phys. Rev. Lett. **58**, 1224.
Norman, M. R., 1987, Phys. Rev. Lett. **59**, 232.
Norman, M. R., 1990, Phys. Rev. B **41**, 170.
Norman, M. R., 1992, Physica C **194**, 205.
Norman, M. R., 1993, Phys. Rev. B **48**, 6315.
Norman, M. R., 1994a, Phys. Rev. Lett. **72**, 2077.
Norman, M. R., 1994b, Phys. Rev. B **50**, 6904.
Norman, M. R., 1995a, Phys. Rev. B **52**, 1421.
Norman, M. R., 1995b, Phys. Rev. B **52**, 15 093.
Norman, M. R., 1996, private communication.
Norman, M. R., R. C. Albers, A. M. Boring, and N. E. Christensen, 1988, Solid State Commun. **68**, 245.
Norman, M. R., and P. J. Hirschfeld, 1996, Phys. Rev. B **53**, 5706.
Norman, M. R., and D. D. Koelling, 1993, in *Handbook on the Physics and Chemistry of Rare Earths and Actinides*, edited by K. A. Gschneidner, Jr., L. Eyring, G. H. Lander, and G. R. Choppin (Elsevier, Amsterdam), Vol. 17, p. 1.
Oguchi, T., and A. J. Freeman, 1985, J. Magn. Magn. Mater. **52**, 174.
Oguchi, T., A. J. Freeman, and G. W. Crabtree, 1987, J. Magn. Magn. Mater. **63-64**, 645.
Ohmi, T., and K. Machida, 1993, Phys. Rev. Lett. **71**, 625.
Ohmi, T., and K. Machida, 1996a, J. Phys. Soc. Jpn. **65**, 3456.
Ohmi, T., and K. Machida, 1996b, J. Phys. Soc. Jpn. **65**, 4018.
Orenstein, J., and A. J. Millis, 2000, Science **288**, 468.
Ott, H. R., E. Felder, A. Bernasconi, Z. Fisk, J. L. Smith, L. Taillefer, and G. G. Lonzarich, 1987, Jpn. J. Appl. Phys. **26**, 1217 Suppl. 26-3.
Ott, H. R., and Z. Fisk, 1987, in *Handbook on the Physics and Chemistry of Actinides*, edited by A. J. Freeman and G. H. Lander (Elsevier, Amsterdam), Vol. 5, p. 85.
Ott, H. R., H. Rudigier, P. Delsing, and Z. Fisk, 1984, Phys. Rev. Lett. **52**, 1551.
Palumbo, M., and P. Muzikar, 1992a, Europhys. Lett. **20**, 267.
Palumbo, M., and P. Muzikar, 1992b, Phys. Rev. B **45**, 12 620.
Palumbo M., P. Muzikar, and J. A. Sauls, 1990, Phys. Rev. B **42**, 2681.
Park, K., and R. Joynt, 1995, Phys. Rev. B **53**, 12 346.
Pethick, C. J., and D. Pines, 1986, Phys. Rev. Lett. **57**, 118.
Pethick, C. J., D. Pines, K. F. Quader, K. S. Bedell, and G. E. Brown, 1986, Phys. Rev. Lett. **57**, 1955.
Phillips, N. E., 1959, Phys. Rev. **114**, 676.
Ponchet, A., J.-M. Mignot, A. de Visser, J. J. M. Franse, and A. Menovsky, 1986, J. Magn. Magn. Mater. **54-57**, 399.
Putikka, W. O., and R. Joynt, 1988, Phys. Rev. B **37**, 2372.
Putikka, W. O., and R. Joynt, 1989, Phys. Rev. B **39**, 701.
Qian, Y. J., M.-F. Xu, A. Schenstrom, H.-P. Baum, J. B. Ketterson, D. Hinks, M. Levy, and B. K. Sarma, 1987, Solid State Commun. **63**, 599.
Ramirez, A. P., N. Stücheli, and E. Bucher, 1995, Phys. Rev. Lett. **74**, 1218.
Rasul, J. W., and A. P. Harrington, 1987, J. Phys. C **20**, 4783.
Rauchschwalbe, U., U. Alheim, F. Steglich, D. Rainer, and J. J. M. Franse, 1985, Z. Phys. B: Condens. Matter **60**, 379.
Rodriguez, J. P., 1985, Phys. Rev. Lett. **55**, 250.
Salomaa, M., and G. E. Volovik, 1987, Rev. Mod. Phys. **59**, 533.
Sarma, B. K., M. Levy, S. Adenwalla, and J. Ketterson, 1992, *Physical Acoustics* (Academic, New York), Vol. 20, p. 107.
Satterthwaite, C. B., 1962, Phys. Rev. **125**, 873.
Sauls, J. A., 1994, Adv. Phys. **43**, 113.
Sauls, J. A., 1996, Phys. Rev. B **53**, 8543.
Scharnberg, K., D. Walker, H. Monien, L. Tewordt, and R. A. Klemm, 1986, Solid State Commun. **60**, 535.
Scheider, W. D., and C. Laubschat, 1981, Phys. Rev. B **23**, 997.
Schenstrom, A., M.-F. Xu, Y. Hong, D. Bein, M. Levy, B. K. Sarma, S. Adenwalla, Z. Zhao, T. Tokuyasu, D. W. Hess, J. B. Ketterson, J. A. Sauls, and D. G. Hinks, 1989, Phys. Rev. Lett. **62**, 332.
Schmitt-Rink, S., K. Miyake, and C. Varma, 1986, Phys. Rev. Lett. **57**, 2575.
Schöttl, S., E. A. Schuberth, K. Flachbart, J. B. Kycia, J. I. Hong, D. N. Seidman, W. P. Halperin, J. Hufnagl, and E. Bucher, 1999, Phys. Rev. Lett. **82**, 2378.
Schuberth, E. A., and M. Fischer, 1994, Physica B **194-196**, 1983.
Schuberth, E. A., B. Strickler, and K. Andres, 1992, Phys. Rev. Lett. **68**, 117.
Shivaram, B., J. Gannon, Jr., and D. Hinks, 1989, Phys. Rev. Lett. **63**, 1723.
Shivaram, B., J. Gannon, Jr., and D. Hinks, 1990, Physica B **163**, 141.
Shivaram, B. S., Y. H. Jeong, T. F. Rosenbaum, and D. G. Hinks, 1986, Phys. Rev. Lett. **56**, 1078.
Shivaram, B. S., Y. H. Jeong, T. F. Rosenbaum, D. G. Hinks, and S. Schmitt-Rink, 1987, Phys. Rev. B **35**, 5372.
Shivaram, B. S., T. F. Rosenbaum, and D. G. Hinks, 1986, Phys. Rev. Lett. **57**, 1259.
Sieck, M., H. v. Löhneysen, and L. Taillefer, 1995, Physica B **206-207**, 603.
Signore, P. J. C., M. W. Meisel, S. E. Brown, and Z. Fisk, 1994, Physica B **199-200**, 157.
Sigrist, M., R. Joynt, and T. M. Rice, 1987, Phys. Rev. B **36**, 5186.
Sigrist, M., and K. Ueda, 1991, Rev. Mod. Phys. **63**, 239.
Simon, S. H., and P. A. Lee, 1997, Phys. Rev. Lett. **78**, 1548.
Sonier, J. E., M. F. Hundley, J. D. Thompson, and J. W. Brill, 1999, Phys. Rev. Lett. **82**, 4914.
Steglich, F., J. Aarts, C. D. Bredl, W. Lieke, D. Meschede, W. Franz, and J. Schäfer, 1979, Phys. Rev. Lett. **43**, 1892.
Steglich, F., U. Rauchschwalbe, U. Gottwick, H. M. Mayer, G. Sparn, N. Grewe, U. Poppe, and J. J. M. Franse, 1985, J. Appl. Phys. **57**, 3054.

Stewart, G., 1984, Rev. Mod. Phys. **56**, 755.
Stewart, G., Z. Fisk, J. Willis, and J. L. Smith, 1984, Phys. Rev. Lett. **52**, 679.
Sticht, J., and J. Kübler, 1985, Solid State Commun. **54**, 389.
Strange, P., and B. Gyorffy, 1985, J. Phys.: Condens. Matter **7**, 5579.
Suderow, H., J. P. Brison, A. D. Huxley, and J. Flouquet, 1997a, Physica B **230-232**, 342.
Suderow, H., J. P. Brison, A. D. Huxley, and J. Flouquet, 1997b, J. Low Temp. Phys. **108**, 11.
Suderow, H., J. P. Brison, A. Huxley, and J. Flouquet, 1998, Phys. Rev. Lett. **80**, 165.
Sulewski, P. E., A. J. Sievers, M. B. Maple, and M. S. Torikachvili, J. L. Smith, and Z. Fisk, 1988, Phys. Rev. B **38**, 5338.
Sulpice, A., P. Gandit, J. Chaussy, J. Flouquet, D. Jaccard, P. Lejay, and J. L. Tholence, 1986, J. Low Temp. Phys. **62**, 39.
Sumiyama, A., S. Shibata, Y. Oda, N. Kimura, E. Yamamoto, Y. Haga, and Y. Onuki, 1998, Phys. Rev. Lett. **81**, 5213.
Sundaram, S. K., and R. Joynt, 1989, Phys. Rev. B **40**, 8780.
Taillefer, L., 1990, Physica B **163**, 278.
Taillefer, L., 1994, Hyperfine Interact. **85**, 379.
Taillefer, L., K. Behnia, K. Hasselbach, J. Flouquet, S. M. Hayden, and C. Vettier, 1990, J. Magn. Magn. Mater. **90-91**, 623.
Taillefer, L., J. Flouquet, Yu. P. Gaïdukov, and N. P. Danilova, 1992, J. Magn. Magn. Mater. **108**, 138.
Taillefer, L., J. Flouquet, and W. Joss, 1988, J. Magn. Magn. Mater. **76-77**, 218.
Taillefer, L., J. Flouquet, and G. G. Lonzarich, 1991, Physica B **169**, 257.
Taillefer, L., and G. G. Lonzarich, 1988, Phys. Rev. Lett. **60**, 1570.
Taillefer, L., R. Newbury, G. G. Lonzarich, Z. Fisk, and J. L. Smith, 1987, J. Magn. Magn. Mater. **63-64**, 372.
Taillefer, L., F. Piquemal, and J. Flouquet, 1988, Physica C **153-155**, 451.
Taillefer, L., B. Ellman, B. Lussier, and M. Poirier, 1997, Physica B **230-232**, 327.
Taillefer, L., B. Lussier, R. Gagnon, K. Behnia, and H. Aubin, 1997, Phys. Rev. Lett. **79**, 483.
Takanaka, K., 1977, in *Anisotropy Effects in Type II Superconductors*, edited by W. Weber (Plenum, New York), p. 93.
Thalmeier, P., B. Wolf, D. Weber, R. Blick, G. Bruls, and B. Lüthi, 1992, J. Magn. Magn. Mater. **108**, 109.
Tokuyasu, T., D. Hess, and J. A. Sauls, 1990, Phys. Rev. B **41**, 8891.
Tinkham, M., 1996, *Introduction to Superconductivity* (McGraw-Hill, New York).
Tou, H., Y. Kitaoka, K. Ishida, K. Asayama, N. Kimura, Y. Onuki, E. Yamamoto, Y. Haga, and K. Maezawa, 1998, Phys. Rev. Lett. **80**, 3129.
Tou, H., Y. Kitaoka, N. Kimura, Y. Onuki, E. Yamamoto, and K. Maezawa, 1996, Phys. Rev. Lett. **77**, 1374.
Trappmann, T., H. v. Löhneysen, and L. Taillefer, 1991, Phys. Rev. B **43**, 13 714.
Tsai, C. L., R. L. Fagaly, H. Weinstock, and F. A. Schmidt, 1981, Phys. Rev. B **23**, 6430.
Tsuei, C. C., and J. R. Kirtley, 2000, Rev. Mod. Phys. **72**, 969.
van Dijk, N. H., 1994, Ph.D. thesis (University of Amsterdam).
van Dijk, N. H., A. de Visser, J. J. M. Franse, S. Holtmeier, L. Taillefer, and J. Flouquet, 1993a, Phys. Rev. B **48**, 1299.
van Dijk, N. H., A. de Visser, J. J. M. Franse, and L. Taillefer, 1993b, J. Low Temp. Phys. **93**, 101.
van Dijk, N. H., A. de Visser, J. J. M. Franse, and L. Taillefer, 1994, Physica B **199-200**, 159.
van Dijk, N. H., B. Fak, L. P. Regnault, A. Huxley, and M-T. Fernandez-Diaz, 1998, Phys. Rev. B **58**, 3186.
Vincent, E., J. Hammann, L. Taillefer, K. Behnia, N. Keller, and J. Flouquet, 1991, J. Phys.: Condens. Matter **3**, 3517.
Volovik, G. E., 1988, J. Phys. C **21**, L221.
Volovik, G. E., 1993, JETP Lett. **58**, 469.
Volovik, G. E., and N. B. Kopnin, 1997, Phys. Rev. Lett. **78**, 5028.
Volovik, G. E., and L. Gor'kov, 1984, JETP Lett. **39**, 674.
Volovik, G. E., and L. Gor'kov, 1985, JETP **61**, 843.
Vorenkamp, T., M. C. Aronson, Z. Koziol, K. Bakker, J. J. M. Franse, and J. L. Smith, 1993, Phys. Rev. B **48**, 6373.
Walko, D. A., J.-I. Hong, T. V. Chandrasekhar Rao, Z. Wawrzak, D. N. Seidman, W. P. Halperin, and M. J. Bedzyk, 2001, Phys. Rev. B **63**, 054522.
Wang, C. S., M. R. Norman, R. C. Albers, A. M. Boring, W. E. Pickett, H. Krakauer, and N. E. Christensen, 1987, Phys. Rev. B **35**, 7260.
Willis, J. O., J. D. Thompson, Z. Fisk, A. de Visser, J. J. M. Franse, and A. Menovsky, 1985, Phys. Rev. B **31**, 1654.
Wölfle, P., 1986, Phys. Lett. A **119**, 40.
Wright, D. A., J. P. Emerson, B. F. Woodfield, J. E. Gordon, R. A. Fisher, and N. E. Phillips, 1999, Phys. Rev. Lett. **82**, 1550.
Wu, W. C., and R. Joynt, 2002, Phys. Rev. B (in press).
Yaron, U., P. L. Gammel, G. S. Boebinger, G. Aeppli, P. Schiffer, E. Bucher, D. J. Bishop, C. Broholm, and K. Mortensen, 1997, Phys. Rev. Lett. **78**, 3185.
Yaouanc, A., P. Dalmas de Réotier, and E. H. Brandt, 1997, Phys. Rev. B **55**, 11 107.
Yaouanc, A., P. Dalmas de Réotier, F. N. Gygax, A. Schenk, A. Amato, C. Baines, P. C. M. Gubbens, C. T. Kaiser, A. de Visser, R. J. Keizer, A. Huxley, and A. A. Menovsky, 2000, Phys. Rev. Lett. **84**, 2702.
Yaouanc, A., P. Dalmas de Réotier, A. Huxley, J. Flouquet, P. Bonville, P. C. M. Gubbens, and A. M. Mulders, 1998, J. Phys.: Condens. Matter **10**, 9791.
Yin, G., and K. Maki, 1994, Physica B **199-200**, 224.
Yip, S. K., and A. Garg, 1993, Phys. Rev. B **48**, 3304.
Yip, S. K., T. Li, and P. Kumar, 1991, Phys. Rev. B **43**, 2742.
Zhao, Z., F. Behroozi, S. Adenwalla, Y. Guan, J. B. Ketterson, B. K. Sarma, and D. G. Hinks, 1991, Phys. Rev. B **43**, 13720.
Zhitomirskii, M., 1989, Pis'ma Zh. Eksp. Teor. Fiz. **49**, 333 [JETP Lett. **49**, 379 (1989)].
Zhitomirskii, M., and I. Luk'yanchuk, 1992, Zh. Eksp. Teor. Fiz. **101**, 1954 [JETP **74**, 1046 (1992)].
Zhitomirskii, M., and K. Ueda, 1996, Phys. Rev. B **53**, 6591.